



저작자표시-동일조건변경허락 2.0 대한민국

이용자는 아래의 조건을 따르는 경우에 한하여 자유롭게

- 이 저작물을 복제, 배포, 전송, 전시, 공연 및 방송할 수 있습니다.
- 이차적 저작물을 작성할 수 있습니다.
- 이 저작물을 영리 목적으로 이용할 수 있습니다.

다음과 같은 조건을 따라야 합니다:



저작자표시. 귀하는 원저작자를 표시하여야 합니다.



동일조건변경허락. 귀하가 이 저작물을 개작, 변형 또는 가공했을 경우에는, 이 저작물과 동일한 이용허락조건하에서만 배포할 수 있습니다.

- 귀하는, 이 저작물의 재이용이나 배포의 경우, 이 저작물에 적용된 이용허락조건을 명확하게 나타내어야 합니다.
- 저작권자로부터 별도의 허가를 받으면 이러한 조건들은 적용되지 않습니다.

저작권법에 따른 이용자의 권리는 위의 내용에 의하여 영향을 받지 않습니다.

이것은 [이용허락규약\(Legal Code\)](#)을 이해하기 쉽게 요약한 것입니다.

[Disclaimer](#)

**Ph.D. DISSERTATION**

**Development of a Local Field Potential-based  
Closed-loop Deep Brain Stimulation System  
for Neuropathic Pain Control**

신경병증성 통증 조절을 위한 뇌 국소전위 기반의  
폐회로 심부 뇌 자극 시스템 개발에 대한 연구

By

Sung Eun Lee

February 2015

**DEPARTMENT OF ELECTRICAL ENGINEERING  
AND COMPUTER SCIENCE  
COLLEGE OF ENGINEERING  
SEOUL NATIONAL UNIVERSITY**

# Development of a Local Field Potential-based Closed-loop Deep Brain Stimulation System for Neuropathic Pain Control

신경병증성 통증 조절을 위한 뇌 국소전위 기반의  
폐회로 심부 뇌 자극 시스템에 개발에 관한 연구

指導教授 金 成 俊

이 論文을 工學博士 學位論文으로 提出함

2015 年 2 月

서울大學校 大學院

電氣情報工學部

李 聖 恩

李 聖 恩의 工學博士 學位論文을 認准함

2015 年 2 月

委員長 : 전 누리 (印)

副委員長 : 김 성 준 (印)

委員 : 장 진 우 (印)

委員 : 김 경 환 (印)

委員 : 서 종 모 (印)

# Abstract

Deep brain stimulation (DBS) is an effective therapy that can be used to alleviate symptoms of neuropathic disorders such as Parkinson's disease, essential tremor, dystonia, and neuropathic pain. Even though the method has matured for widespread implantation of the device worldwide, the therapeutic mechanisms of DBS are still unclear. Moreover, current DBS system is an open-loop system so a flexible and effective neuromodulation that depends on severity of patients' symptoms is yet to be made available. The open-loop configuration also wastes power due to its continuous generation of stimulation current pulses, requiring frequent exchange of implanted battery.

In this dissertation, we studied a local field potential-based closed-loop deep brain stimulation (CDBS) system and its use for controlling neuropathic pain. A multichannel DBS electrode was developed based on a novel LCP material using improved fabrication process. Stimulation parameters of the CDBS system were determined from preliminary experiments including behavioral tests and neural recordings. A correlation analysis was performed between changes in recorded local field potential (LFP) and changes in scored results of behavioral tests related to neuropathic pain proved to yield important information for the closed-loop strategy. Finally, a prototype CDBS system for neuropathic pain was developed and validated *in vivo*.

**Keywords:** Closed-loop deep brain stimulation, DBS, neuropathic pain

**Student Number: 2010-30944**

# Contents

<b>ABSTRACT</b> .....	<b>iii</b>
<b>Contents</b> .....	<b>iv</b>
<b>List of Figures</b> .....	<b>vii</b>
<b>List of Tables</b> .....	<b>ix</b>

## Chapter

<b>1. Introduction</b> .....	<b>1</b>
<b>1.1 Biological background</b> .....	<b>2</b>
1.1.1 Neuropathic pain .....	2
1.1.2 Neural pathway of neuropathic pain and current treating methods .	3
1.1.3 Anatomical characteristics of ventral posterior lateral nucleus .....	5
<b>1.2 Overview of brain stimulation</b> .....	<b>6</b>
1.2.1 Brain stimulation .....	6
1.2.2 Mechanisms and stimulation condition of DBS .....	13
1.2.3 Deep brain stimulation for neuropathic pain .....	16
<b>1.3 Closed-loop deep brain stimulation system</b> .....	<b>18</b>
1.3.1 Current deep brain stimulation system: Open-loop system .....	18
1.3.2 Closed-loop concept for neural prosthetic devices .....	18
1.3.3 Requirements for closed-loop deep brain stimulation system .....	20
<b>1.4 Objectives of this dissertation</b> .....	<b>24</b>
<b>2. Materials and methods</b> .....	<b>25</b>
<b>2.1 Multichannel deep brain stimulation electrode</b> .....	<b>26</b>
2.1.1 Liquid crystal polymer (LCP) .....	26
2.1.2 Electrode design .....	28
2.1.3 Volume of tissue activated (VTA) simulation .....	31
2.1.4 Surgical process design: Electrode implantation .....	33
2.1.5 Fabrication process .....	34
2.1.6 Characteristics measurements .....	43
<b>2.2 Preliminary experiments</b> .....	<b>45</b>
2.2.1 TST neuropathic modeling .....	45

2.2.2 Electrode implantation .....	46
2.2.3 Deep brain stimulation (DBS) .....	47
2.2.4 Behavioral tests (von Frey test and duration test) .....	50
2.2.5 Neural recording .....	50
2.2.6 Signal processing .....	52
2.2.7 Correlation analysis .....	54
<b>2.3 Closed-loop stimulator .....</b>	<b>56</b>
2.3.1 Overview of closed-loop DBS system for neuropathic pain .....	56
2.3.2 Closed-loop deep brain stimulation strategy for neuropathic pain ..	58
2.3.3 Prototype implementation .....	60
2.3.4 Prototype measurements: performance test .....	63
2.3.5 Animal experiments: <i>in vivo</i> application .....	64
<b>3. Results .....</b>	<b>66</b>
<b>3.1 Multichannel deep brain stimulation electrode .....</b>	<b>67</b>
3.1.1 Results of VTA simulation .....	68
3.1.2 Fabrication process .....	68
3.1.3 Developed electrode .....	70
3.1.4 Results of characteristics measurements .....	71
<b>3.2 Results of preliminary experiments .....</b>	<b>73</b>
3.2.1 Results of behavioral tests (von Frey tests and duration tests) .....	73
3.2.2 Results of neural recording (Local field potential, LFP) .....	75
3.2.3 Results of correlation analysis (Pearson analysis) .....	79
3.2.4 Results of histological study .....	79
<b>3.3 Closed-loop stimulator .....</b>	<b>80</b>
3.3.1 Developed closed-loop deep brain stimulation strategy .....	80
3.3.2 Developed prototype closed-loop stimulator .....	82
3.3.3 Results of performance measurements .....	83
3.3.4 Results of <i>in vivo</i> experiments .....	84
<b>4. Discussion .....</b>	<b>86</b>
<b>4.1 Improved LCP process for multiple LCP layers .....</b>	<b>87</b>
<b>4.2 Volume of tissue activated (VTA) issues .....</b>	<b>90</b>
<b>4.3 Correlation analysis .....</b>	<b>92</b>

<b>4.4 Closed-loop stimulator</b> .....	94
4.4.1 Correction method based on neural spikes .....	94
4.4.2 Power consumption .....	94
4.4.3 Size of the system .....	95
4.4.4 Response time of closed-loop control .....	96
<b>4.5 Gliosis</b> .....	98
<b>5. Conclusion</b> .....	<b>99</b>
<b>References</b> .....	101
<b>Acknowledgement</b> .....	117
<b>Abstract in Korean</b> .....	118
<b>감사의 글</b> .....	120

# List of Figures

Figure 1-1. Pain signaling pathways .....	4
Figure 1-2. Rodent brain anatomy of ventral posterolateral nucleus (VPL) .....	6
Figure 1-3. Image of stimulating the brain with electroconvulsive therapy (ECT) ..	8
Figure 1-4. Image of configuration for transcranial magnetic stimulation (TMS) ...	9
Figure 1-5. Image of configuration for vagus nerve stimulation (VNS) .....	10
Figure 1-6. Image of configuration for cortical stimulation .....	11
Figure 1-7. Diagram of deep brain stimulation .....	13
Figure 1-8. VL neuron pathway .....	16
Figure 1-9. Overview of deep brain stimulation for neuropathic pain .....	17
Figure 1-10. Schematic diagram of a closed-loop algorithm .....	19
Figure 1-11. Quantitative scoring methods for neuropathic pain .....	20
Figure 1-12. CDBS related researches of other groups .....	22
Figure 2-1. Chemical structure of liquid crystal polymer .....	27
Figure 2-2. Electrode design process .....	28
Figure 2-3. Designed multichannel DBS electrode .....	30
Figure 2-4. Mask designs for lithography .....	30
Figure 2-5. Electrode structure for FEM simulation .....	32
Figure 2-6. Designed surgical procedure and electrode holder .....	33
Figure 2-7. LCP-based electrode fabrication process of previous studies .....	36
Figure 2-8. Modified method for fabrication .....	38
Figure 2-9. Misalignment problems with the previous method .....	40
Figure 2-10. Improved interlayer alignment method .....	40
Figure 2-11. Iridium oxide (IrOx) electroplating process .....	42
Figure 2-12. Setup for the buckling tests and an <i>in vivo</i> insertion tests .....	44
Figure 2-13. Process of preliminary experiments for characterizing responses .....	45
Figure 2-14. TST modeling method .....	46



Figure 2-15. Procedure of electrode implantation .....	47
Figure 2-16. Definitions of stimulation parameters and the shape of the pulse .....	48
Figure 2-17. Developed and applied stimulator for preliminary experiments .....	49
Figure 2-18. System composition for neural recording of preliminary experiments	52
Figure 2-19. Steps for signal process for preliminary experiments .....	53
Figure 2-20. Overview of the suggested CDBS system for neuropathic pain .....	57
Figure 2-21. Closed-loop deep brain stimulation strategy for neuropathic pain .....	59
Figure 2-22. System diagram of CDBS system for neuropathic pain .....	61
Figure 2-23. Schematic of the CDBS system .....	62
Figure 2-24. Performance measurements .....	64
Figure 2-25. <i>In vivo</i> experimental setup .....	65
Figure 3-1. Results of FEM simulation for VTA .....	67
Figure 3-2. Images of the whole fabrication process for the LCP-based electrode ..	68
Figure 3-3. Application of the improved LCP process .....	69
Figure 3-4. Developed LCP-based deep brain stimulation electrode .....	70
Figure 3-5. Results of electrochemical measurements .....	71
Figure 3-6. Results of material-dependent mechanical characteristics measurements	72
Figure 3-7. Changes in behavioral responses before and after DBS stimulation .....	74
Figure 3-8. Changes in neural signals related to neuropathic pain .....	75
Figure 3-9. Results of neural recording with different configuration .....	77
Figure 3-10. Changes in pain-related neural responses .....	77
Figure 3-11. Changes in LFPs depending on painful stimulus and DBS .....	78
Figure 3-12. Results of histological study and the rodent brain atlas .....	79
Figure 3-13. Final finite state machine (FSM) for controlling prototype CDBS .....	81
Figure 3-14. Implemented prototype CDBS system for neuropathic pain .....	82
Figure 3-15. Results and test environment for performance measurements .....	83
Figure 3-16. <i>In vivo</i> performance tests of prototype CDBS system for NP .....	85
Figure 4-1. Layer arrangement for double-side LCP-based electrode .....	89

Figure 4-2. Problems during new interlayer alignment method .....	89
Figure 4-3. Results of TVA simulation for Thalamic VIM stimulation .....	91
Figure 4-4. Hexagonal electrode design and its various stimulation scheme .....	92
Figure 4-5. Compensation circuit for DC offset .....	95
Figure 4-6. Integrated circuit-based CDBS system .....	96
Figure 4-7. Comparison of changes in LFP and system response time .....	97

## List of Tables

Table 1-1. Comparison of various electrical brain stimulation configurations .....	7
Table 2-1. List of the properties of polymers used for implantable devices .....	27
Table 2-2. FEM simulation parameters .....	32
Table 2-3. Recipes for laser process .....	37
Table 2-4. Custom designed current stimulation chip specification .....	48
Table 2-5. Various stimulation condition for specifying stimulation parameter .....	49
Table 2-6. Strength of relationship depending on correlation coefficient $r$ .....	55
Table 2-7. Functions of Microcontroller for closed-loop control .....	63
Table 3-1. Measured electrochemical characteristics .....	71
Table 3-2. $p$ -value of statistical analysis on results of behavioral tests .....	74
Table 3-3. $p$ -value of statistical analysis on results of neural recording .....	77
Table 3-4. Results of correlation analysis .....	79
Table 3-5. System response time .....	84

# ***1. Introduction***

---

***1.1 Biological background***

***1.2 Overview of brain stimulation***

***1.3 Closed-loop neural prosthetic system***

***1.4 Objectives of this thesis***

Neural prosthesis is a technology related to neuroscience and biomedical engineering. Neural prostheses are a series of devices that can substitute a motor, sensory or cognitive modality that might have been damaged or lost because of injury or disease. Such devices might represent an important tool in clinical cases where neural control is lost or significantly reduced like a cochlear implant for hearing [4, 5], a retinal implant for vision [6-8], a deep brain stimulation (DBS) for treating neuropathic disorders [9, 10]. Commercialized neural prosthetic devices such as cochlear implants and retinal implants are based on already known their biological functional mechanisms. In contrast, mechanisms of deep brain stimulation are still unclear, despite it has already commercialized [11, 12]. In this chapter, we discussed the biological background about neuropathic pain and the DBS method to explain the proposed closed-loop DBS system for neuropathic pain.

## **1.1 Biological background**

### **1.1.1 Neuropathic pain**

We focused on deep brain stimulation system for neuropathic pain control. Pain is a multidimensional sensory experience that is intrinsically unpleasant and associated with hurting and soreness. Pain can be essentially divided into two broad categories; adaptive and maladaptive pain (neuropathic pain, NP). Adaptive pain contributes to survival by protecting the organism from injury or promoting healing when injury has occurred. In contrast, neuropathic pain is an abnormal pain syndrome. The current definition of neuropathic pain as proposed by the International Association for the Study of Pain (IASP) is “pain initiated or caused by a primary lesion or dysfunction of the nervous system” [13-16]. It is estimated that 2 – 3 % of the population in the developed world experience neuropathic pain [17]. It is pain as disease.

There are two common pathological conditions that develop after tissue or nerve injury; allodynia and hyperalgesia. In allodynia, there is a reduction in pain threshold and, consequently, nonnoxious stimuli that normally do not cause pain now induce pain.

In hyperalgesia, there is an enhanced response to noxious stimuli. [18, 19].

Several research approaches, including the use of human brain imaging and manipulated rats, have consistently suggested that neuropathic pain is due to long-term plastic changes along sensory pathways. Plastic changes not only take place in peripheral nociceptors and spinal dorsal horn and subcortical areas but also in cortical areas that are involved in the processing of painful information [19]. Although many patients suffer from neuropathic pain, its mechanisms and appropriate treating methods are still unclear [20].

### **1.1.2 Neural pathway of neuropathic pain and current treatments**

Pathophysiological mechanisms underlying neuropathic pain have been reviewed extensively within recent years [21-24]. Addressing the neural pathway related to neuropathic pain is not still clear, but the pain occurring after peripheral nerve damage has been suggested a general cause of neuropathic pain. Injured peripheral nerve fibers give rise to an intense and prolonged input of ectopic activity to the central nervous system and in some cases also secondary changes of the excitability of dorsal horn neurons. At the cellular level formation of new channels, up-regulation of certain receptors and down-regulation of others, altered local or descending inhibition are some of the biological features that can contribute to a hyper-excitability. The neuronal hyper-excitability has a wide spectrum of manifestations including increase in cellular excitability. And the threshold of a single neuron was simultaneously reduced resulting in burst or irregular spike firing patterns can be occurred [25]. The typical neural pathway is known as Figure 1-1. Afferent nociceptive information enters the brain from the spinal cord. Afferent spinal pathways include the spinothalamic, spinoparabrachio–amygdaloid and spinoreticulo–thalamic pathways. Nociceptive information from the thalamus is related to the insula (IS), anterior cingulate cortex (ACC), primary somatosensory cortex (S1) and secondary somatosensory cortex (S2), and amygdala [26].

The nociceptive neurons from the ventrobasal complex mainly project to the S1 and

this pathway constitutes the lateral pain system that plays an important role in the discrimination of stimuli [27]. The affective-motivational aspect of pain is mediated by the medial pain pathway, which includes the intralaminar thalamic nuclei [28] and posterior aspect of ventromedial thalamic nuclei [29] that project to somatosensory cortex and limbic structures [24]. Neurons originated from lamina VII/VIII project to the medullary reticular formation [30], ventrolateral periaqueductal [31] and intralaminar thalamic nuclei [23]. There is extensive projection from the intralaminar nuclei to the cortex, including to the ACC, subserving the motivational aspects of pain [32].

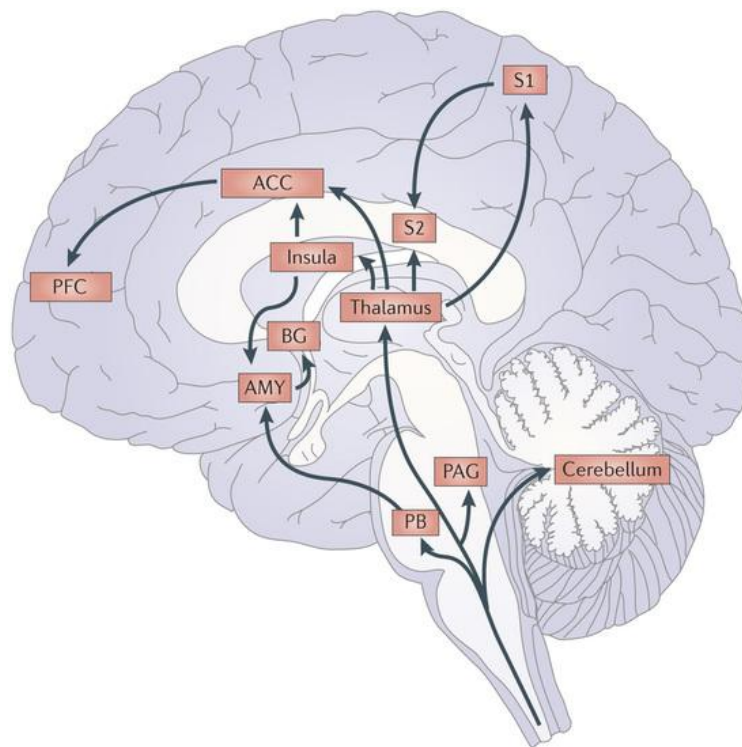


Figure 1-1. Pain signaling pathways. Addressing the complex pains remains an ongoing challenge. Pain signaling pathways involve many neural tissues that could be potentially targets for deep brain stimulation

(Abbreviations: ACC - anterior cingulate cortex, S1 and S2- primary and secondary somatosensory cortex, AMY - amygdala, PAG - periaqueductal grey, BG - basal ganglia, PB - parabrachial nucleus, PFC - prefrontal cortex) [20, 26].

Current treatments for neuropathic pain, pharmacological and surgical methods, were based on this pathological map. First, pharmacological method using morphine, anticonvulsants, antidepressants, opioids, NMDA blockade and topical agents is common. This method has severe side effects such as constipation and addiction. Moreover, many of these analgesic agents have been administered in an uncontrolled fashion, with the long-term effectiveness of these approaches uncertain. Recent randomized controlled trials and meta-analyses of randomized controlled trials indicate a beneficial effect of opioids [33]. The other method is one of the past neurosurgical interventions for neuropathic pain called 'lesioning' [22]. However, lesioning procedures could be harmful to patients because of their lack of reversibility. Deep brain stimulation, an alternative solution for these methods, is less invasive than lesioning procedures because it stimulates a specific site by inserting a small electrode to modulate neuronal activity [34, 35]. If necessary, the stimulation device can be removed from the brain.

### **1.1.3 Anatomical characteristics of ventral posterior lateral nucleus**

This study is aimed to develop a closed-loop brain stimulation system for suppressing the neuropathic pain by stimulating a neuropathic pain. The selected stimulation target is a part of thalamic nuclei called ventral posterior lateral nucleus (VPL). The coordinates of the VPL were AP: -2.2 mm (from bregma), ML: 2.8 mm (right side from midline) and DV: -6.0 mm (from skull). The volume of VPL is similar to a capsule with a diameter of 500  $\mu\text{m}$  and a height of 1 mm as shown in Figure 1-2 [36]. As briefly aforementioned at section 1.1.2, the VPL receives information from the neospinothalamic tract (nociception) by which potentially damaging mechanical, thermal, and chemical stimuli are detected. It projects this sensory information to the S1 of the brain as shown in Figure 1-1. The thalamic nuclei is one of the supra-spinal structures that has been extensively investigated as it receives projections from multiple ascending pathways. Spinal lamina I neurons project extensively to the ventrobasal complex (VPL+ VPM) and to the posterior group thalamic nuclei [21, 37].

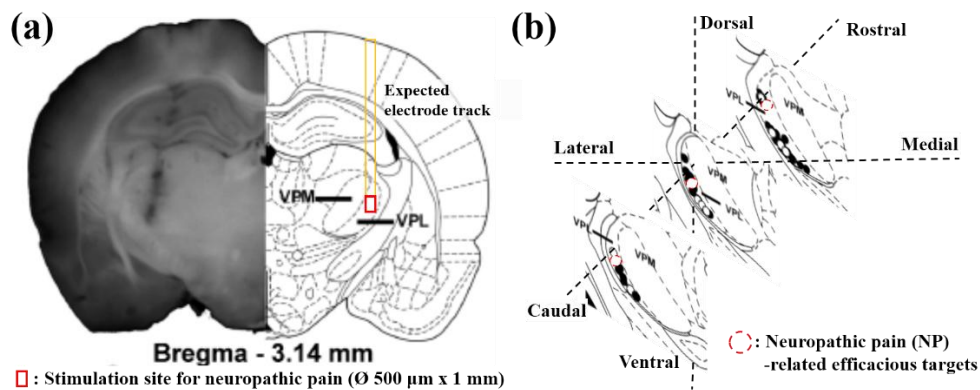


Figure 1-2. Rodent brain anatomy of ventral posterolateral nucleus (VPL). (a) Coronal view and (b) 3D view graph to calculate the volume of VPL for electrode design.

## 1.2 Overview of brain stimulation

### 1.2.1 Brain stimulation

Since conventional treatment methods for neuropathic pain control have several limitations like other neuropathic disorders, then brain stimulations have been on the rise as alternative approaches (Section 1.1.2). Brain stimulations are methods to inhibit or excite neuronal cells to modulate the brain. Several brain stimulation approaches have been developed such as Electro-convulsive therapy (ECT), transcutaneous magnetic stimulation (TMS), cortical stimulation (CS), and deep brain stimulation (DBS) depending on their configurations for deriving stimulation currents [38, 39]. Various configurations to stimulate the brain are described as following (Table 1-1).



Table 1-1. Comparison of various electrical brain stimulation configurations

	<b>Current application</b>	<b>Pulse delivery</b>	<b>Targeting quality</b>	<b>Advantages</b>	<b>Disadvantages</b>
<b>Electroconvulsive therapy (ECT)</b>	Depression, mania, catatonia, Parkinson's disease	Skin electrodes	Good	Noninvasive	Nonfocal, Memory side effects, Requires anesthesia
<b>Transcranial magnetic stimulation (TMS)</b>	Depression	Magnetic field	Good	Noninvasive	Nonfocal, Limited to surface brain
<b>Vagus nerve stimulation (VNS)</b>	Epilepsy, depression	Implanted electrodes	Fair	Brain surgery is not required	Effects modest
<b>Cortical stimulation (CS)</b>	Pain	Epidural electrodes on cortex	Excellent	Minimally invasive	Limited on the cortex
<b>Deep brain stimulation (DBS)</b>	Parkinson's disease, Tremor, Obsessive-compulsive disorder, Pain	Depth-type implanted electrode	Excellent	Discrete targeting, Marked effects	Invasive surgery

### (1) Electroconvulsive therapy (ECT)

Electroconvulsive therapy (ECT) is first considered as a potential therapeutic treatment. In procedure of ECT, electrodes are attached to the scalp of an anesthetized patient (Figure 1-3). The clinical applications of ECT are generalized seizure, mood disorders, and occasional catatonia or Parkinson's disease [40]. Nobler *et al.* have found that those patients who go on to respond to ECT have a greater reduction in prefrontal blood flow immediately following ECT [41]. There appears to be anatomic specificity to where the ECT stimulus is most needed and is most effective for the treatment of depression.

Although mechanisms of ECT are still unclear, repeated ECT over the course of several weeks are an effective treatment for depression, mania, and catatonia. Unfortunately, the skull acts as a large resistor when electrical current is applied to the scalp, so the bulk of the energy of an ECT pulse does not go directly into brain, and the electrical energy cannot be focused. ECT cannot be focused on or directed to specific targets within the brain. Due to the diffuse nature of the application of the current and the inability to focus the induced seizure, ECT has not proven effective for the treatment of primary Obsessive compulsive disorder (OCD) unless its effectiveness for depression symptoms. The use of ECT remains somewhat problematic for various reasons. The technique is associated with memory loss and requires repeated general anesthesia.

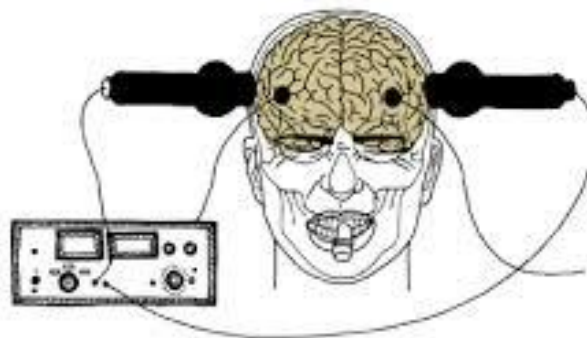


Figure 1-3. Image of stimulating the brain with electroconvulsive therapy (ECT). ECT is the most effective treatment for severe depression, curing up to 80 percent of cases (ref: <http://www.colors magazine.com/>).

## (2) Transcranial magnetic stimulation (TMS)

Transcranial magnetic stimulation (TMS) uses a powerful hand-held to create a time-varying magnetic field where a localized pulsed magnetic field over the surface of the head depolarizes underlying superficial neurons [42]. High-intensity current is rapidly turned on and off in the electromagnetic coil through the discharge of capacitors (Figure 1-4). Producing powerful but brief magnetic fields that induce electrical currents in the brain, TMS rapidly differs from the currently popular use of low-level static magnetic fields as alternative therapies. If TMS pulse are delivered repetitively and rhythmically, it is called repetitive TMS (rTMS). The first modern TMS device was developed and introduced by A. Barker *et al.* in 1985 [43]. TMS as a treatment tool for depression has studied clinical application. Neuronetics, Inc., a privately-held medical device company, announced that the United States Food and Drug Administration (FDA) have cleared its TMS therapy system for the treatment of depression. Many researchers worldwide are currently conducting studies on TMS in subjects with schizophrenia, Parkinson's disease, Tourette's syndrome, epilepsy, and some anxiety disorders [44].

The most critical safety concern with TMS may be inadvertently causing a seizure [44]. And like magnetic resonance imaging (MRI), TMS could cause the movement of paramagnetic objects. TMS can cause heating of metallic implants. Moreover, TMS devices can excite only the surface cortex of the brain because magnetic field strength falls off sharply with distance from the coil.

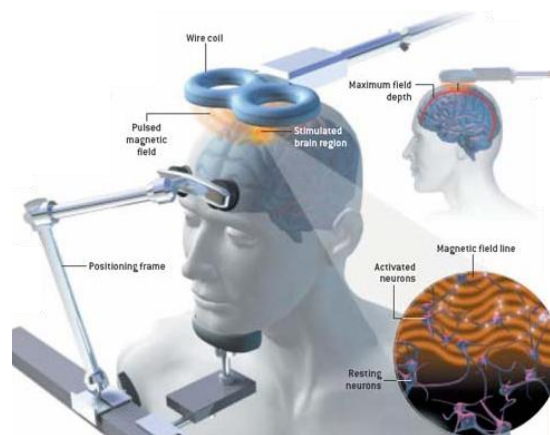


Figure 1-4. Image of configuration for transcranial magnetic stimulation (TMS) [45].

### (3) Vagus nerve stimulation (VNS)

Vagus nerve stimulation (VNS) is a minimal invasive neuromodulation method in neurosurgery. As shown in the Figure 1-5, the direct vagus nerve stimulation method is currently and widely used method for VNS. the generator sends electric impulses to the vagus nerve at regular intervals [46]. The vagus nerve is an important cranial nerve that connects the brain with the body's viscera. Jake Zabara of Temple University discovered that the excitation of the vagus nerve could abort a seizure occurring in dogs in 1985 [47]. From these important observations and ideas have come patents by a company (Cyberonics, Inc). This technique has been available for treatment of refractory partial onset seizures in Europe since June 1994. The US FDA also approved VNS therapy for partial-onset epilepsy and treatment-resistant depression in 1997 and 2005, respectively [48].

Although VNS is an effective, safe, and well-tolerated treatment in patients with long-standing, refractory partial-onset seizures, data indicate that the full effect of VNS may be delayed for as long as a year and those patients continue to improve during that time. Moreover, there is a possibility of operative and postoperative complications. Left vocal cord paralysis with postoperative hoarseness can rarely occur, presumably due to injury to the efferent motor fibers of the vagus nerve. Migration of the pulse generator under the skin can also occur. Lead failure from tension on the electrode wire develops after several times [46, 49].

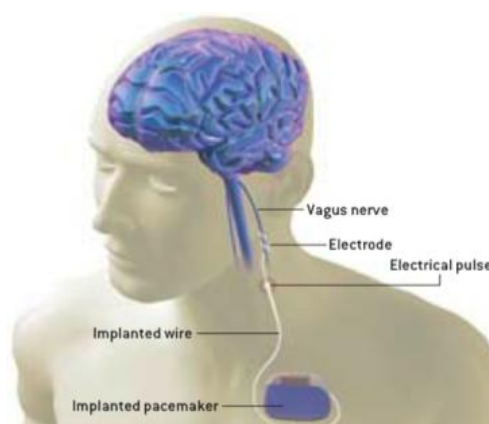


Figure 1-5. Image of configuration for vagus nerve stimulation (VNS) [45].

#### (4) Cortical stimulation

Cortical stimulation is a type of electrocorticography that involves a physically invasive procedure and aims to modulate the function of specific brain regions through direct electrical stimulation of the cerebral cortex [50]. Leads and electrode arrays implanted on the surface of the brain derive stimulation pulses for modulation as shown in Figure 1-6. It's conceivable that once implanted, surface electrode arrays would be in a position to perform multiple applications as new stimulation regimes and neurophysiological mechanisms are uncovered.

Both Neuropace and Northstar Neuroscience are looking at applications for cortical stimulation and vendors like Cyberkinetics Neurotechnology Systems have made process implanting recording electrodes in the cortex [51].

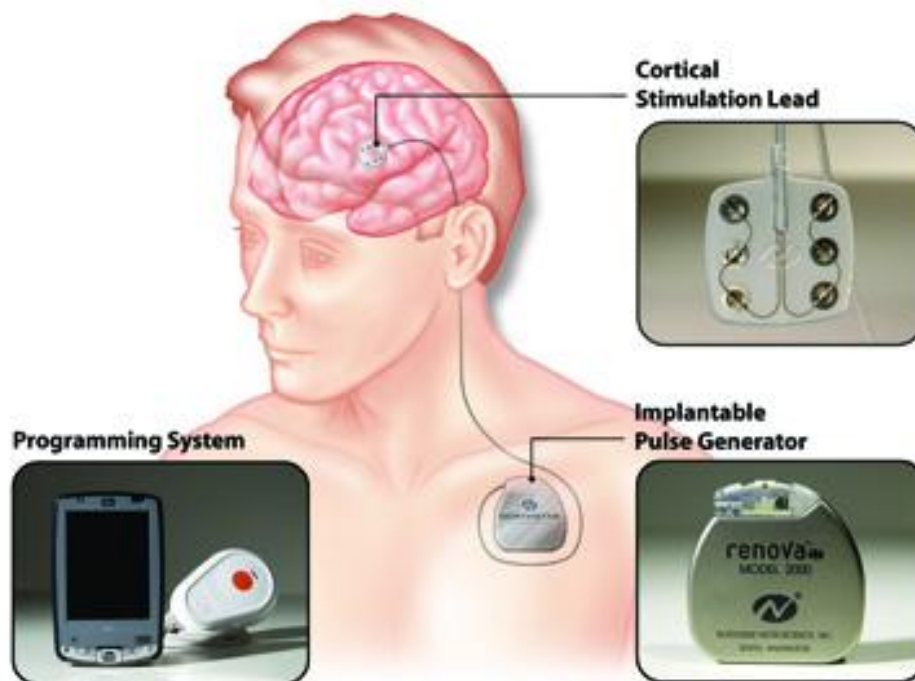


Figure 1-6. Image of configuration for cortical stimulation ([www.medgadget.com](http://www.medgadget.com)). The configuration of cortical stimulation is similar to its of DBS.

## **(5) Deep brain stimulation**

Deep brain stimulation (DBS) is a neuromodulation method to alleviate the symptoms of neuropathic disorders by electrically stimulating into specific regions of the brain. Electrical stimulation pulses generated by the neurostimulator interfere with and block the electrical signals that cause neuropathic disorders. The DBS has been already approved by the United States Food and Drug Administration (FDA) as a treatment for essential tremor since 1997 [52], for Parkinson's disease (PD) in 2002 [53], and dystonia in 2003 [54] since its first trial in 1987 by Benabid [38]. DBS is also used in research studies to treat chronic pain and has been used to treat various affective disorders including major depression [55], neither of these applications of DBS have yet been FDA-approved. Despite these effective clinical applications, the therapeutic mechanisms of DBS are still not completely understood [56].

DBS is considered reversible, and less potentially damaging to delicate brain structures than other surgical options. Instead of making a permanent cut or lesion the idea is to use precisely configured pulses of electric current from an implanted programmable device. One big advantage is the ability to remove the stimulator if it proves ineffective [40]. DBS directly changes brain activity in a controlled manner, its effects are reversible unlike those of lesioning techniques, and it is one of only a few neurosurgical methods that allow blinded studies.

The DBS system consists of three components as shown in Figure 1-7; the electrode, the stimulator, and the external controller. The electrode is inserted through a small opening in the skull, which is called 'burr hole', and the site of the electrode is positioned within the targeted brain area using a stereotaxic tool. The stimulator is usually implanted under the skin near the collarbone, because there is enough space to place the device. The third part, the external controller is used for setting stimulation conditions like current amplitude, pulse frequency, and duration of the stimulation. Such stimulation parameters are usually set via wireless link by a clinical specialist.

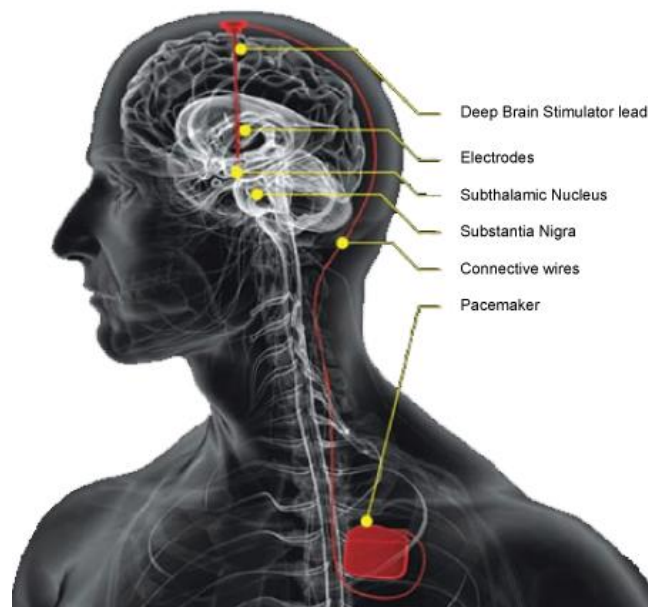


Figure 1-7. Diagram of deep brain stimulation. The deep brain stimulation system generally includes two electrodes, lead wires, connective wires and two pacemakers, which are implanted under the skin near the collarbone. (<http://news.brown.edu/>).

### 1.2.2 Mechanisms and stimulation conditions of DBS

Clearly, clinical developments in the past did not require a detailed knowledge of the neuronal mechanisms of DBS but at the minimum, notions as to the mechanisms have inspired or given confidence to pursuing new clinical applications. The remarkable effectiveness of DBS must be saying something about the underlying neuronal pathophysiology. For example, DBS for Parkinson's disease is effective when all manner of medications [57] and indeed, when brain fetal dopamine cell transplantation fails [58]. Clearly, DBS must be addressing neuronal pathophysiological mechanisms not addressed by pharmacological or cellular replacement of dopamine.

Contrary to earlier notions that only high frequency DBS was clinically effective, recent studies demonstrate that low frequency DBS, in some circumstances such as the pedunculopontine (PPN) nucleus for gait disorders [59] or of the STN for speech [60] in Parkinson's disease. The same high frequency DBS of the GPi is effective for both

hypokinetic disorders, such as chorea [61, 62], as well as hypokinetic disorders such as Parkinson's disease [57]. This is inconsistent with current theories that hold that the mechanisms underlying hypo- and hyperkinesia are reciprocal.

There are as many different DBS mechanisms as there are effective targets or some common mechanisms that are not unique to any particular targets. This suggests that it may be profitable to view DBS from a "systems" perspective rather than just its local effect [63].

Montgomery *et al.* [63] evaluated motor function pattern of contralateral upper extremity while blinded to the pattern of stimulation. Stimulation frequencies varied regularly from 6 to 256 Hz. DBS at 130 Hz resulted in an improvement in the finger tapping performance, while stimulation with 130 Hz irregular caused a worsening of finger tapping performance. However, DBS at 130 Hz modulate with the rate of 2 Hz produced the greatest worsening of motor performance [63]. Given the state of uncertainty as to the pathophysiological mechanism, the importance for the development of new treatments.

### **(1) Inhibition or excitation**

One of the first controversies is whether high frequency DBS inhibits the stimulated target. Originally, the hypothesis of inhibition was based on the similarity of clinical efficacy with ablation and high frequency DBS. A number of mechanisms have been proposed to explain how DBS can reduce neuronal activity within the stimulated target [64]. These include depolarization blockage, neurotransmitter depletion [65] and stimulation of presynaptic terminals with neurotransmitter release. Anderson *et al.*, [66] demonstrated predominant decreases in ventrolateral thalamus (= ventrolateral thalamic nuclei, VL) activity with globus pallidus internal segment (GPi) stimulation consistent with activation of inhibitory projections from GPi to VL.



In contrast, computation modeling suggests a resolution. McIntyre and Grill demonstrated that stimulation could hyperpolarize the cell body and dendrites yet still excite an action potential at the axon initial segment or proximate inter-nodes [67]. But there is also neurophysiological evidence of such phenomena [68-70]. It is unlikely that direct DBS effects would inhibit axons. Many studies demonstrated increased activity approximately 5-7 ms following the STN DBS pulse in GPi [71, 72], VL thalamus [71] and VL thalamus [73] with GPi stimulation.

In reality, the question of DBS effects is more complicated than simple excitation or inhibition. A number of investigators have demonstrated complex patterns of both inhibition and excitation [72-74]. The question of the origins of these complex responses remains [63].

## **(2) Local *versus* system effects**

The large majority of other laboratories have focused on the DBS effects at the site of stimulation [74-77] or the first order neurons immediately downstream of the stimulated target [66, 72, 73]. Likewise, computational modeling have focused on local effects [67] or effects immediately downstream [78]. The focus on local or immediately downstream structures follows from a conceptualization of the basal ganglia-thalamic-cortical (BG-Th-Ctx) system as a hierarchical and sequential organization of local processors [79]. However, there is empirical evidence that the BG-Th-Ctx system acts more as a parallel and distributing system [80]. Consequently, focus on local *versus* immediate downstream effects of DBS still may be too narrow [61]. As shown in Figure 1-8, some VL neurons demonstrate a remarkable post-inhibitory rebound increased excitability. The immediate effect of the DBS pulse and the late effect of the previous DBS pulse,

could interact and summate producing a resonance effect, which could be one mechanism of DBS therapeutic effects [63].

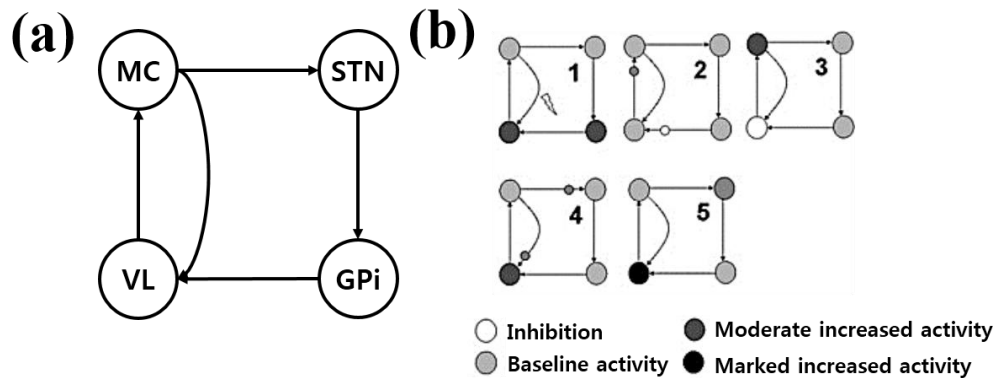


Figure 1-8. VL neurons demonstrate a remarkable post-inhibitory rebound increased excitability. (a) A nested two oscillator systems, (b) A potential mechanism is schematically represented. The first oscillator is the disynaptic feedback loop between MC and VL. The second loop consists of the motor cortex (MC) to STN to GPi to VL and then back to MC. (Step 1) The subsequent activations beginning with the synchronized activation of VL and GPi neurons. (Step 2) The activity in VL is transmitted to MC while activity in GPi is transmitted to VL. (Step 3) This results in excitation of MC and inhibition of VL. (Step 4) MC activity is transmitted back to VL and there is a post-inhibitory rebound increased activity in VL. (Step 5) The excitation from MC in step 4 then combines with the post-inhibitory rebound increased excitability in VL to result in a marked increase in activity shown. Modified from [73].

### 1.2.3 Deep brain stimulation for neuropathic pain

The concept of treating neuropathic pain by brain stimulation is about 50 year-old. There have been several researches since Wall and Sweet tried the temporary abolition of pain in man with brain stimulation in 1967 [19, 31, 81, 82]. It has been suggested that

descending biphasic modulation with high amplitude and frequency on the brain contributes to various cortical functions, including the perception of pain, learning processes associated with the prediction or avoidance of noxious stimuli and influencing on transmission nociceptive information by noxious stimuli to undergo pain [39, 83-85]. Several researches suggest proper stimulation target and optimal neuromodulation parameters [85-87]. Rodent stimulation researches suggested periventricular (PVG) and periaqueductal gray (PAG) regions as DBS target [88], findings translated to humans in the 1970s [89, 90]. Evidence supporting ventral posterior lateral and medial (VPL and VPM) thalamic nuclei and adjacent structures as putative targets for limb and head pain, respectively, to be treated first by intermittent then chronic thalamic DBS [91-93]. Other researchers also targeted the internal capsule and more medial thalamic nuclei [94, 95]. Physiological coherence between PVG and VPL/VPM has also led to implantation of both structures together to synergize analgesia [96].

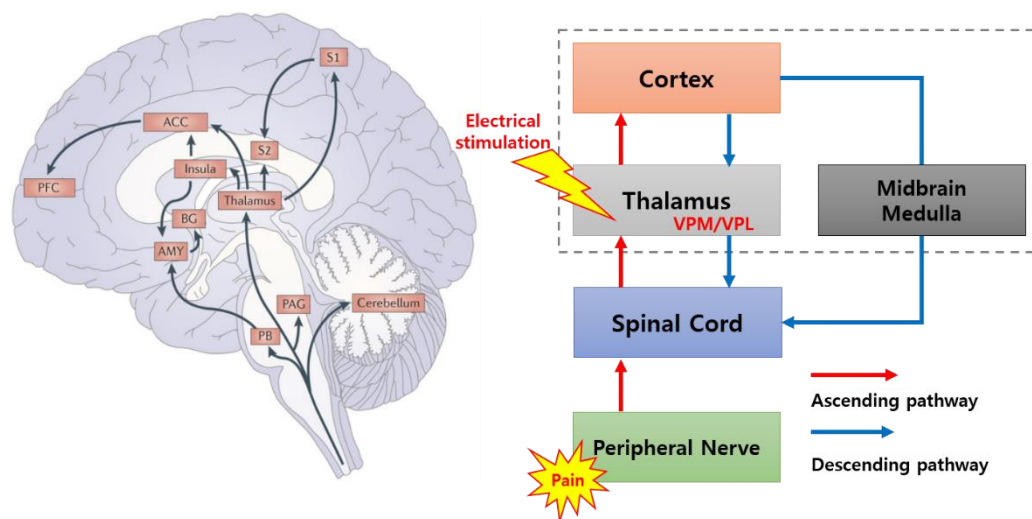


Figure 1-9. Overview of deep brain stimulation for neuropathic pain related to this study. This study is aimed to stimulate and record on VPL for suppressing nociception.

## **1.3 Closed-loop deep brain stimulation system**

Many neurological diseases are associated with clinically detectable and altered brain dynamics. In principle, the aberrant brain activity can be restored through electrical stimulation. In this dissertation, we focused on principles and methods for developing a prototype closed-loop deep brain stimulation system for neuropathic pain, which is one of closed-loop neural prosthetic devices.

### **1.3.1 Current deep brain stimulation system: Open-loop system**

The lack of understanding makes the selection of the stimulation parameters such as voltage, pulse duration, and frequency, which are programmed by a clinician following implantation of the device, quite challenge. Moreover, as aforementioned at section 1.2.2, there are few guidelines available to guide the selection of appropriate stimulus parameters, and programming is largely an ad-hoc process that relies on clinical expertise and does not necessarily result in optimal outcomes. The selection of parameters has important implications for power consumption and thus the battery life of the implanted pulse generator, because current commercial deep brain stimulation systems are open-loop system which derive continuous stimulation pulses with conditioned parameters at once [97].

### **1.3.2 Closed-loop concept for neural prosthetic devices**

#### ***Concept of general closed-loop control***

Closed-loop control concept is based on conventional closed-loop transfer function in control theory that was described in Figure 1-10 (a). The net result of the effects of a closed-loop on the input signal to the circuits enclosed by the loop. The closed-loop transfer function is measured at the output. The output signal waveform can be calculated from the closed-loop transfer function and the input signal waveform. Next signal notated as  $G(s)$  summing up  $H(s)$ , reflects the feedback signal resulting from the previous signal notated as  $G(s)$ . The summation node of Figure 1-10 (a) means that reflection of the

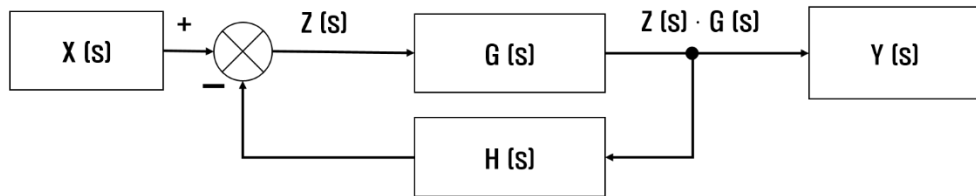
feedback index signal ( $H(s)$ ), which would have the following transfer functions;

$$Y(s) = Z(s)G(s) \rightarrow Z(s) = \frac{Y(s)}{G(s)} \quad (\text{Eq. 1-1})$$

$$X(s) - Y(s)H(s) = Z(s) = \frac{Y(s)}{G(s)} \rightarrow X(s) = \frac{Y(s)}{G(s)} [1 + G(s)H(s)] \quad (\text{Eq. 1-2})$$

$$\frac{Y(s)}{X(s)} = \frac{G(s)}{1 + G(s)H(s)} \quad (\text{Eq. 1-3})$$

(a)



(b)

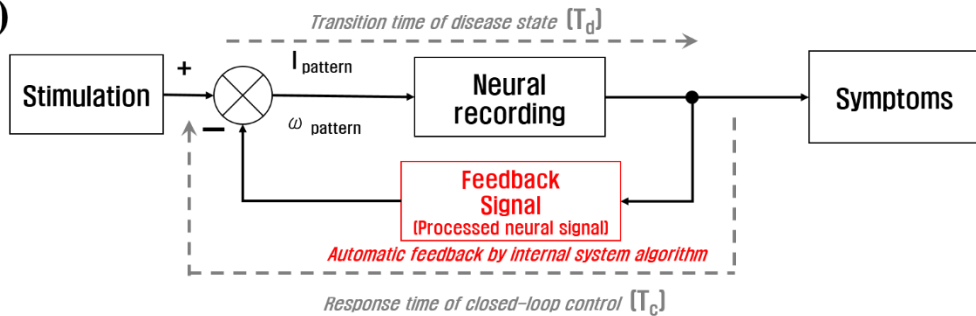


Figure1-10. Schematic diagram of a closed-loop algorithm. (a) General closed-loop concept (closed-loop transfer function for control algorithm).  $Z(s)$  is intermediate signal. (b) Closed-loop diagram for neural prosthetic systems. Recorded and signal processed signals give feedback information for conditioning stimulation parameters.

### ***Closed-loop control for neural prosthetic systems***

For neural prosthetic systems, the closed-loop control can be described as Figure 1-10(b) and is used for purposes as following: (1) To prevent excessively stimulating on central nerve systems which causes the damage of tissues and patient discomforts. (2) To extend the battery lifetime related to the operation period. (3) To derive suitable

stimulation pulse into the target tissues depending on the patient's condition immediately. For this requirement, the closed-loop control response time ( $T_c$  as shown in Figure 1-10 (b)) of the system is also big issue for real-time closed-loop control systems. If the closed-loop control response time ( $T_c$ ) were longer than the transition time of disease state ( $T_d$ ), the closed-loop system could not function in real-time. For practically real-time closed-loop control, the ' $T_c$ ' should be short as possible as or shorter than ' $T_d$ '.

### 1.3.3 Requirements for a closed-loop deep brain stimulation system

#### *Limitation of behavioral tests as an indicator for closed-loop control*

As aforementioned at section 1.3.2, the feedback factor has to include the objective information to acquire high reliability and accuracy. For that, a closed-loop DBS system (CDBS system) for neuropathic pain requires systematic and quantitative methods. Conventional quantitative testing and scoring methods for the neuropathic pain such as visual analogue scale (VAS) and von Frey of Figure 1-11 have been described as providing a convenient, easy, and rapidly administered measurement. However, these methods have several limitations to be directly used as feedback factors for closed-loop system because these methods are based on behavior reactions of test subjects, which are easy for experimenters to become subjective in measurements [98]. Moreover, a test-retest approach was used in most studies to investigate the reliability testing of tools such as measures of internal consistency are prohibited by the single item format.

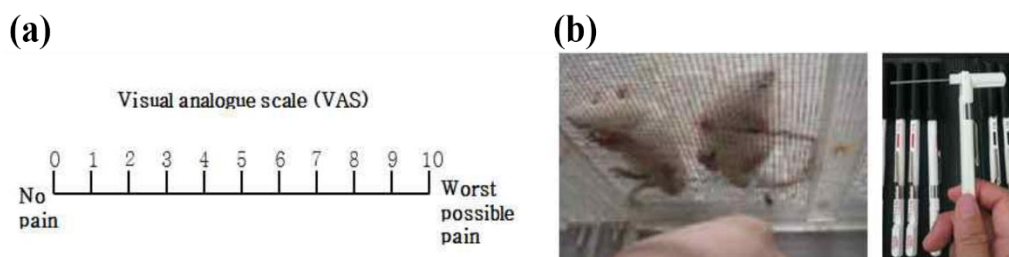


Figure 1-11. Quantitative scoring methods for neuropathic pain. (a) Visual analogue scale (VAS) method[98]. (b) Von Frey test method. wire mesh is the commonly used apparatus to allow their application [99].

### ***Local field potential (LFP)***

We used local field potentials (LFPs) resulting from the superposition of the aggregate activity of a population of neurons around the electrode (i.e., amount of nociceptive information) for source of neural signal index of closed-loop control in this study. It is common belief that the LFP, a population signal obtained from electrophysiological recordings of the brain, should reflect the synchronized spiking activity of neurons near the recording electrode [100]. Indeed, the average postsynaptic effect in the LFP at a given recording site triggered on spikes initiated across a patch of cortex is predictive of the LFP [101]. Distinct spike patterns across neurons and their phase relationship to LFP oscillations encode a substantial amount of surplus of information about the stimulus compared to information contained in the firing rate alone [102]. A previous study has demonstrated that the amplitude of LFPs oscillations (LFP-power) encodes, within certain frequencies, motion direction and speed [103].

LFPs have been suggested an appropriate feedback signal as they can be readily measured using the clinically implanted DBS electrode [104, 105], and there is very high correlation between field potentials and nociceptive information. LFPs contain oscillations with frequencies below 200 Hz that can be recorded from the same electrode as higher frequency spikes fired by single units as well. LFPs are thought to represent synaptic activity within a local network. Further, changes in the LFPs along the BG-Th-Ctx motor loop are correlated with symptoms of neuropathic pain. The nature of the LFP, however, remains ambiguous in important ways, including its spatial resolution, which has always been poorly defined. It is well known that low-frequency electrical signals can be recorded at substantial distances from their point of origin within a filtering medium such as the human body.

### ***Requirements for closed-loop control***

The requirements for a closed-loop deep brain stimulation system are as below. Required elements should be organically connected each other for closed-loop neural prosthetic systems.

- (1) Multichannel electrode for simultaneous stimulation and recording.
- (2) Neural response monitoring for determining the time of stimulating and conditioning stimulation parameters
- (3) Signal processing for identifying an index signal related to the symptoms.
- (4) Closed-loop control logic (algorithm) using the processed signals for adjusting stimulation parameters such as amplitude, duration, and frequency.
- (5) Continuous feedback using the closed-loop control logic.
- (6) The system should operate with short response time ( $T_c$ ) for real-time control.

Currently, there is no commercially available closed-loop systems for neuropathic disorders yet. A repetitive nerve stimulation system for epilepsy (NeuroPace Inc., CA, USA) of Figure 1-12 (a) that is known as the device in advanced clinical stage is also still in the clinical trial. It is seizure-triggered feedback electrical stimulation for effectively suppressing pathological brain activities [106]. Besides, there have been several researched related to closed-loop DBS for various neuropathic disorders as shown in Figure 1-12. Oxford university group has been working on local field potential (LFP)-based closed-loop DBS system for Parkinson's disease (PD) as shown in Figure 1-12 (b). However, it is a just conceptual design for CDBS system because they have been struggling with finding the indicator from recorded LFP related to PD [107]. Michigan university group has been working on CDBS system for PD as well as shown in Figure 1-12 (c) based on their system integration technologies including neural probes and ICs for neural recording and signal processing for many years. Nonetheless, they also have difficulties relating to low reliability due to methods for extracting neural signal



index [108]. On the other hand, Mayo clinic (Minnesota, MN, USA) have been working on developing CDBS systems for depression, obsessive compulsive disorder (OCD), and PD using electrochemical measurement of neurotransmitters relating to neuropathic disorders such as serotonin and dopamine as shown in Figure 1-12 (d). However, the speed of the scanning neurotransmitters is much slower than electrical recording of neural signals, then it is difficult to apply for real-time closed-loop neuromodulation [109]. In addition to this, other many groups have been working on developing CDBS system for epilepsy, OCD, PD, and tremor and the principles of them, yet they are still conceptual designs [110, 111].

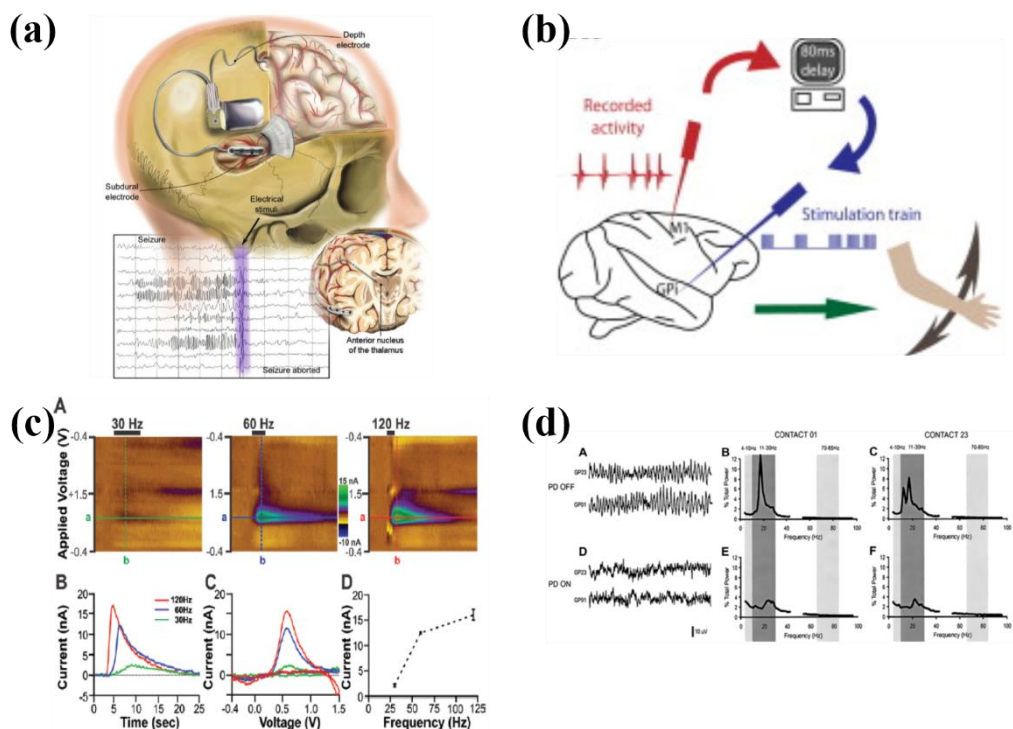


Figure 1-12. CDBS related researches of other groups. (a) Commercial CDBS system of Neuro Pace Inc. (<http://www.medscape.com>), (b) performance measurements of prototype CDBS system for PD of Michigan university [108], (c) conceptual CDBS design for PD of Oxford university [107], and (d) neurotransmitter scanning for neurochemical CDBS system of Mayo clinic [109].

## 1.4 Objectives of this dissertation

In this dissertation, we proposed a nociceptive information (local field potential, LFP)-triggered closed-loop deep brain stimulation system for neuropathic pain control.

### Objectives

- 1) We developed a closed-loop deep brain stimulation (CDBS) system for neuropathic pain control including a multichannel electrode and a closed-loop stimulator.
- 2) We determined effective stimulation parameters and objective neural signal index (indicator) of neuropathic pain for CDBS system control from results of preliminary experiments (behavioral tests and LFP recording). For considering recorded and signal-processed LFP as objectively nociceptive information, a correlation analysis between changes in averaged power spectral density (PSD) of recorded LFPs and changes in scored results of behavioral tests was performed.
- 3) Reflecting results of preliminary experiments and correlation analysis, we developed a closed-loop strategy and applied to a prototype closed-loop deep brain stimulation system. To validate the developed closed-loop DBS system, we applied it to *in vivo* experiments.

## ***2. Materials and Methods***

---

***2.1 Multi-channel deep brain stimulation electrode***

***2.2 Preliminary experiments***

***2.3 Closed-loop deep brain stimulator***

## **2.1 Multichannel deep brain stimulation electrode**

Multichannel electrode is an essential part for CDDBS system. It is required that the CDDBS electrode works for not only neural recording but also for stimulation in a small region of the brain (VPL). We developed a multichannel DBS electrode based on liquid crystal polymer (LCP), which has good mechanical and electrical characteristics with good reliability. We suggested a new design for stimulation in small region of the brain and an enhanced fabrication method. We performed electrochemical and mechanical characteristics measurements of the developed electrode for validation before applying animal experiments.

### **2.1.1 Liquid crystal polymer (LCP)**

We developed the DBS electrode using a polymer called liquid crystal polymer (LCP). The fabrication process was based on previous studies [1, 2, 8, 112]. We used LCP for both substrate and insulation materials in this study. LCP has lower moisture absorption rate that is essentially related to the durability than conventional polymers such as polyimide and parylene-C [113-115]. As shown in Figure 2-1, LCP is built up of rigid and flexible monomers that are linked to each other, and hence they can organize in aligned molecule chains with a crystal-like spatial regularity. The main properties of LCP are high mechanical strength at high temperatures, extreme chemical resistance, and low moisture permeability, and good barrier properties for other gases [115-117]. Some information of polymers used for neural implants was shown in Table 2-1. LCP has been used as a high-performance thermoplastic material for high-density printed circuit board fabrication and semiconductor packaging. Today, many different types of LCPs are available, including LCPs which are specially designed for use in medical engineering (FDA approved, USP class VI) [115, 118]. The previous study also described that LCP has high biocompatibility *in vitro* [119]. Moreover, the LCP used in this study is a film-type with predefined thickness from 25  $\mu\text{m}$  to 3 mm to be handled easily [115]. These

LCP films are melt-processible and can be structured by laser machining and reactive ion etching [1, 2, 8, 114, 115, 117].

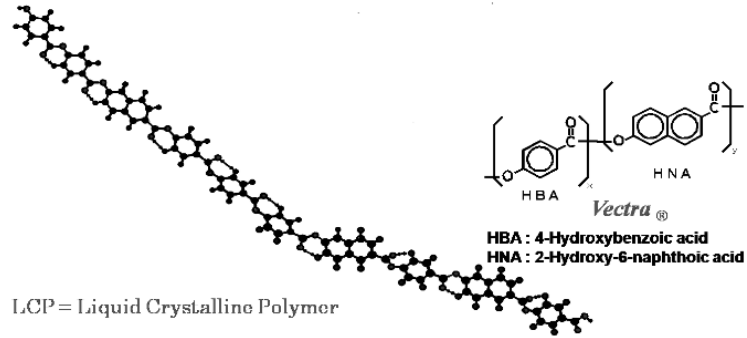


Figure 2-1. Chemical structure of liquid crystal polymer [120]. LCP is built up of rigid and flexible monomers that are linked to each other.

Table 2-1. List of the properties of polymers used for implantable devices

Properties of polymers	Polyimide	Parylene-C <sup>b</sup>	PDMS <sup>c</sup>	SU-8 <sup>d</sup>	LCP <sup>e</sup>
Possible of thickness [μm]	1-15	1-100	10-100	1-300	25-3000
Density [g/cm <sup>3</sup> ]	1.10-1.11	1.29	1.08	1.08-1.24	1.4
Moisture absorption [%]	0.8-1.4	0.06	< 1	0.55-0.65	0.03
Melting temperature [°C]	-	290	-	-	280
Thermal decomposition temperature [°C]	> 550	-	~250	300-315	-
Glass transition temperature [°C]	-	-	-	200-215	-
Thermal conductivity [W/cm K]	0.29	8.2	15-25	0.002-0.003	-
Thermal coefficient of expansion [ppm/K]	12	35	-	52	4-38
Specific resistivity [Ω cm]	> 10 <sup>16</sup>	> 10 <sup>15</sup>	10 <sup>15</sup>	7.8×10 <sup>14</sup>	1.3×10 <sup>13</sup>
Disruptive strength [V/cm]	1.5×10 <sup>5</sup>	2.6-10 <sup>6</sup>	2000	> 4×10 <sup>5</sup>	4.7×10 <sup>6</sup>
Dielectric coefficient [ε <sub>r</sub> ]	3.5 (@ 1kHz)	3.1 (@ 1kHz)	2.6 (@ 50 Hz)	3.2 (@ 50 Hz)	3 (@ 1 MHz)
Tensile strength [MPa]	392	69	6.2	60	182
Tensile module [MPa]	8830	20	0.1-0.5	20	10,600
Elongation [%]	30	200	600	4.8-6.5	3.4
USP class	-	VI	VI	-	VI

\* This table was reposted and modified from the reference [115]. <sup>a</sup>UBE U-Varnish-S [121], <sup>b</sup>PCS Parylene C [122], <sup>c</sup>NuSil MED-1000 [123], <sup>d</sup>MicroChem SU-8 2000 & 3000 Series [124], <sup>e</sup>Vectra MT1300 [125].

### 2.1.2 Electrode design

There were some requirements for a CDBS electrode. First, the simultaneous stimulation and neural recording should be available in a small region of the brain (VPL). Second, although the electrode contact has small geometric surface area (GSA), it requires small impedance, high injection limit, and large storage capacitance for signal to noise ratio and derivable current range, respectively [126]. Finally, the electrode structure should reflect the fabrication process. Whole process for the electrode design was described as Figure 2-2.

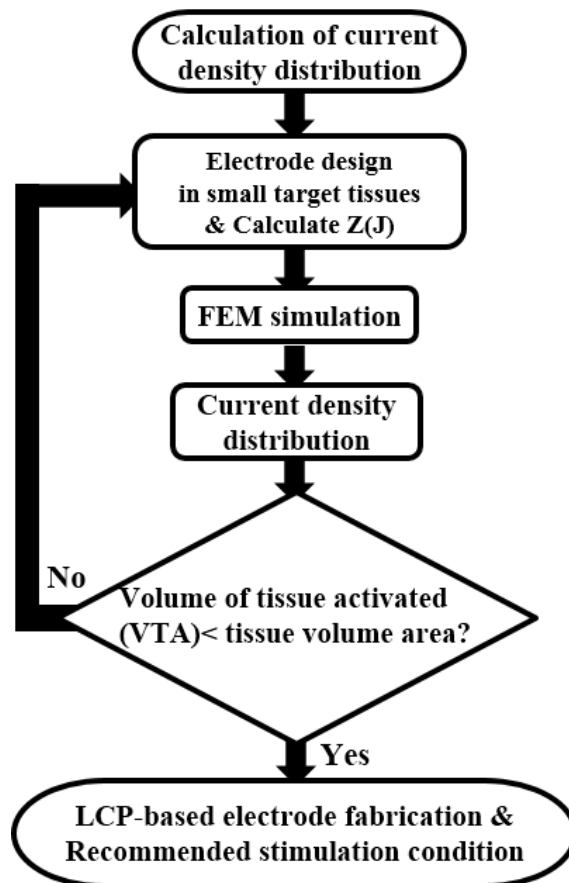


Figure 2-2. Electrode design process. Calculating the charge density distribution, we could estimate the volume of tissue activated. This volume should be smaller than that of a target region (VPL which has the volume of about  $0.196 \mu\text{m}^3$ ) in the rodent brain.

We designed all four contacts of the electrode to be all inserted into VPL region of a rodent brain. The precise dimension, of course, should be modified reflecting results of volume of tissue activated (VTA) simulation of section 2.1.3. Moreover, we also designed the electrode for both monopolar and bipolar recording. The monopolar configuration needs a global reference contact that has large size for referencing the potential. For this reason, we designed a reference contact that has large GSA of about  $7.8 \text{ mm}^2$  as shown in Figure 2-3 (a). The electrode design also reflected the fabrication process, especially the mask design for lithography process and multiple-layer alignment. First, we designed the electrode as the thickness of  $200 \sim 300 \mu\text{m}$  because the thickness over  $200 \mu\text{m}$  had the sufficient strain to be straightly inserted in the brain without buckling in previous study [1]. Second, each layers had nonmultiplying metal patterns such as lead lines and contacts as shown in Figure 2-3 (b) for preventing short and signal coupling. With an improved LCP process for multiple LCP layers of section 2.1.5, we could assign two or three lines on each LCP layers, and the margin for final laser cutting process was guaranteed upto  $50 \mu\text{m}$ . In general, the margin for final laser cutting process is empirically required upto  $100 \mu\text{m}$  from side to side using the conventional LCP process. It was also available to prevent overlapping and shorting between metal lead lines during thermal press bonding process by the new method. Although signal interference between each layers would be smaller because the dielectric coefficient of LCP is much small as shown in Table 2-1, this kind of metal-line arrangement could additionally decrease signal coupling between metals. Finally, the probe design reflected electroplating process including via process and IrOx process. After via drilling and top metal deposition, we electroplated Au to connecting between the bottom metal pattern and largely deposited contact pattern on the top cover layer using a common pad of Figure 2-3 (b) and 2-4. In addition, we electroplated IrOx right after Au electroplating because the electroplating process was not available after connecting the electrode to an interface board using DC block capacitors. Reflecting these factors, we designed lithography masks for electrode fabrication as Figure 2-4.

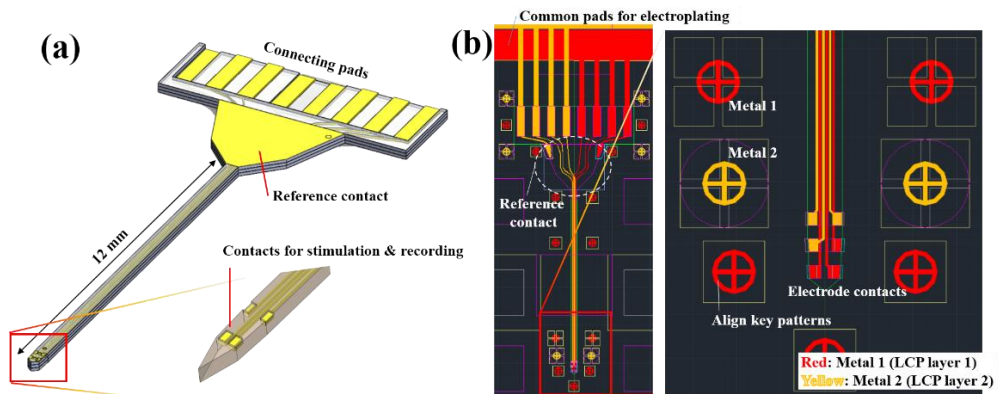


Figure 2-3. Designed multichannel DBS electrode. (a) Overview of the designed multichannel DBS electrode. We designed a reference contact for monopolar recording configuration. (b) Mask design for lithography process. Nonmultiplying lead-line and contact placements allowed to guarantee high yield and the improved margin during thermal press bonding process and final laser cutting step.

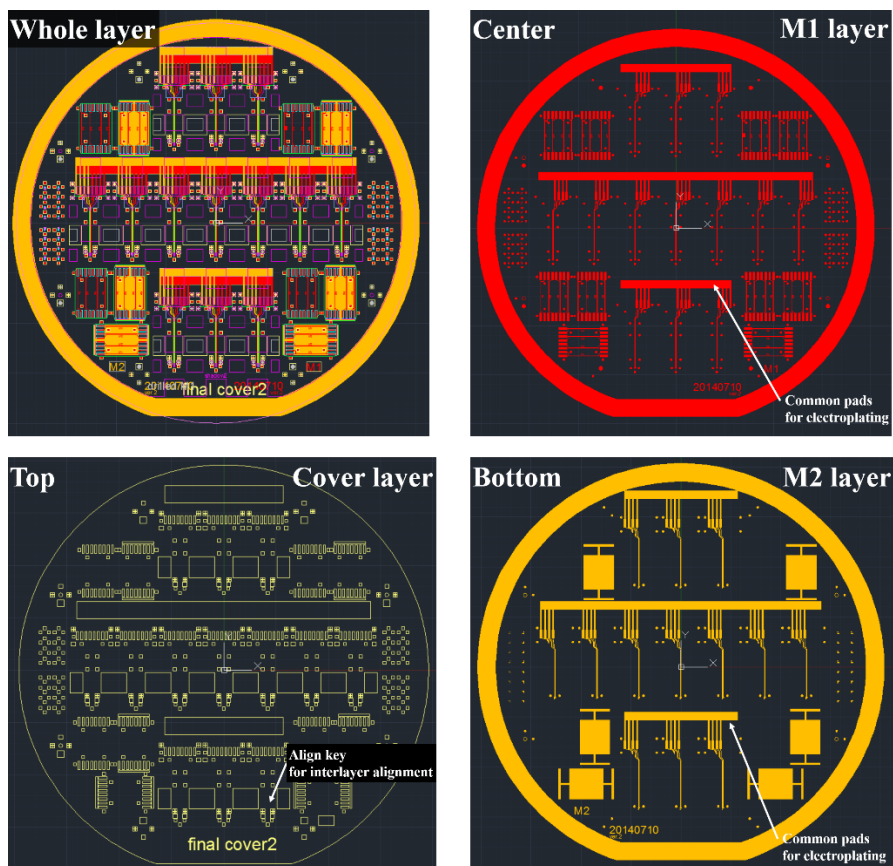


Figure 2-4. Mask designs for lithography.



### 2.1.3 Volume of tissue activated (VTA) simulation

Several research groups including McIntyre *et al.* [63, 67] have demonstrated the importance of the consideration about electrode structures. Then they have suggested that customizing DBS electrodes for different anatomical targets and/or disease states should start from the characterization of the electric field and volume of tissue activated (VTA) by stimulation. The contact geometry, the distribution of cathode(s) and anode(s), and biophysical properties of the tissue should be considered for the VTA-considered structure. With this claim, McIntyre *et al.* [63, 67] have suggested methods for calculating and simulating the VTA dependency of the electrode contact structures. These methods are based on the converging theoretical results and experimental results. The VTA of DBS electrode was simulated and was designed to build VTA within the rodent VPL region applying the formula (Eq. 2-1) and using software for finite element methods (Comsol, version 4.3b, Comsol Multiphysics, Inc., MA, USA). The model boundary was determined by a 100 x 100 x 100 mm<sup>3</sup> cube that surrounded the electrode encapsulated with a homogenous isotropic tissue conductivity of 0.96 S/m [127]. The boundary was set to 0 V, and the electrode contact set to the port of current injection (Amplitude = 700  $\mu$ A, duration = 60  $\mu$ sec, frequency = 130Hz).

$$\text{Volume of Tissue Activated} = \frac{\Delta^2 V_e}{\Delta x^2} \quad (\text{Eq. 2-1})$$

where,

$x$ : distance from the electrode

$V_e$ : potential distribution

We designed four or more contacts to be inserted into VPL region at once. The dimension of an electrode was temporarily determined as Figure 2-5 (a). Considering the IrOx-based electrode contacts that have lower impedance and larger charge storage capacitance comparing to other metal-based ones, we designed the size of the electrode

contact. Validating the characteristics of designed electrode, we simulated VTA of a temporary design of LCP electrode and a commercial electrode (TM33CINS, World Precision Instrument, Inc., FL, USA) to compare as Figure 2-5. Used parameters were listed in Tables 2-2.

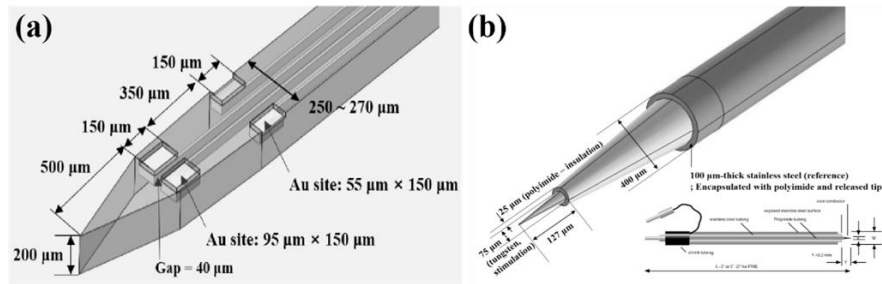


Figure 2-5. Electrode structure for FEM simulation: (a) structure of a LCP-based electrode. The size of the contact is designed with IrOx . (b) Structure of a tungsten-based commercial electrode (TM33CINS, World Precision Instrument, Inc.)

Table 2-2. FEM simulation parameters

Simulation Parameters		Value	
Electrical Conductivity [S/m]	Tissue		0.96
	LCP electrode	LCP	$10^{-17}$
		Au	$4.5 \times 10^7$
	Commercial electrode*	W	$1.8 \times 10^7$
		Stainless	$4.0 \times 10^6$
		Polyimide	$10^{-12}$
Relative Permittivity	Tissue		49.5
	LCP electrode	LCP	1
		Au	5.6
	Commercial electrode*	W	1
		Stainless	1
		Polyimide	3.4
Amplitude of stimulation current [ $\mu$ A]		700	

\* TM33CINS of World Precision Instruments, Inc.

### 2.1.4 Surgical process design: Electrode implantation

The DBS electrode should be long-term implantable, more than 5 weeks (the preliminary experiments of this study had been performed for even 8 weeks). We designed a surgical procedure for the LCP-based multichannel electrode for precise implantation. Moreover, we also needed a strong fixation method to fix the electrode on a rodent skull of electrode because we performed behavioral tests under unanesthetized condition. Additionally, the surgical procedure and newly developed surgical tools should be compatible to commercial stereotaxic tools.

We designed the electrode implantation procedure as shown in Figure 2-4 (a). First, we drilled a hole called ‘burr hole’ on the top of VPL region of the skull (AP: -2.2 mm, ML: 2.8 mm from the bregma). Second, we inserted the electrode into the VPL region (DV: -6.0 mm from the skull) in holding the electrode on the stereotaxic electrode holder (Figure 2-6 (b)). Third, we fixed the electrode with a bioglue and dental cement. Finally, we bent the electrode and fixed the interface board on the skull using stainless steel screws and bioglue [128]. The electrode holder was designed as shown in Figure 2-6 (b). It was compatible to a commercial stereotaxic frame and a small groove on the clip of the holder allowed the electrode to be straightly held.

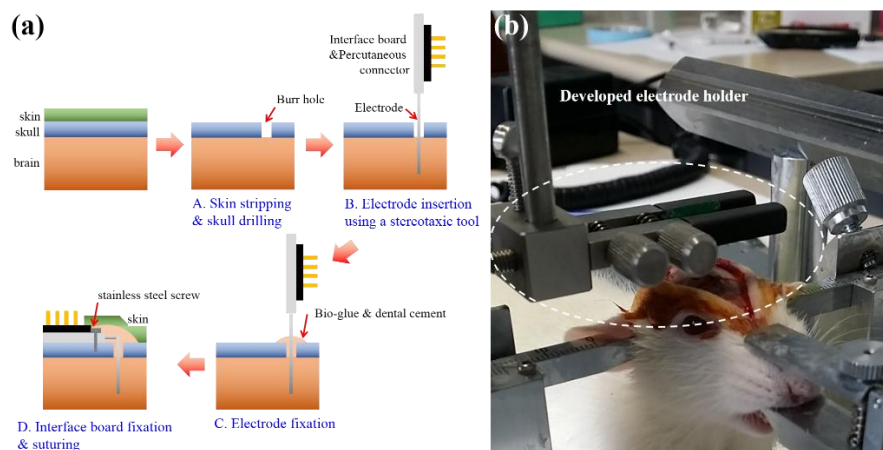


Figure 2-6. Designed surgical procedure and surgical tools for electrode implantation. (a) Developed surgical procedure. (b) Custom designed electrode holder is compatible to a commercial stereotaxic frame (SR-6R, Narishige, Tokyo, Japan).

## 2.1.5 Fabrication process

### (1) LCP-based electrode fabrication process

We fabricated the designed electrode using an improved LCP process based on the conventional LCP process of previous studies as shown in Figure 2-7 [1-3].

- (i) LCP-substrate was fixed on a handle silicon wafer using silicone elastomer (MED-6233, NUSIL, Carpinteria, CA, USA). The attached LCP sample was slightly treated in the oxygen plasma condition ( $O_2$  100 sccm, 0.1 mTorr, 4 min.) for enhancing adhesion between LCPs and metal layer.
- (ii) Seed metal layers (Ti : Au = 1000 Å : 3000 Å) were deposited using E-beam evaporator (ZZS550-2/D, Maestech, Seoul, Korea).
- (iii) The negative MEA metal pattern of photoresist (PR) were composited using PR (AZ4620, Clariant, NJ, USA) with spin-coated HMDS.
- (iv) The *i*-line lithography (MA6/BA6, SUSS MicroTec, Garching, Germany).
- (v) We deposited the gold layer up to 10 μm using electroplating process.
- (vi) After PR strip process, (vii) the seed layers were wet-etched using diluted aqua regia solution (DIW : HCl : HNO<sub>3</sub> = 5 : 3 : 1) and diluted hydrofluoric acid solution (DIW : HF = 10:1).
- (vii) The LCP substrate was detached at an acetone solution.
- (viii) The LCP-DBS electrode was monoencapsulated with another LCP cover layer (100 μm in thickness) which has laser-opened site holes by a thermal press bonding process (lamination) at a temperature of 285 °C and pressure of 2.1 MPa. The monolithic structure of LCP encapsulation blocks the penetration ions and moisture through the LCP seals. After cover LCP layer lamination process, laser drilling for electrode contacts and laser thinning for reference electrode were performed using UV laser machine (Samurai UV Laser marking system, DPSS Laser Inc., CA, USA) as previous study [129]. It was too stiff and thick to be bent without thinning process. The established recipes of laser process are described in Table 2-3. The thinning

of LCP was implemented using laser patterns of several straight line. The gap between each line has to be smaller than 25  $\mu\text{m}$  because the spot size of the UV laser beam is larger than 50  $\mu\text{m}$ .

- (ix) After laser micromachining process, additional metal layer was deposited with screening using a shadow mask for implementing larger electrode sites than pre-patterned at the process (iv)~(ix).
- (x) After 2nd metal deposition, additional electroplating was performed to deposit the via metal over of 25  $\mu\text{m}$ . With this step, the large contact pattern was contacted to the small patterns on the LCP substrates. Finally, the fabricated electrodes were cut using laser-micromachining process.

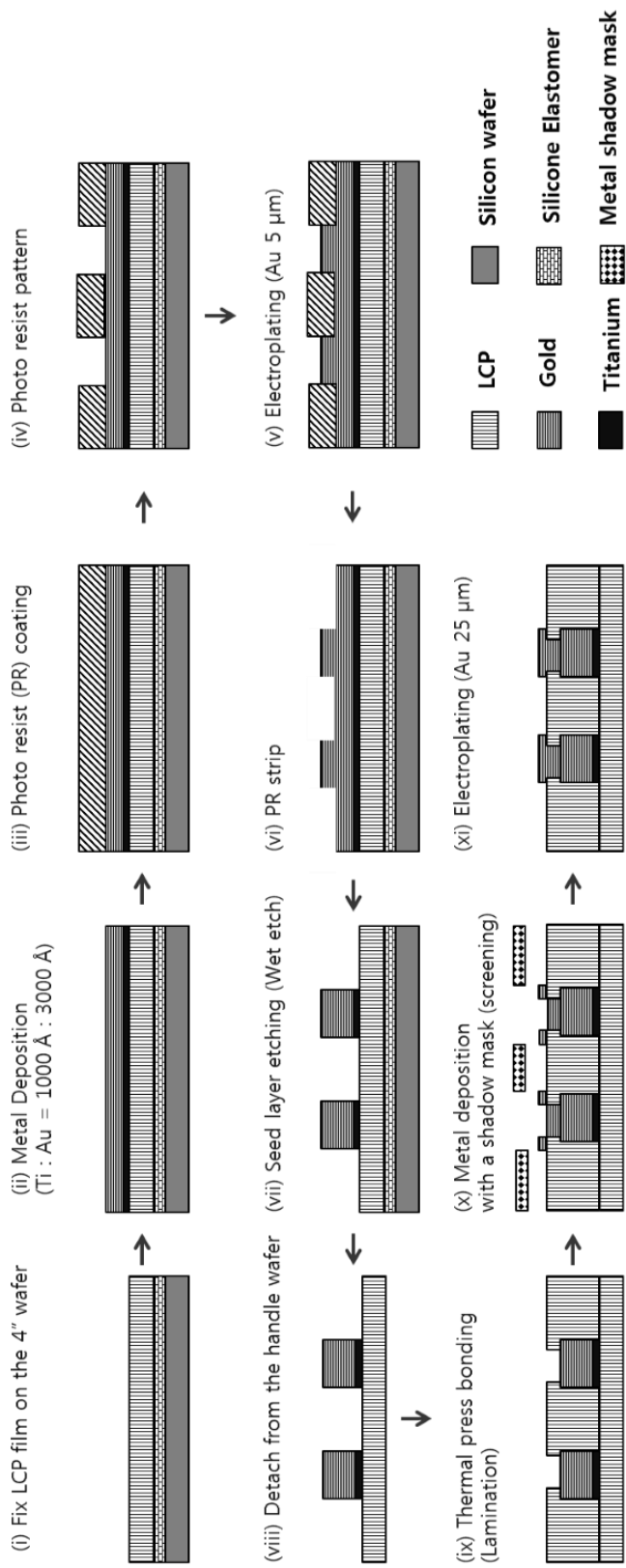
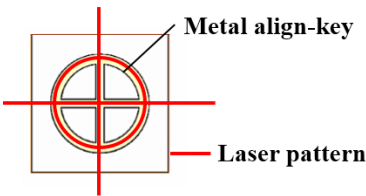
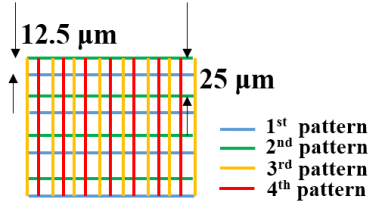


Figure 2-7. LCP-based electrode fabrication process of previous studies [1-3]. LCP process includes semiconductor process (i ~ iv, vi ~ viii), thermal press bonding process (ix), electroplating process (v, xii) and laser micromachining process (xi).

Table 2-3. Recipes for laser process

Process and fabrication recipe	Pattern design
<p><b>Guide beam</b></p> <p><b>Power</b> Unnecessary</p> <p><b>Mark speed</b> 500 mm/sec</p> <p><b>Frequency</b> 5 kHz</p> <p><b>Pulse width</b> 100 <math>\mu</math>sec</p>	 <p>Metal align-key</p> <p>Laser pattern</p>
<p><b>Thinning &amp; Ablation</b></p> <p><b>Power</b> 80 %</p> <p><b>Mark speed</b> 200 mm/sec</p> <p><b>Frequency</b> 10 kHz</p> <p><b>Pulse width</b> 10 <math>\mu</math>sec</p>	 <p>12.5 <math>\mu</math>m</p> <p>25 <math>\mu</math>m</p> <p>— 1<sup>st</sup> pattern</p> <p>— 2<sup>nd</sup> pattern</p> <p>— 3<sup>rd</sup> pattern</p> <p>— 4<sup>th</sup> pattern</p>
<p><b>Final cutting</b></p> <p><b>Power</b> 80 %</p> <p><b>Mark speed</b> 100 mm/sec</p> <p><b>Frequency</b> 20 kHz</p> <p><b>Pulse width</b> 20 <math>\mu</math>sec</p>	<p>Electrode figure</p>

\* The whole recipe is for Samurai UV Laser Marking system (DPSS Laser Inc, USA)

## (2) Multi-layer arrangement method and alignment method

While the LCP process of previous studies used a LCP substrate for multichannel, this study suggests modified arrangement and alignment methods based on multilayered LCP process for integrating multichannel on a narrow and small shaft of the electrode.

### *Modified metal pattern arrangement method*

This method is a feedback into the electrode design step of section 2.1.2. Integrating many channels on small region, the width of the line and the gap between each lines should decreased. However, the narrower gap brings the larger interference of signal transmission due to the coupling capacitance and the more overlapping during thermal press bonding process of fabrication. Minimizing the interference between each lead lines and preventing the overlapping as shown in Figure 2-8 (a), small patterns were patterned on the substrate LCP layers for contacts and larger metal patterns of contacts was added on the insulation LCP layer using metal deposition with a shadow mask and electroplating process. It is because the metal pattern for contact is the largest pattern in the metal layer which limits the number of integrated lead lines on a narrow electrode shaft as shown in Figure 2-8 (b) [1-3]. As our group have suggested, the laser ablation process helped this new integration process. Small via could be formed using the laser drilling process which is a kind of laser ablation [129].

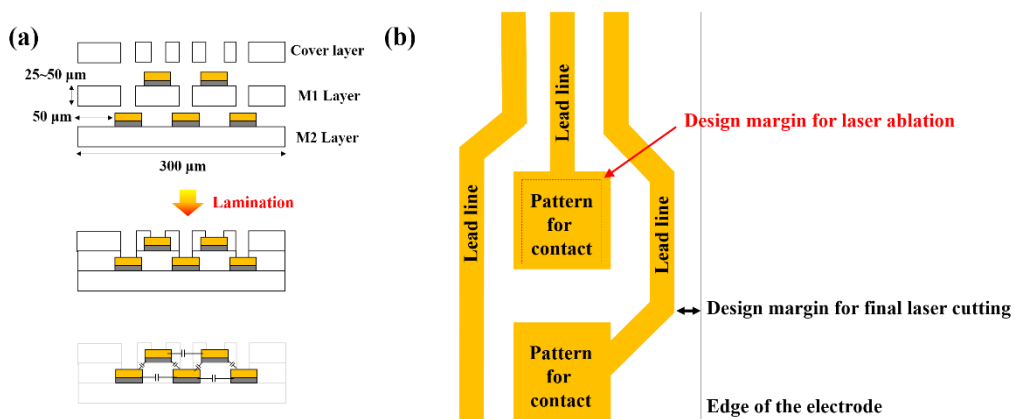


Figure 2-8. Modified method for fabrication. (a) Modified metal-line arrangement method. (b) Design margin for laser ablation and final laser cutting.



### ***Interlayer alignment method for multiple LCP layers***

We suggested an interlayer alignment method for multiple LCP layers. It is an improved method from previous studies which used four stainless steel pins of 1 mm in diameter on the jig for thermal press bonding and laser micromachining process [1-3, 114]. The margin of alignment with the previous method was upto 500  $\mu\text{m}$ . It was the critical reason of low yield during thermal press bonding and final laser cutting process as shown in Figure 2-9. These problems cause low yield. Although the laser drilling and ablation method [129] partially improved the yield, the yield of depth-type electrodes was still low due to its difficulties of alignment. It is caused by the expansion of LCP during thermal-related steps such as laser marking (drilling), metal deposition, soft bake for lithography, laser cutting, and thermal press bonding process or handling by body temperature. A new alignment method is similar to multiple mask alignment process for photography of silicon process (Figure 2-9). Two metal patterned layers and one insulation layer composite one side of the electrode. Each layers was physically aligned with pins on a press jig. During the layer alignment, align keys of A ~ D of Figure 2-9 (b) are additionally used for precise alignment in observing the whole process with a microscope. After alignment, each point was fixed with adhesive (polyimide tape). Align-keys were also used for laser ablation for contact opening and final cutting process using laser micromachining. After laser ablation and final laser cutting process, the  $\text{O}_2$  plasma cleaning was performed for ashing of burnt residues. For the CDBS electrode fabrication, both the new method and the previous physical pin alignment method were applied. This method could be applied for not only three and more LCP layers but also double-faced electrode fabrication that needs over twice number of layers as one-side electrode. Requirement for precise alignment of multiple layers is just multiple alignment keys that are crossing each other.

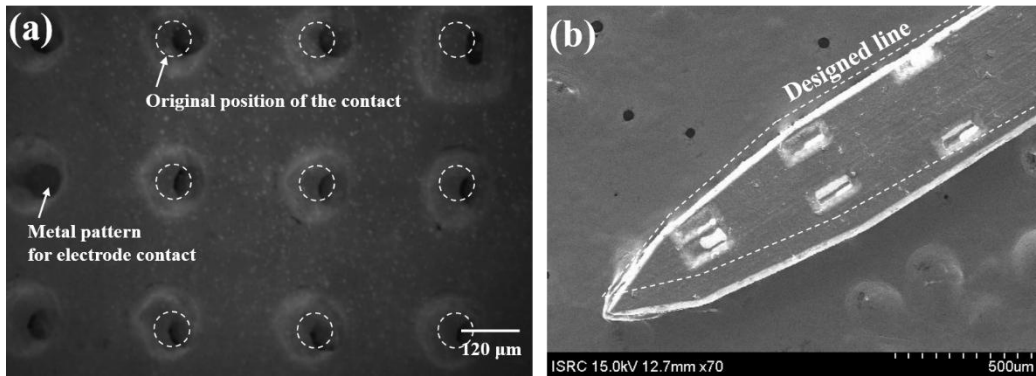


Figure 2-9. Misalignment problems with the previous method [1-3]. These problems cause low yield. Although the laser drilling and ablation method [129] were applied, the yield was still low due to its difficulties of alignment. (a) Misalignment between electrode contacts and opened cover LCP layer before and during the thermal press bonding process. (b) Failure by misalignment during the final laser cutting process.

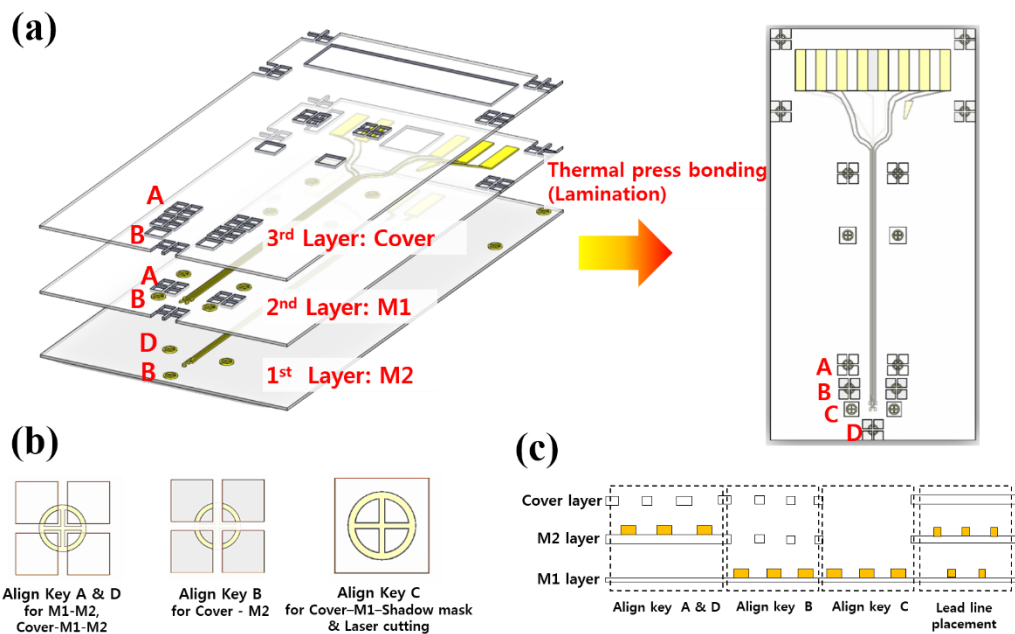


Figure 2-10. Improved interlayer alignment method. (a) Overview of the whole alignment method. (b) Top view of align keys for new method and (c) cross sectional view. During the layer alignment, align-keys of A ~ D are additionally used.

### **(3) Iridium oxide electroplating process**

As aforementioned in section 2.1.2, the iridium oxide (IrOx) electroplating process should be performed before connecting the fabricated LCP electrode to interface PCB board using DC block capacitors. It is because the triangle wave and square pulse wave, which are induced into the electrode for IrOx electroplating, cannot be DC block capacitor of 0.1 ~ 1  $\mu$ F. The electrode contacts were 75  $\mu$ m x 75  $\mu$ m gold sites.

After the end of the fab process, The IrOx contacts were electroplated using an anodic electrochemical process with three-electrode configuration. For electroplating IrOx, the common pads for electroplating were used as shown in Figure 2-3(b) and 2-4. The electroplating process was performed using a potentiostat (Solartron 1260/1287, AMEMTEK, UK) at room temperature with a stabilized 4 mM IrCl<sub>4</sub> solution. This solution was supported electrolyte of 40 mM oxalic acid and 340 mM K<sub>2</sub>CO<sub>3</sub>, similar method reported by Yamanaka [130]. A powder formed Iridium oxide hydrate was dissolved in deionized water, and 40 mM oxalic acid was added to form a stable complex of iridium oxide. Then by gradual addition of 340 mM K<sub>2</sub>CO<sub>3</sub>, the pH of the solution was set to '10.3'. After 7 days of stabilization period, electroplating was conducted. The whole process of solution preparation was summarized in Figure 2-8. After sequential electrochemical processes composed by cyclic voltammetry (CV) scanning with a triangular waveform and a rectangular potential pulses was used in this study. The scanning rate of triangular waveform repeated 50 cycles was 50 mV/s from 0.0 V to 0.55 V versus Ag|AgCl. Followed 2000 of rectangular potential pulses with 1 Hz frequency and 0.5 sec duration, had same potential limits to the triangular waveform.

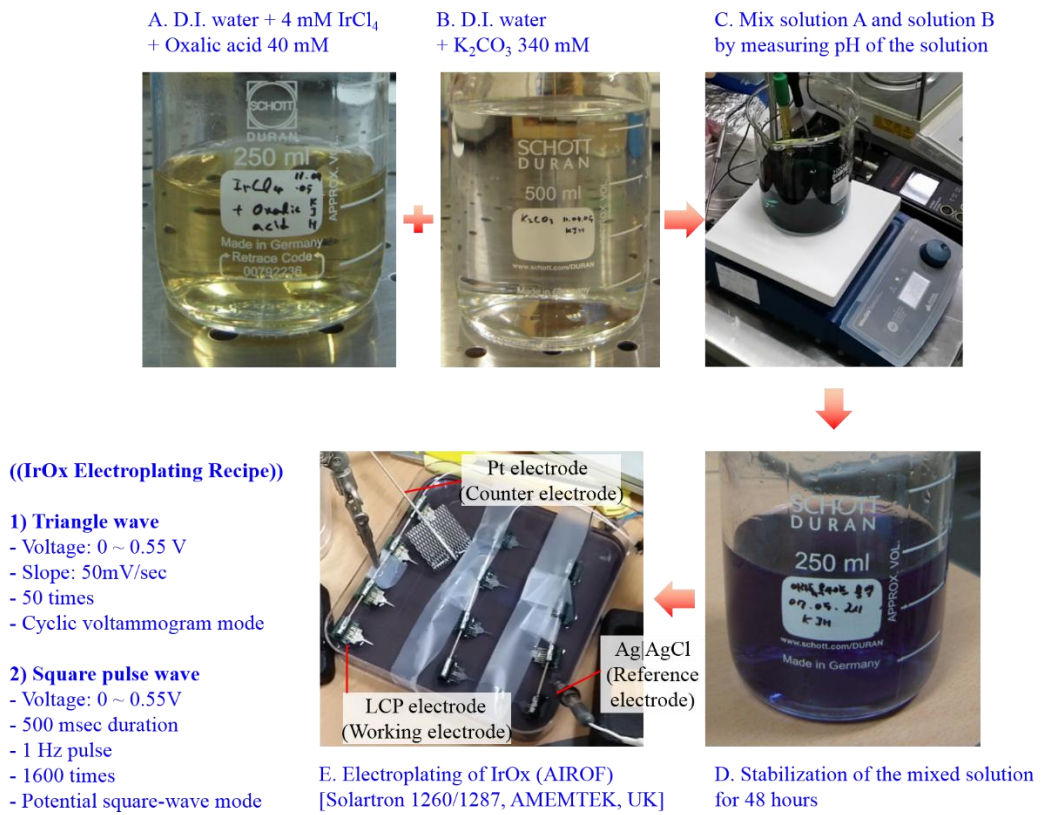


Figure 2-11. Iridium oxide (IrOx) electroplating process. After IrOx solution preparation (A~D), the electrode was electroplated using 3-electrode composition by a potentiostat (Solartron 1260/1287, AMEMTEK, UK).

### **2.1.6 Characteristics measurements**

We performed electrochemical and mechanical characteristic measurements for fabricated electrode before applying *in vivo* experiments.

#### **(1) Electrical characteristics measurement**

We performed electrochemical impedance spectroscopy (EIS), cyclic voltammetry (CV) for calculating charge storage capacitance, and observation of the derived biphasic pulse for calculating charge injection limit. Whole measurements were performed in a phosphate-buffered saline solution (PBS solution, Gibco #10010, Invitrogen Life Technologies, NY, USA) using an impedance analyzer (Solartron 1260/1287, AMETEK, UK) in three electrode arrangement with a Ag/AgCl reference electrode (K0260, AT Frontier, Inc., Kyeonggi-do, Korea) and Pt counter electrode (RDE0021, AT Frontier). The root-mean-square magnitude of the excitation voltage input was 5 mV and the impedance was measured over a broad frequency range from 1 Hz to 100 kHz.

#### **(2) Mechanical characteristics measurement**

We performed buckling tests [131-133] for measuring mechanical characteristics. The test examined the stiffness of the probes using a single-axis oil hydraulic micromanipulator with a motor drive (MO-81, Narishige, Tokyo, Japan) attached with a force/torque sensor (Nano17, Pinnacle Park Apex, NC, USA) (Figure 2-12). The probe was fixed at the sensor assembly unit and the probe shank was pinned vertically to the acrylic plate at the bottom (after placing the LCP neural probe on the surface, the stress (force) loaded on a probe was monitored while the probe was advanced downwards at a speed of 100  $\mu\text{m/s}$ ). From this test, we obtained the elastic modulus. Using Euler's buckling load formula (Eq. 2-2 and Eq. 2-3) and the required insertion force from the literature [134], the maximum length of the probe (L) could be calculated, if a threshold value of the buckling force ( $P_{cr}$ ) was given [132, 135]. (This work was performed an

extended study of the author's thesis for M.S. degree. We examined additional four samples of each electrodes after the previous work for reliable data)

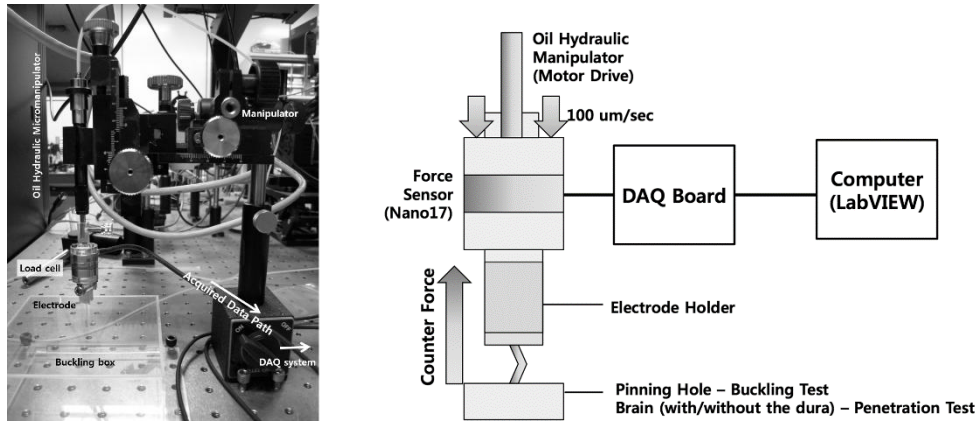


Figure 2-12. Setup for the buckling tests and an *in vivo* insertion tests. An acrylic customized electrode holder was fixed to the force sensor, which was held onto the oil hydraulic micromanipulator with the pulse motor drive. The measured counter force was acquired by the DAQ board and transferred to the computer [1].

$$P_{cr} = \frac{K \pi^2 E I}{L^2} \quad (\text{Eq. 2-2})$$

$$I = \frac{1}{12} w h^3 \quad (\text{Eq. 2-3})$$

where,

- $P_{cr}$  buckling force threshold
- $K$  column effective length factor (one-pinned/one fixed end) = 2.045
- $E$  elastic modulus
- $I$  area moment of inertia
- $L$  unsupported column length or maximum probe length
- $w$  column width
- $h$  column thickness
- $K/L^2$  effective length of the column

## 2.2 Preliminary experiments

We performed behavioral tests (von Frey test and duration measurement) and neural signal recording experiments using tibial and sural nerve transection (TST) model SD-rats depending. It was for characterizing and identifying neural signal index (indicator) and effective stimulation parameters as shown in Figure 2-13.

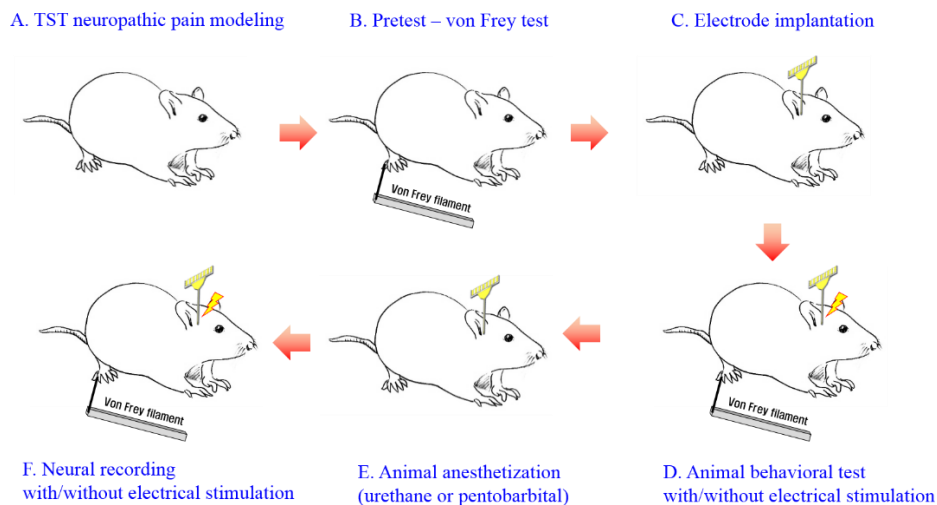


Figure 2-13. Process of preliminary experiments for characterizing responses to neuropathic pain. We performed behavioral tests (von Frey test and latency measurement) and neural signal recording experiments using tibial and sural nerve transection (TST) model SD-rats with or without DBS.

### 2.2.1 TST neuropathic pain modeling [136, 137]

This study was conducted according to the guidelines of the Ethical Committee of International Association for the Study of Pain [138] and the Institution Animal Care and Use Committee of Seoul National University, Yonsei University, and Hallym University. Male Sprague-Dawley rats, weighing 180 ~ 200 g, were used. They were housed in groups of three per cage, with food and water available ad libitum under a light-dark cycle of 12 hour-12 hour. All experiments were performed during the light phase. Animals were allowed to acclimate at least for a week before surgery and behavioral testing.

The rats were anesthetized with phentobarbital sodium solution (50 mg/kg). Atropine (1 mg/kg) was used to reduce airway secretion. Then a segment of the left sciatic nerve was exposed between the mid-thigh levels. Surrounding tissues were carefully removed. Under a surgical microscope (Olympus, Tokyo, Japan), the three major division of the sciatic nerve (tibial, sural and common peroneal nerves) were clearly separated. To generate an efficient neuropathic pain model, the tibial and sural nerves were completely ligated and tightly transected as shown in Figure 2-14. The peroneal nerve was left intact. Hemostasis was completed and the cut was closed with muscle and skin sutures [137].



Figure 2-14. Tibial and sural nerve transection (TST) modeling method. The tibial and sural nerves were completely ligated and tightly transected.

### 2.2.2 Electrode implantation

For the first trial, a tungsten electrodes (200  $\mu\text{m}$  in diameter) insulated with 5  $\mu\text{m}$  of parylene-C were used. For the second trial was performed with a LCP-based DBS electrode. The procedure of electrode implantation for both electrodes was the same as the designed surgical procedure of section 2.1.4. The rats were anesthetized with phentobarbital sodium solution (50 mg/kg). Atropine (1 mg/kg) was used to reduce airway secretion. The electrodes were inserted into the VPL (AP: -2.2 mm, ML: 2.8 mm, DV: -6.5 mm from bregma). The electrodes were firmly secured on skull with glue [128]. Then, the electrode was bent and fixed on the rodent skull. Remaining the connector on the interface board, the skin of the rat was sutured.



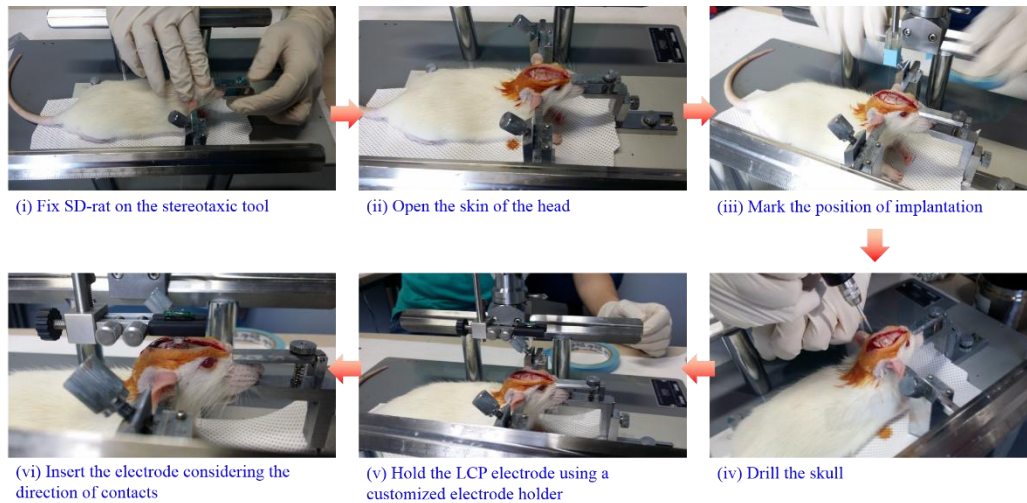


Figure 2-15. Procedure of electrode implantation. This procedure was based on the designed surgical procedure in section 2.1.4.

### 2.2.3 Deep brain stimulation (DBS)

We used a custom designed stimulator for preliminary experiments, which had the same structure as the following CDBS system using a custom designed current stimulation chip (IDEC 80<sup>th</sup> 0.35- $\mu$ m MPW process, Samsung semiconductor) and a microcontroller (Atmega 128, ATMEL, TX, USA). The stimulator could derive stimulation pulses with various stimulation conditions such as amplitude, duration, and frequency to determine the effective stimulation parameters. The definitions of these stimulation parameters were shown in Figure 2-16. The range of controllable stimulation parameters were listed in Table 2-4. We summarized used stimulation parameters in Table 2-5. The effects of stimulation was classified by changes in animal behaviors and LFPs depending on DBS. We determined the default stimulation parameter based on empirical condition for human neuropathic pain (1.4 mA, 60  $\mu$ sec and 130 Hz) [139]. Then we additionally applied several parameteres near the default stimulation condition. Additionally, large number of animal tests were required for determining effective stimulation conditions. Then, we designed the stimulator to be wirelessly controllable using a PC. We could simultaneously control several stimulators using only a PC via Zigbee protocol as shown in Figure 2-17.

Table 2-4. Custom designed current stimulation chip specification

Stimulation condition*	Range	resolution
<b>Amplitude</b>	10 $\mu$ A – 2550 $\mu$ A	10 $\mu$ A
<b>Pulse rate</b>	16 $\mu$ sec – 512 $\mu$ sec	2 times per bit (5 bit)
<b>Duration</b>	512 $\mu$ sec – 16 msec	2 times per bit (5 bit)
<b>Polarity</b>	Monophasic – Biphasic	
<b>Time for stimulation</b>	0.1 sec – 10 sec	0.1 sec

\* We summarized definitions of each stimulation parameters in Figure 2-16.

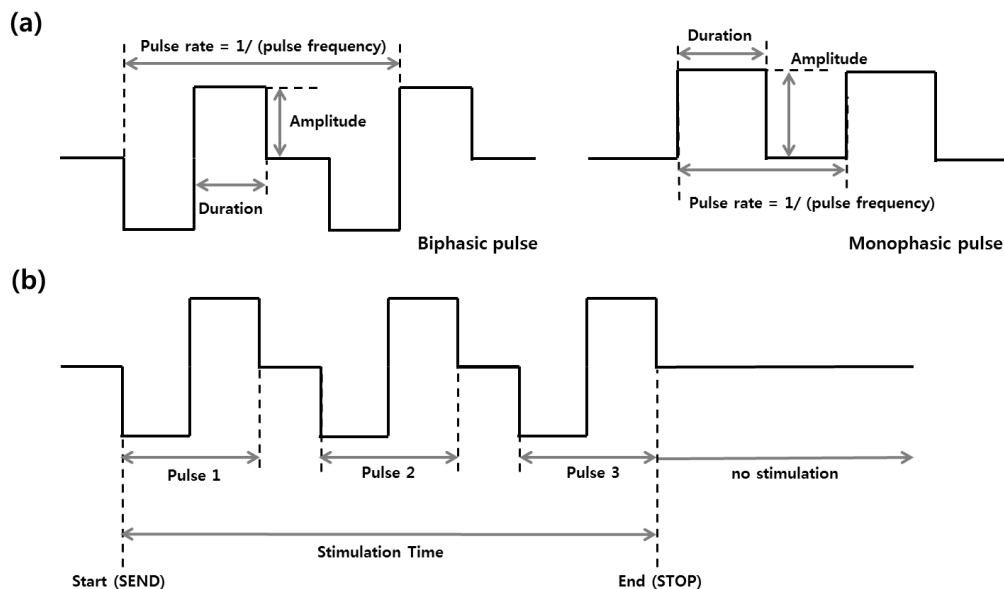


Figure 2-16. Definitions of stimulation parameters and the shape of the pulse. The developed stimulator could be derived with (a) polarity (mono- or bi-phasic), amplitude, duration, pulse frequency ( $\text{Hz} = 1 \text{ sec/pulse rate}$ ) and (b) stimulation time (period).

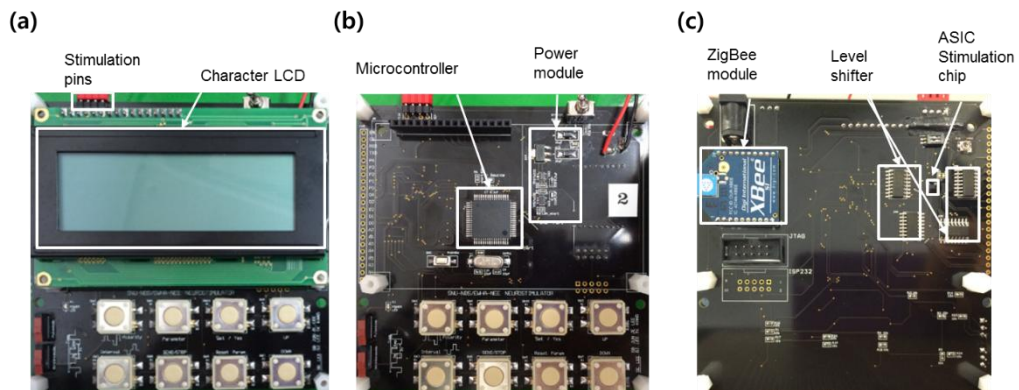


Figure 2-17. Developed and applied stimulator for preliminary experiments (a) Top image of the stimulator part. A pair of reference and stimulation ports for a bipolar stimulation are placed on the top side. Current stimulation parameter could be monitored on a LCD. (b) Backside of the LCD panel. (c) Bottom of the stimulator. A PC could control this system via Zigbee protocol.

Table 2-5. Various stimulation condition for specifying stimulation parameter

Stimulation condition	Amplitude	Duration	Frequency	Period
	[ $\mu\text{A}$ ]	[ $\mu\text{sec}$ ]	[Hz]	[min]
Amplitude dependency	300	60	130	10 or 20
	700	60	130	
	1400	60	130	
Duration dependency	1400	60	130	
	1400	120	130	
	1400	240	130	
	1400	300	130	
Frequency dependency	1400	60	10	
	1400	60	50	
	1400	60	90	
	1400	60	130	

\*Default condition: amplitude of 1.4 mA, duration of 60  $\mu\text{sec}$ , and frequency of 130 Hz

#### **2.2.4 Behavioral tests (von Frey test and duration test)**

Von Frey hairs are tools for mechanism study of cutaneous stimulation-induced sensory input. Mechanical force was exerted via application of a particular hair to the cutaneous receptive field until buckling of the hair occurs. To date, wire mesh is the commonly used apparatus to allow their application. Specifically, the elevated wire mesh floor supports a rat while the hairs were applied from below to the surface of the paw through the wire mesh. Rats were placed inside acrylic cages (8 x 10 x 20 cm) on top of a wire mesh grid for accessing to the paws. After 30 min of adaptation, innocuous mechanical stimulation was applied with a von Frey filament (8 mN bending force) 10 times to the lateral edge of the left and right hind paws [137]. The time of showing withdrawal response such as lifting, biting, shaking its left hind paw by painful stimulus was measured (von Frey scoring method) and the neural signal of that time was also measured (duration scoring method). These two kinds of behavioral tests were used for scoring changes of animal behaviors.

#### **2.2.5 Neural recording**

Neural activities in the VPL of normal and neuropathic pain model rats were recorded. We used urethane (1.3 g/kg) and pentobarbital (5 ml/kg) with atropine (1 mg/kg) to anesthetize SD-rats for the first and second trial, respectively. An hour after electrode implantation, we recorded neural activities for 300 sec. Mechanical stimulus (pain stimulus) was applied to both normal and pain group rats by applying a von Frey hair for 20 sec at 30 sec from the start of recording.

Recorded local field potentials (LFPs) were amplified ( $G = 100\sim 1000$  V/V), low-pass filtered (0.1 ~ 300 kHz) and sampled using a commercial amplifier (model 1700, A-M Systems, WA, USA) and a commercial recording device (Micro 1401, Cambridge Electronic Design Ltd., Cambridge, UK). The recorded data was stored by Spike 2 (version 7, Cambridge Electronic Design Ltd.). The recording system composition was shown in Figure 2-18.

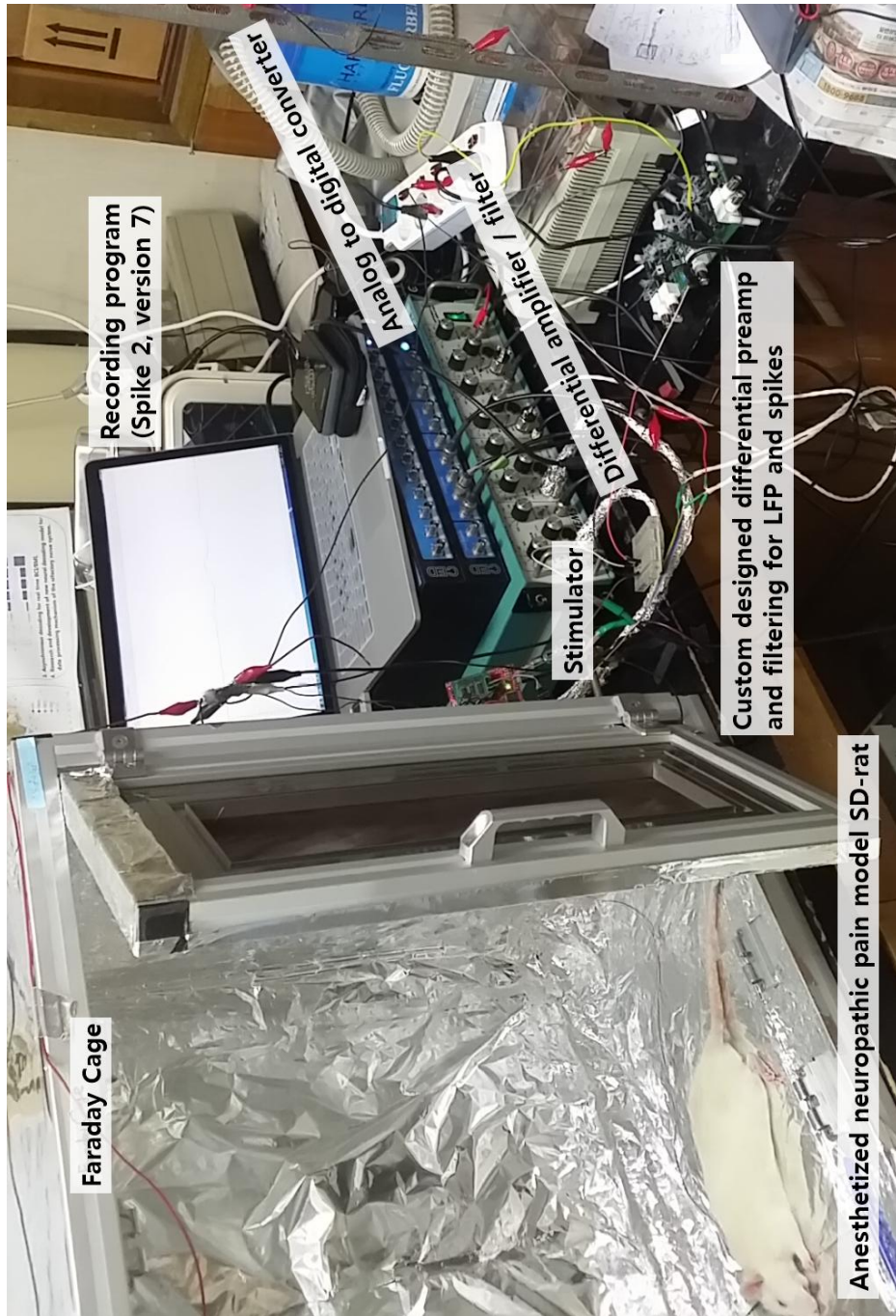


Figure 2-18. System composition for neural recording of preliminary animal experiments.

### 2.2.6 Signal processing

The stored neural signals are signal processed by Neuroexplorer (Version 4, Nex Technologies, AL, USA). The short term Fourier transform (STFT) was applied containing the hanning window with 50 % overlap rate [140]. STFT method have been generally used to determine the sinusoidal frequency and phase content of local sections of a signal as it changes over time and the governed equation is (Eq. 2-4). Because of its fast algorithm and simplicity of synthesis, STFT was applied for this study. Using STFT, we could display recorded LFPs as spectrogram. The time range was divide by window function  $w(n)$ , and the Fourier transform of divide window is as following:

$$X_k(w) = \sum_{n=0}^{M-1} x_k(n) \exp(-jwn) , \quad k = 1, 2, \dots, K \quad (\text{Eq. 2 - 4})$$

$$\text{where, } x_k(n) = x(n)w(n - (k - 1)M), \quad 1 \leq k \leq K \quad (\text{Eq. 2 - 5})$$

$$w(n) = \begin{cases} 1, & 0 \leq n \leq M - 1 \\ 0, & \text{otherwise} \end{cases} \quad (\text{Eq. 2 - 6})$$

When the time is 'm', the result of the Fourier transform of (M-1)th section is as following:

$$X(m, w) = \sum_{n=0}^{M-1} x(n)w(n - m) \exp(-jwn) , \quad k = 1, 2, \dots, K \quad (\text{Eq. 2 - 7})$$

After the STFT process (2048 points for fast Fourier transform, hanning window of 1 sec, overlap of 50 %) using Neuroexplorer (version 4, Nex Technologies, AL, USA), normalization was applied for obvious extraction of index pain signal using MATLAB (version 2013b, MathWorks, MA, USA) as the reference [141]. The governed equation

of normalization is

$$Z(m, w) = \frac{X(m, w) - B(m, w)}{\delta(m, w)} \quad (\text{Eq. 2 - 8})$$

where,

$Z(m, w)$ : the normalized spectrogram

$X(m, w)$ : spectrogram resulting from STFT

$B(m, w)$ : mean value of  $X(m, w)$

$\delta(m, w)$ : standard deviation of  $X(m, w)$

After normalization, a 4 x 4 sized smoothing filter was applied for observing the trends of neural signal changes and effective extracting the index signal. Differences of each step were shown as Figure 2-19.

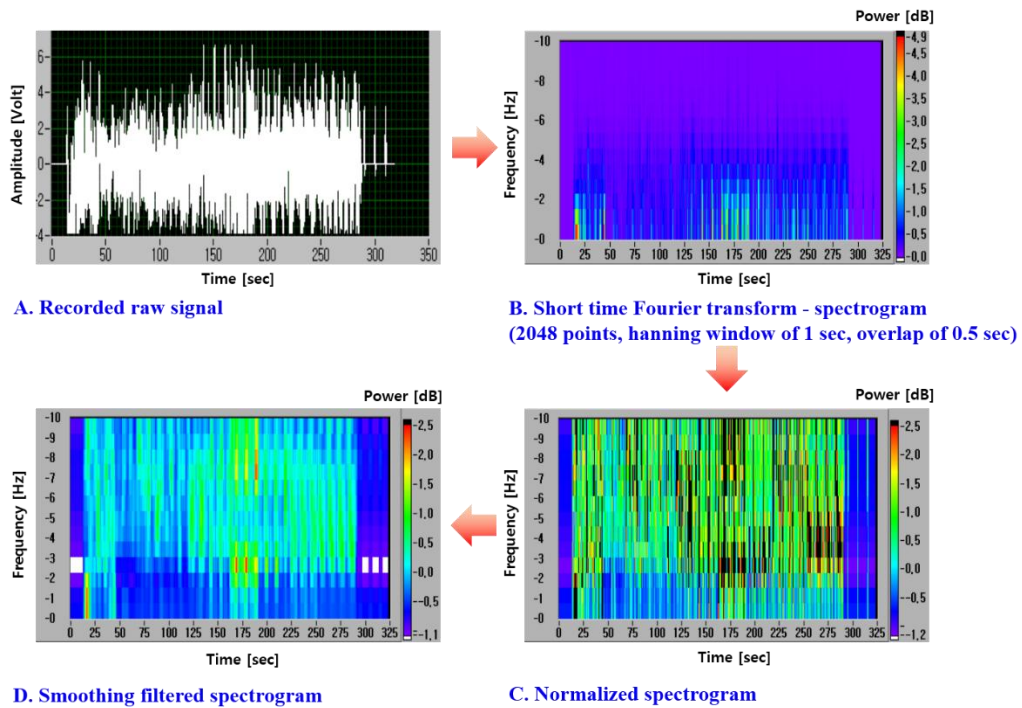


Figure 2-19. Steps for signal process for preliminary experiments. (a) Recorded and low-pass filtered LFP. (b) Using STFT, a spectrogram was acquired. (c) After normalization, shadowy signals was observed. (d) With smoothing filtering, it is easy to identify the change of neural signal relating to neuropathic pain (50 ~ 150 sec).

### 2.2.7 Correlation analysis

Correlation can tell you something about the relationship between two or more variable data. Statistical correlation is validated by what is called coefficient of correlation ( $r$ ) as shown in Table 2-6. Its numerical value ranges from +1.0 to -1.0. It gives us an indication of the strength of relationship. In general,  $r > 0$  indicates positive relationship,  $r < 0$  indicates negative relationship while  $r = 0$  indicates no relationship (or that the variables are independent and not related). Here,  $r = +1.0$  describes a perfect positive correlation and  $r = -1.0$  describes a perfect negative correlation. Closer the coefficients are to +1.0 and -1.0, greater is the strength of the relationship between the variables. As a rule of thumb, the following formula and guidelines on strength of relationship are often useful;

**Step 1:** First, we made a chart with our data for two variables, labeling the variables  $x$  (= averaged PSD level of LFPs, PSD) and  $y$  (= scored results behavioral tests, SR). Then we added 3 more columns labeled  $(xy)$ ,  $(x^2)$ , and  $(y^2)$ . A simple data chart might look like this:

No.	( $x$ )	( $y$ )	( $xy$ )	( $x^2$ )	( $y^2$ )
1					
2					
3					

**Step 2:** Then we completed the chart using basic multiplication of the variable values.

No.	( $x$ )	( $y$ )	( $xy$ )	( $x^2$ )	( $y^2$ )
1	20	30	600	400	900
2	24	20	480	576	400
3	17	27	459	289	729

**Step 3:** After we had multiplied all the values to complete the chart, as shown above, next we added up all the columns from top to bottom.

No.	( $x$ )	( $y$ )	( $xy$ )	( $x^2$ )	( $y^2$ )
1	20	30	600	400	900
2	24	20	480	576	400
3	17	27	459	289	729
Total	61	77	1539	1265	2029



**Step 4:** Then, we used the following formula (Eq. to find the Pearson Correlation Coefficient value.

$$r = \frac{N \sum xy - (\sum x)(\sum y)}{\sqrt{[N \sum x^2 - (\sum x)^2][N \sum y^2 - (\sum y)^2]}} \quad (\text{Eq. 2 - 9})$$

Where, N = number of pairs of scores

**Step 5:** Once we completed the formula above by plugging in all the correct values, the result was our coefficient value.

Table 2-6. Strength of relationship depending on correlation coefficient  $r$

Variable of $r$	Strength of relationship
- 1.0 to - 0.5 or 1.0 to 0.5	Strong
- 0.5 to - 0.3 or 0.3 to 0.5	Moderate
- 0.3 to - 0.1 or 0.1 to 0.3	Weak
- 0.1 to 0.1	None or very weak

We tried to use the changes in averaged PSD levels, which were acquired from the low frequency bands (delta-band of 0.1 ~ 4 Hz, theta-band of 4 ~ 7 Hz, and alpha-band of 7 ~ 15 Hz) of recorded local field potential (LFP) as the neural signal index for the neuropathic pain. However, LFPs were recorded from anesthetized neuropathic pain models. For that reason, it was required to validate whether the recorded signal reflects the practical neuropathic pain or not. For considering recorded and signal-processed LFP as objectively nociceptive information, we performed the correlation analysis between changes in averaged level of PSD ( $x$  factor) and changes in scored results of behavioral tests ( $y$  factor). Using the Pearson's method, the ratio of changes in averaged PSDs to changes in scored results of behavioral tests depending on various stimulation parameters.

## **2.3 Closed-loop stimulator**

We need to consider several elements for implementing closed-loop DBS system. First, we should identify the neural signal index related neuropathic pain from results of section 2.2. Second, we needed to determine the effective stimulation parameters for neuropathic pain based on results of section 2.2. Finally, we should develop a closed-loop strategy including a finite state machine of stimulation parameters using results of section 2.2. Considering these elements, we developed a prototype system including the electrode and the CDBS stimulator and examined the system performance and its efficacy through *in vivo* application.

### **2.3.1 Overview of closed-loop DBS system for neuropathic pain**

The CDBS for neuropathic pain system of this study has similar compositions to other general closed-loop neural prosthetic devices [142]. After signal processing of the recorded neural signal, the system extracted specific signal index (changes in averaged PSD level) related to symptoms by STFT and averaging. The extracted neural signal index was used as a triggering signal for controlling a stimulator. The CDBS system for neuropathic system should be controlled in two points depending the monitored neural signal of VPL region; (1) It should control power of the stimulator (on/off state). (2) It should adjust stimulation parameters depending on changes in feedback signal (index). If there was a negative feedback signal that means effectiveness, the controller should adjust stimulation state as ‘lower stimulation state’ compared to before. On the other hand, the stimulator should adjust the state to ‘higher stimulation state’.

The classification method of neuropathic pain information was based on results of preliminary experiments of section 2.2. Moreover, stimulation parameters should be fitted depending on each animals. Because the degree and tendency of nociceptive information were different each other. After the fitting process, the system should operate in stand-alone mode. This concept was considered devices for human. The whole system was also summarized in Figure 2-20.

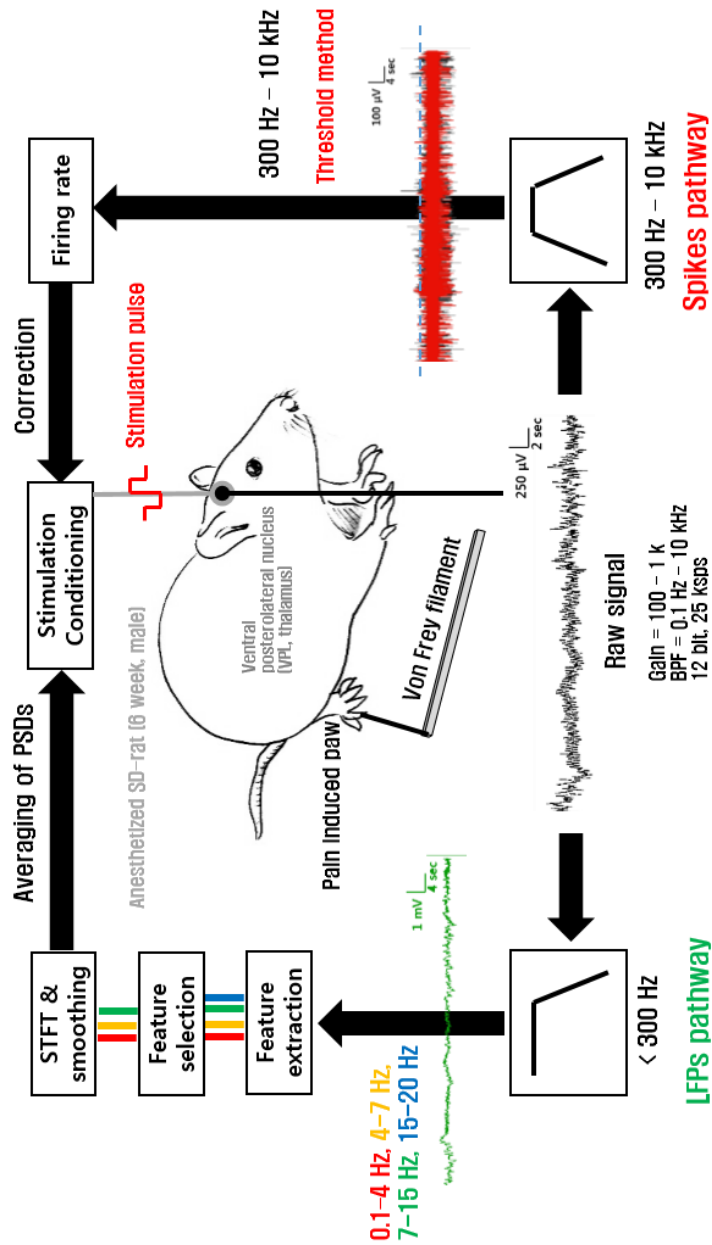


Figure 2-20. Overview of the suggested CDDBS system for neuropathic pain. The CDDBS system of this study use the monitored signal from VPL region, which is the stimulation target as well. The stimulation pulse should be derived to VPL region when the nociceptive information detected and stimulation parameters should be adjusted depending on the level of remission. Changes of the spike rate could be used for correction method of LFP-based closed-loop control. Then, the threshold method was applied for detecting changes of the spike rate.

### **2.3.2 Closed-loop deep brain stimulation strategy for neuropathic pain**

The CDBS system for neuropathic pain should be differently controlled in two cases (higher- and lower-direction) depending changes in neural signal (Figure 2-21). One is 'no pain' state, which is small mechanical stimulus like 'touch' or no physical stimulus. The other is 'pain' state. When there was 'no painful stimulus', the system has to be in 'standby-mode (state 0)' and store the averaged level of PSD as reference level for comparison during preset duration. On the other hand, if the averaged level of PSD was changed over the preset rate (neural signal index), the CDBS system should derive stimulation pulse into the brain with the default stimulation parameter (state 1). The changes of PSD level could be upper or lower. In spite of DBS with condition of 'state 1', the nociceptive state could be kept. Then, the stimulation condition should be changed as 'higher stimulation condition (state 2 ~ 4)'. If the suppression of nociception was detected (changes in PSD level toward reference level), the state should be changed as lower level. The effective time should be acquired from results of preliminary experiments of section 2.2 and previous study [143]. Previous study showed the general transition time of pain states was about a few minutes (time of changes in neural response after electrical stimulation was 3~5 sec). If the system response time is fast enough, we tried to use averaged levels of several PSDs for correction. The adjustable stimulation parameters are amplitude, duration, and pulse frequency for each states was determined reflecting results of preliminary experiments.

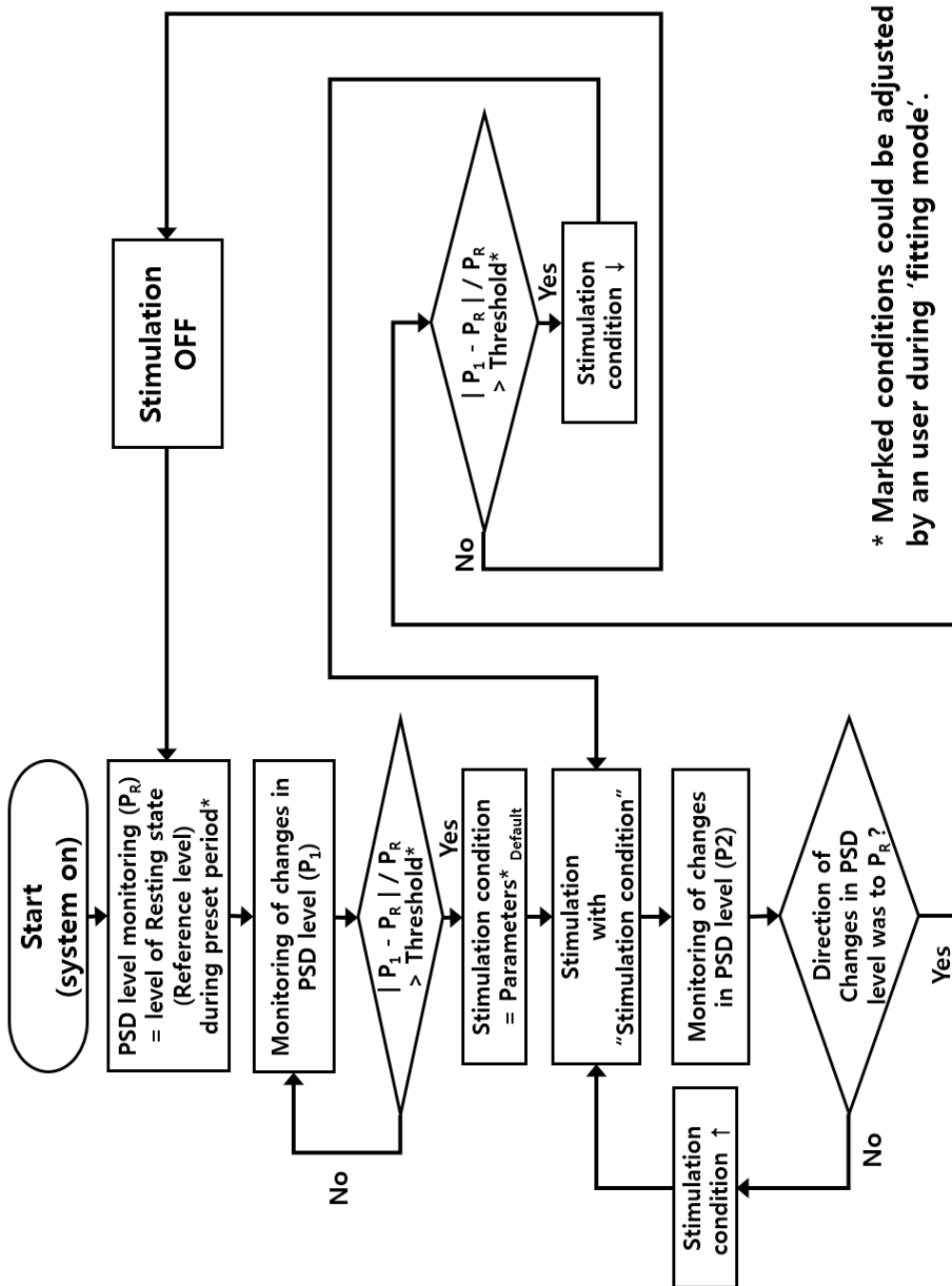


Figure 2-21. Closed-loop deep brain stimulation strategy for neuropathic pain.

### 2.3.3 Prototype implementation

Applying the developed CDBS strategy of section 2.3.2, we developed the prototype CDBS system for neuropathic pain as shown in Figure 2-22 and 2-23. The CDBS system was controlled based on recorded and signal-processed LFPs and MUAs as Figure 2-22(a).

We implemented the CDBS system as following. First, a preamplifier and filters were applied as Figure 2-22 (b). An instrumentation amplifier (AD620, Texas Instruments, TX, USA) was used as a preamplifier for both LFPs ( $A_v = 10$  V/V) and MUA ( $A_v = 1000$  V/V). A variable gain amplifier (VGA, LTC6901-1, Linear Technology, CA, USA) was also used for preventing saturation during DBS period of LFPs part ( $A_v = 1 \sim 100$  V/V). During DBS period, the gain of VGA decreased and the decreased value of gain was compensated by embedded software of main controller. The filters were implemented using LF441 (National Instrument Corp., TX, USA) for antialiasing during ADC sampling process (0.1 ~ 20 Hz for LFPs, 300 ~ 10 kHz for spikes). A comparator was also used for separating the rate of spikes based on threshold method. Second, the microcontroller (MCU, Tiva™ C series LaunchPad Evaluation kit, ARM Cortex M4, Texas Instrument, USA) that has internal ADC and two TIMERS for multi-thread control was used for fast closed-loop control. We summarized the main functions of embedded software of MCU in Table 2-7. It was available to achieve fast system response time using double thread scheduling method. Finally, the MCU also worked for signal processing as section 2.3.1. As shown in Table 2-7, STFT processing and averaging were performed with 320 samples/sec and 4 levels/sec, respectively. The software-based low pass filtering was required to reduce the fluctuation of averaged PSD level as Figure 2-22(b). Applying the developed closed-loop control logic and an established FSM from results of preliminary experiments, the MCU controls the power and adjusts stimulation parameters of the stimulation chip (IDEC 80) with parallelized 20 bits through level shifters (74HC4049D, NXP Semiconductors, Eindhoven, Netherlands).

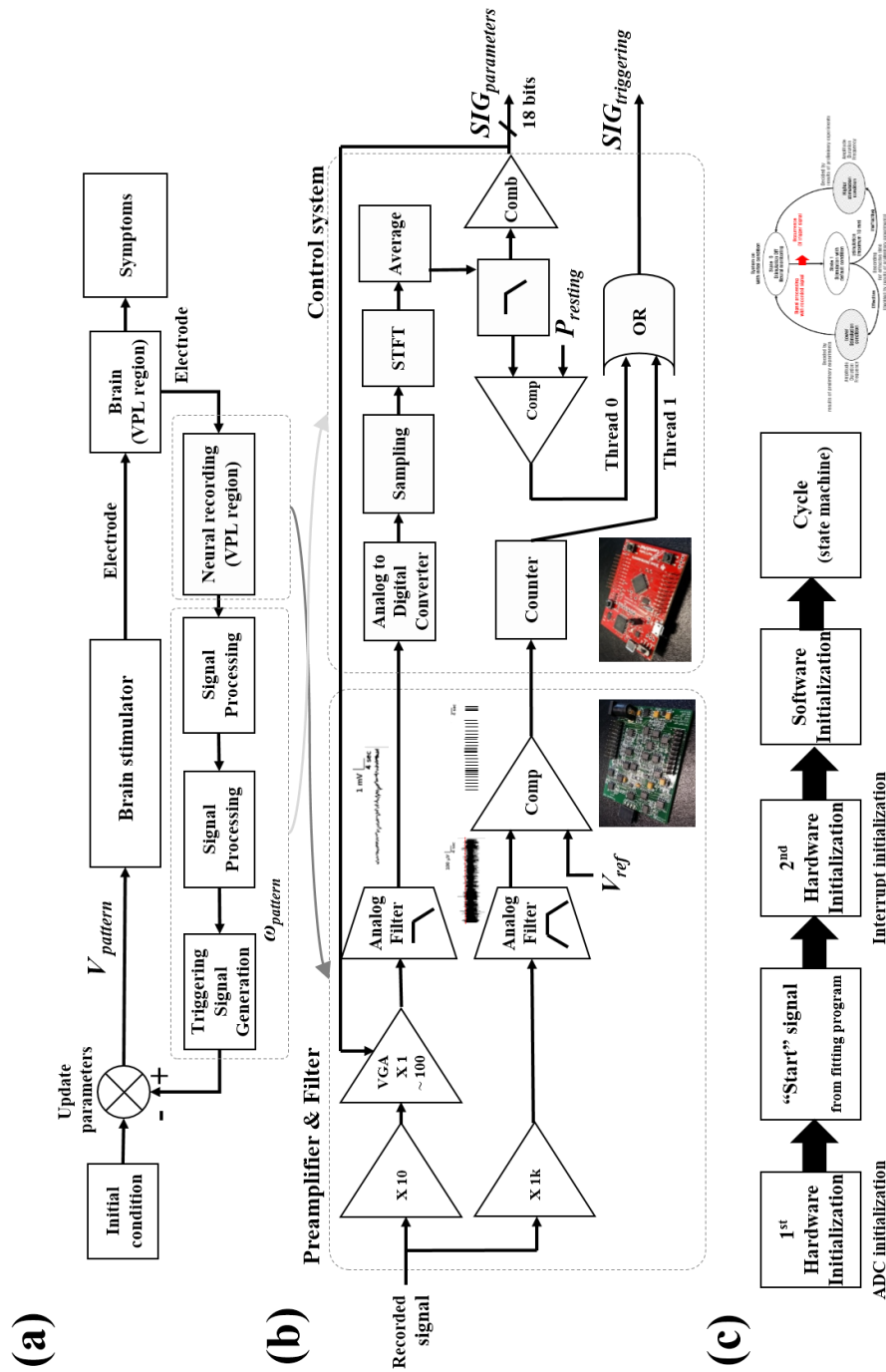


Figure 2-22. System diagram of CDBS system for neuropathic pain; (a) feedback control for NP, (b) system composition for CDBS, and (c) operation of embedded SW.

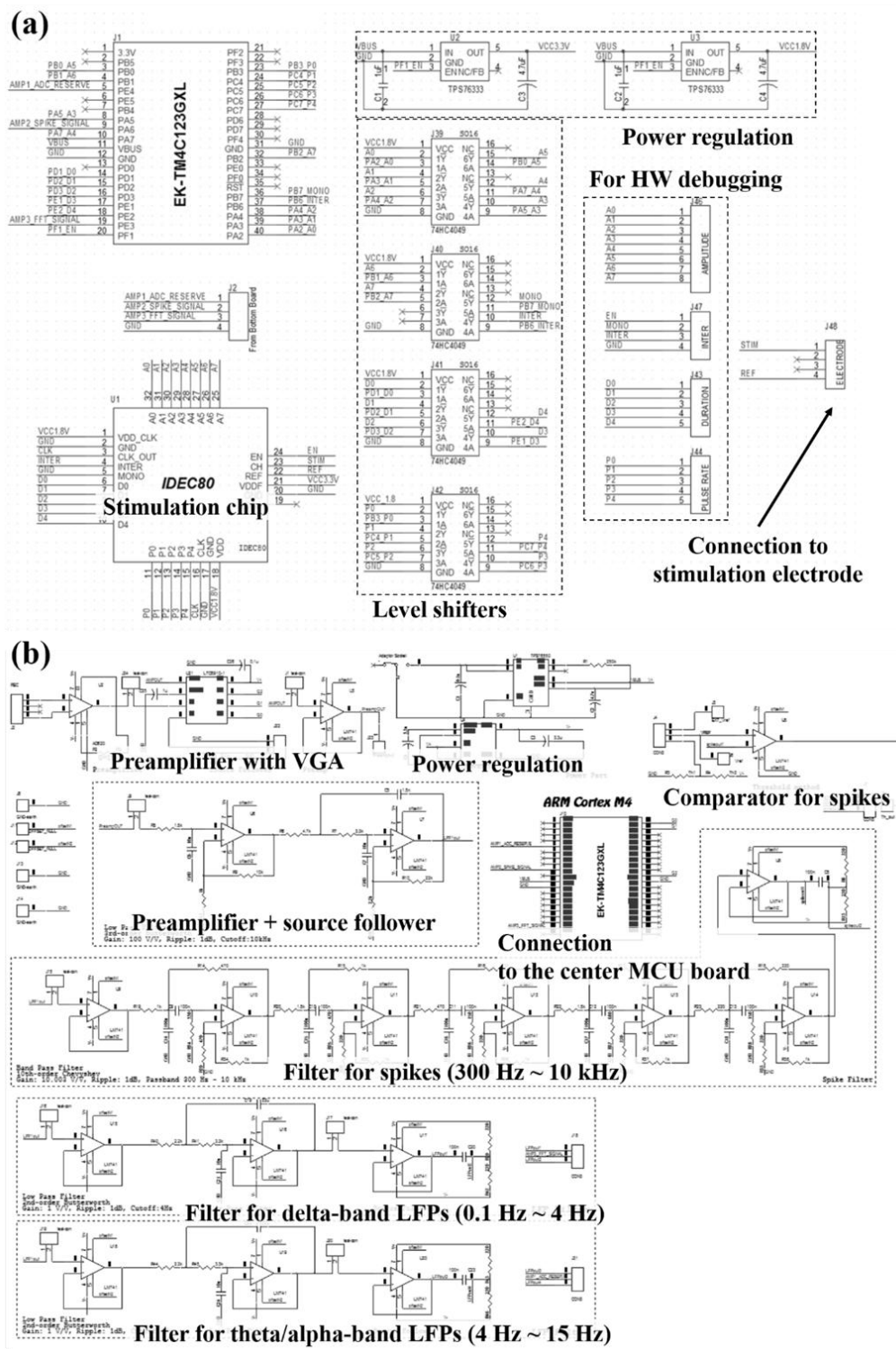


Figure 2-23. Schematic of the CDBS system. (a) Top board for stimulation current derive and (b) bottom board for neural recording.



Table 2-7. Functions of embedded software for closed-loop control

<b>TIMER No.</b>	<b>Function</b>	<b>Description</b>
<b>Thread 0</b> <b>TIMER 0</b> <b>(320 Hz)</b>	<b>(1) Flag management</b>	Changes of neural signal (LFPs and MUAs), system on-off
	<b>(2) Correction method</b>	Correction using a flag of MUAs
	<b>(3) ADC sampling</b>	20,000 samples/sec (internal ADC)
	<b>(4) Interrupt management</b>	Interrupts of ADC, TIMERS
	<b>(5) Signal processing</b>	STFT with 320 samples/sec, averaging process using four samples per a sec.
<b>Thread 1</b> <b>TIMER 1</b> <b>(500 Hz)</b>	<b>(6) TX/RX with a PC</b>	for an external fitting program (PC)
	<b>(7) System on-off control</b>	Power control using a flag of (1)
	<b>(8) Count the number of spikes ( flag for (2) )</b>	Make a flag for correction of (2)

### 2.3.4 Prototype measurements: performance test

We examined functionalities of the developed system using pre-recorded signal during preliminary experiments. We inputted the played pre-recorded signal using an arbitrary wave generator (digital to analog converter, DAC, 33500B series, Agilent, CA, USA) to the recording part and measured the derived current by stimulator part with a resistor of 1 k $\Omega$  using an oscilloscope (DPO3000 series, Tektronix Communications, TX, USA) as shown in Figure 2-24. The playtime of the pre-recorded LFP was over 300 sec and the painful stimulus lasted for 20 sec after 30 sec from the start point as Figure 2-24 (b). We examined the main functions of the system such as power control of On/Off and adjustment of stimulation parameter depending on the its pain state resulting from the recorded and signal-processed PSD level (neural signal index).

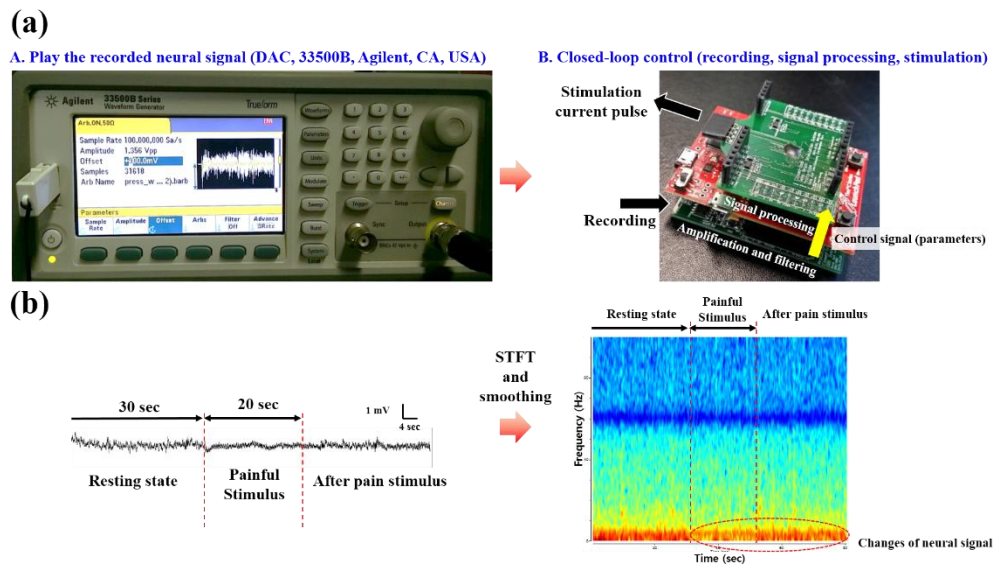


Figure 2-24. Performance measurements. (a) Test methods for performance tests. We played the pre-recorded neural signal using a DAC device. (b) Replayed neural signal. The playtime was 300 sec and the painful stimulus was induced at 30 sec from the starting point (for 20 sec).

### 2.3.5 Animal experiments: *in vivo* application

We applied the developed CDBS system to *in vivo* application. As shown in Figure 2-25, the experimental setup is similar to that of the preliminary experiments of Figure 2-18.

We anesthetized rats with pentobarbital (5 ml/kg) with atropine (1 mg/kg) for reducing airway secretion. The CDBS device was connected to the percutaneous connector of the implanted electrode using shielded wires. The more deeply inserted electrode contacts (channel 1 and 2) were used for DBS, and the other contacts (channel 3 and 4) were used for recording LFP. During the experiments, changes in nociceptive neural signals depending on DBS were monitored using the same system of preliminary experiments on the sidelines of the recording part of the CDBS system. Mechanical stimulus (pain stimulus) was applied to pain model rats with a von Frey hair.

The system firstly operated in ‘fitting mode’ for setting the reference level of

averaged PSDs and number of averaging levels for correction. We could set the threshold rate of change in averaged PSD levels for differentiating ‘pain state’ from the resting state using a fitting program in a connected PC. We used the fitting program only for assignment of initial value, initialization of the hardware, and threshold rate of changes in averaged PSD levels for closed-loop control. After the fitting mode, the system operated in the ‘stand-alone mode’.

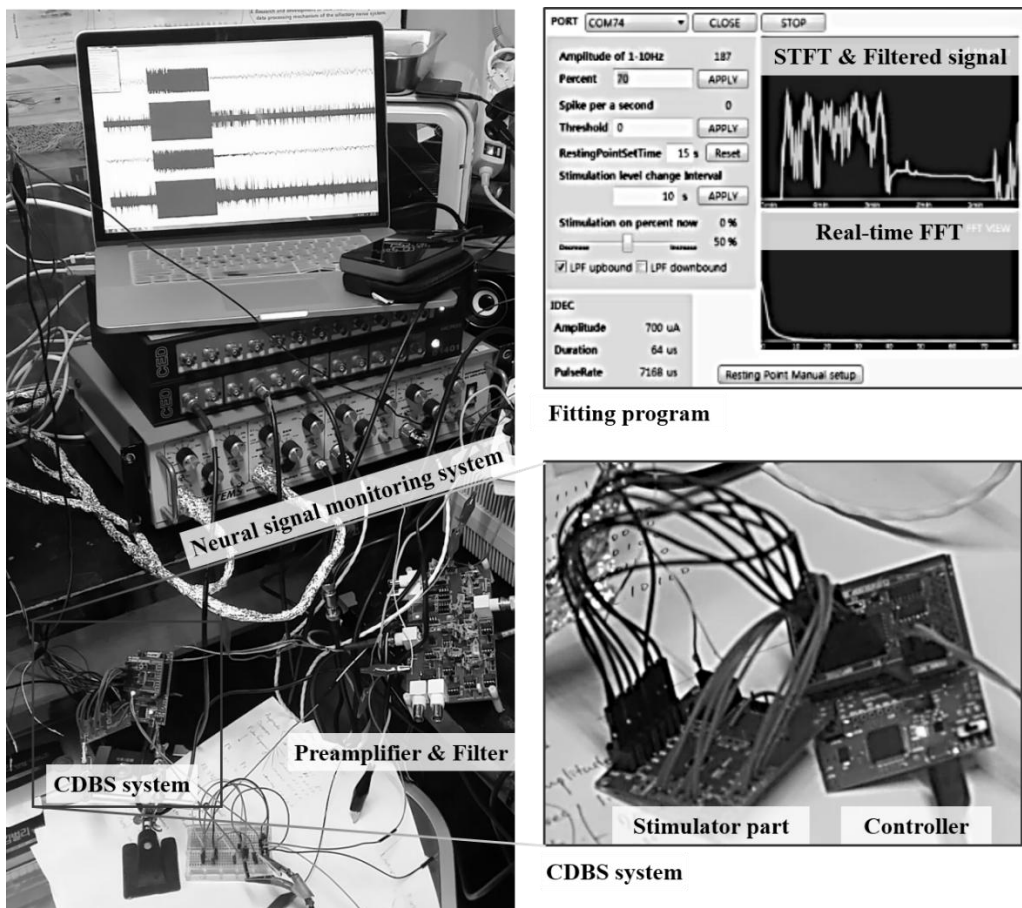


Figure 2-25. *In vivo* experimental setup. The system operated in ‘stand-alone’ mode and the neural signal was monitored using the same system as preliminary experiments of section 2.2.

### ***3. Results***

---

***3.1 Multi-channel deep brain stimulation electrode***

***3.2 Results of preliminary experiments***

***3.3 Closed-loop stimulator***

### 3.1 Multichannel deep brain stimulation electrode

We fabricated the multichannel electrode using an improved LCP process for multiple LCP layers. We performed volume of tissue activated (VTA) simulation of the electrode and measurement of electrochemical and mechanical characteristics before implantation.

#### 3.1.1 Results of VTA simulation

The calculated VTAs of the designed electrode and a commercial electrode (TM33CINS, World Precision Instrument Corporation, USA) with the default bipolar-stimulation condition (1.4 mA, 130 Hz, 60  $\mu\text{sec}$ ) were  $0.043 \mu\text{m}^3$  and  $0.056 \mu\text{m}^3$ , respectively, that were smaller than the volume of VPL region of  $0.196 \mu\text{m}^3$ . The charge distribution of developed LCP electrode was half-cylinder form as shown in Figure 3-1.

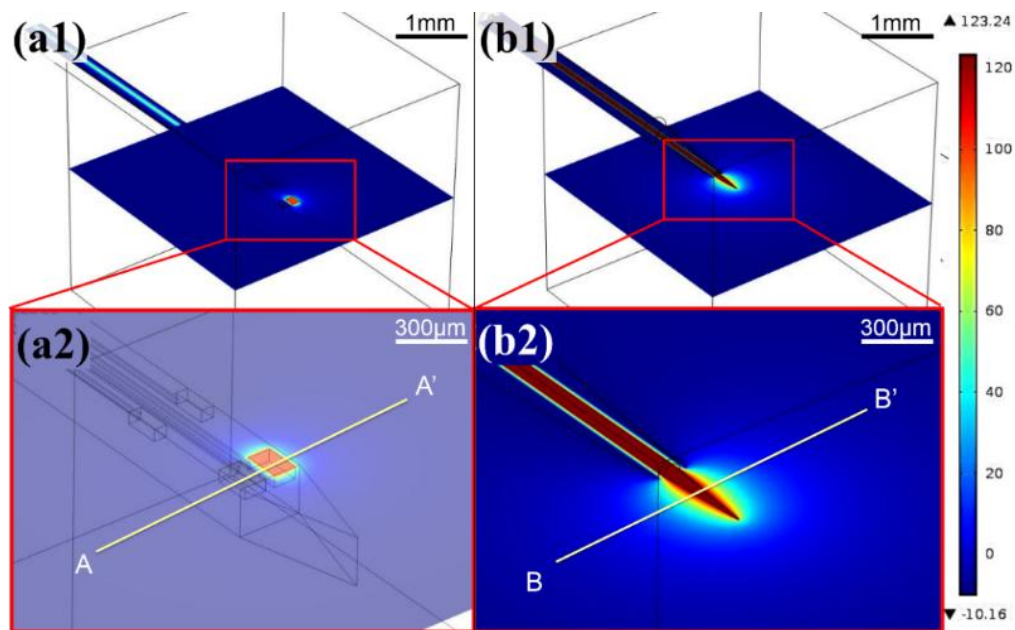


Figure 3-1. Results of FEM simulation for VTA. (a1~a2) LCP-based multichannel electrode and (b1~b2) a commercial electrode (TM33CINS, WPI corp., USA) The formed VTAs of the LCP-based electrode and a commercial bipolar electrode were  $0.043 \mu\text{m}^3$  and  $0.056 \mu\text{m}^3$ , respectively, that were smaller than the volume of VPL region of  $0.196 \mu\text{m}^3$ .

### 3.1.2 Fabrication process

We fabricated the LCP-based CDBS electrode using the suggested multi-layered LCP process of Figure 3-2. We applied the improved LCP process including modified metal pattern arrangement and interlayer alignment methods for fabricating multichannel DBS electrode. We performed thermal press bonding (lamination), laser ablation, and final laser cutting process applying the newly suggested alignment method as shown in Figure 3-3. The design margins for laser ablation and final cutting improved as 100  $\mu\text{m}$  and 50  $\mu\text{m}$ , respectively. The yield of electrode increased  $69.23 \pm 0.68 \%$  (= about 9/13 per a 4" wafer). The number of working electrodes was the same as the one of the practically working electrodes *in vivo*. The working or fail electrode could be determined at the electrochemical characteristics measurement step of section 3.1.3. After IrOx was electroplated, the electrode was connected to the interface board using DC-block capacitors.

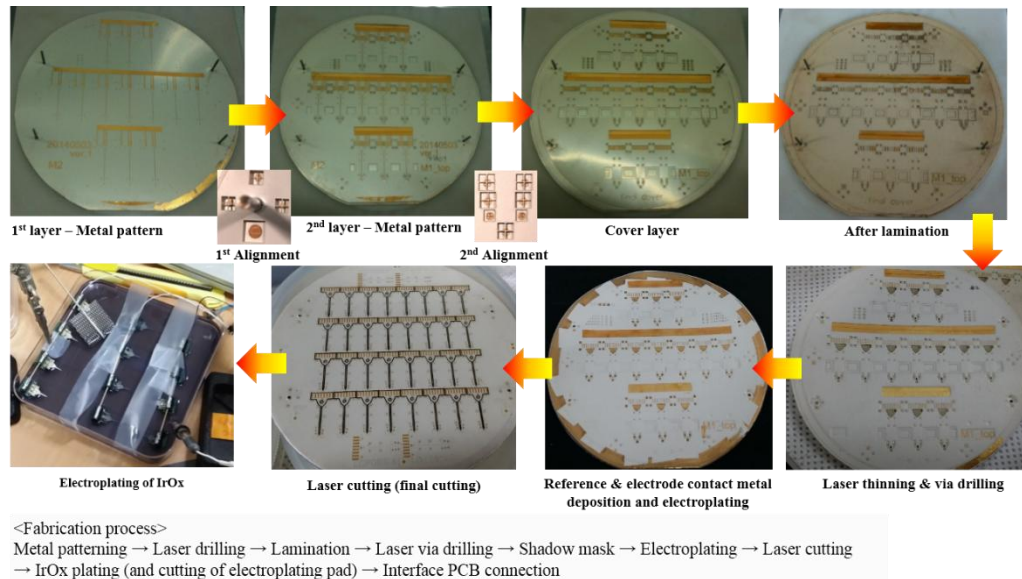


Figure 3-2. Images of the whole fabrication process for the LCP-based CDBS electrode. Before lamination process, the new interlayer alignment method was used to align LCP alignment. The IrOx electroplating process was performed using common pads of the LCP samples.

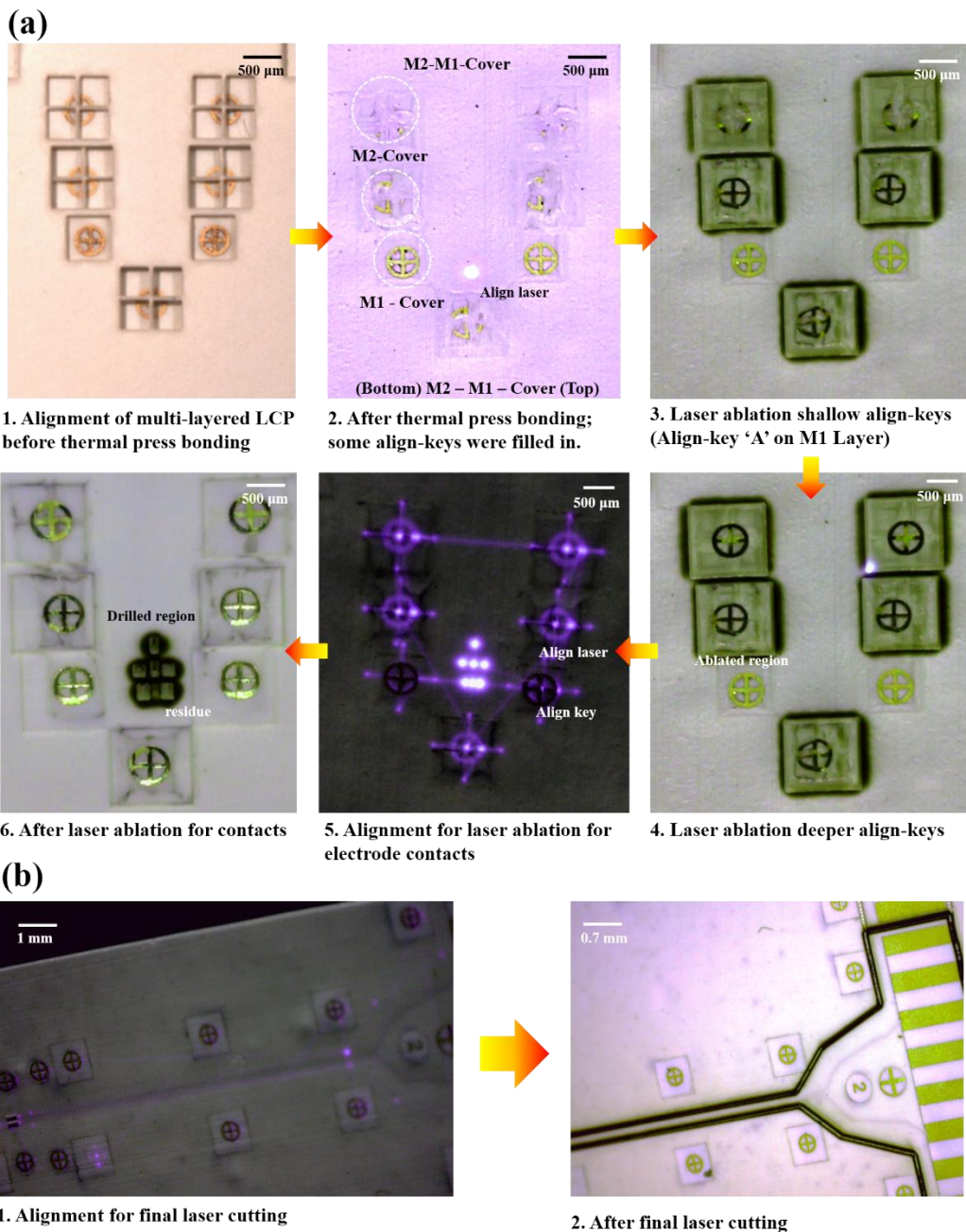


Figure 3-3. Application of the improved LCP process. (a) Thermal press bonding process. After the lamination, the align-keys could be filled in. Using two or more 'M1-Cover' align-key, buried align-key could be exposed by laser ablation process. After align-key exposure, whole align-keys could be used to align for laser drilling and (b) final laser cutting.

### 3.1.3 Developed electrode

The developed multichannel DBS electrode was shown in Figure 3-4. Results of aforementioned fabrication process of section such as IrOx-plated contacts, DC-block capacitor-based connection on the interface board, and a via for a global reference electrode in section 3.1.2 were also shown in Figure 3-4. It was difficult to try electroplating IrOx after connecting to the interface board. The contact for a global reference electrode was sufficiently flexible to bend and there was no differences in resistance during bending as mentioned in section 2.1.2.

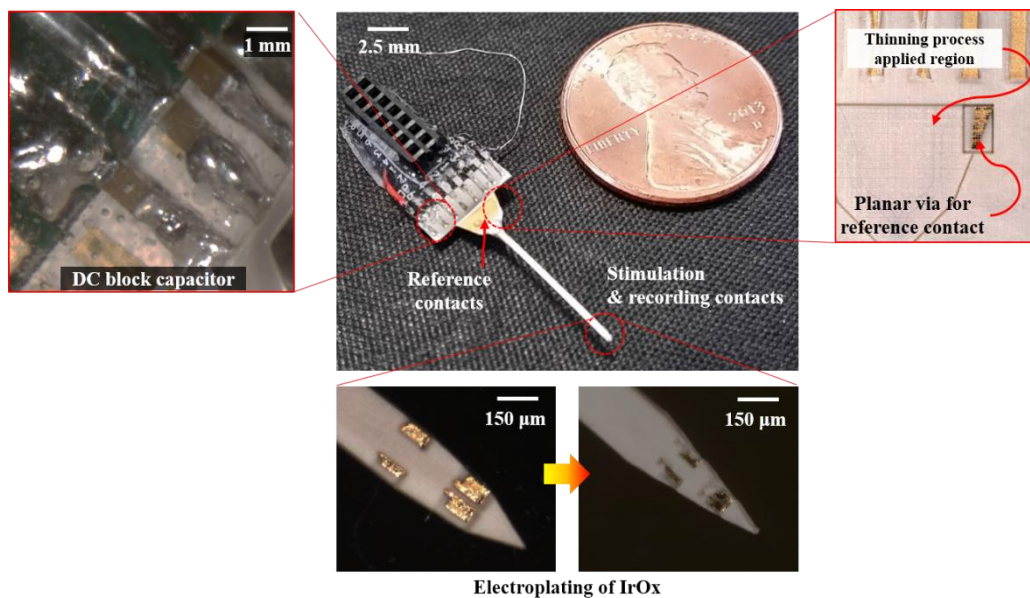


Figure 3-4. Developed LCP-based deep brain stimulation electrode. The recording and stimulation contacts were electroplated with IrOx and the global reference contact was laser thinned before metal deposition using laser thinning method of previous study [129].



### 3.1.4 Results of characteristics measurements

#### (1) Electrical characteristics

The measured electrical characteristics were listed in Table 3-1 and Figure 3-5. The electrochemical impedance was decreased before and after the IrOx electroplating as  $125 \pm 15 \text{ k}\Omega$  and  $16.53 \pm 1.56 \text{ k}\Omega$  at 1 kHz, respectively. The calculated charge storage capacitance was also changed from  $384.4 \pm 0.78 \text{ }\mu\text{C}/\text{cm}^2$  to  $1.29 \pm 0.54 \text{ mC}/\text{cm}^2$  after IrOx electroplating against the GSA of  $9,750 \text{ }\mu\text{m}^2$ . The calculated charge injection limit of the developed CDBS with IrOx contacts was  $1.2 \text{ mC}/\text{ph} \cdot \text{cm}^2$  at 120  $\mu\text{sec}$  and 130 Hz condition.

Table 3-1. Measured electrochemical characteristics

Measured characteristics	Value	Measurement condition
Impedance	$16.53 \pm 1.56 \text{ k}\Omega$	At 1 kHz
Charge storage capacitance	$1.29 \pm 0.54 \text{ mC}/\text{cm}^2$	Cyclic voltammetry
Charge injection limit	$1.2 \pm 0.21 \text{ mC}/\text{ph} \cdot \text{cm}^2$	120 $\mu\text{sec}$ , 130 Hz

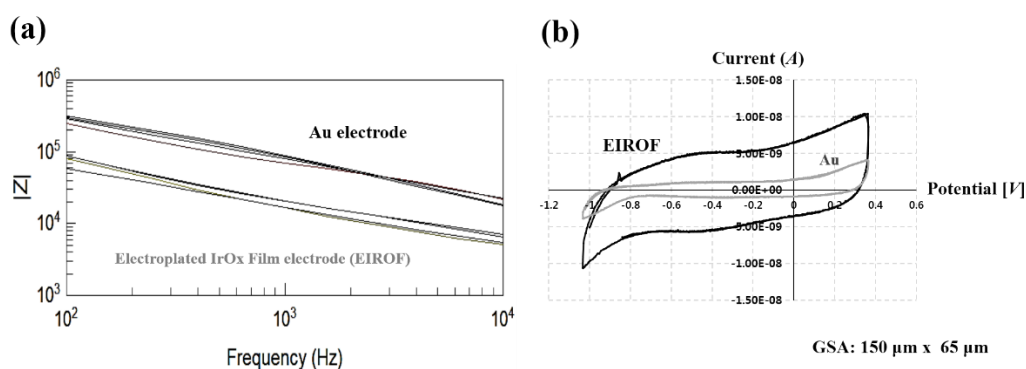


Figure 3-5. Results of electrochemical measurements. (a) Electrochemical impedance spectroscopy and (b) cyclic voltammetry before and after IrOx electroplating.

## (2) Measured mechanical characteristics

The applied force-displacement curves were obtained from the buckling tests of the fabricated LCP-based DBS electrode (200  $\mu\text{m}$  (W) x 200  $\mu\text{m}$  (T)), a tungsten rod (200  $\mu\text{m}$  in diameter), and a silicon probe (100  $\mu\text{m}$  (W) x 100  $\mu\text{m}$  (T)) shown in Figure 3-6. As the displacement increased, the force (stress) applied to the silicon probe linearly increased and rapidly dropped due to the breakage of the silicon shank. On the other hand, both the LCP probe and the tungsten rod showed smoothly increasing applied force-displacement curves [1]. (This work was performed an extended study of the author's thesis for M.S. degree. 4 samples for each kinds of electrodes were additionally examined after the previous work for validating reliability and reproducibility)

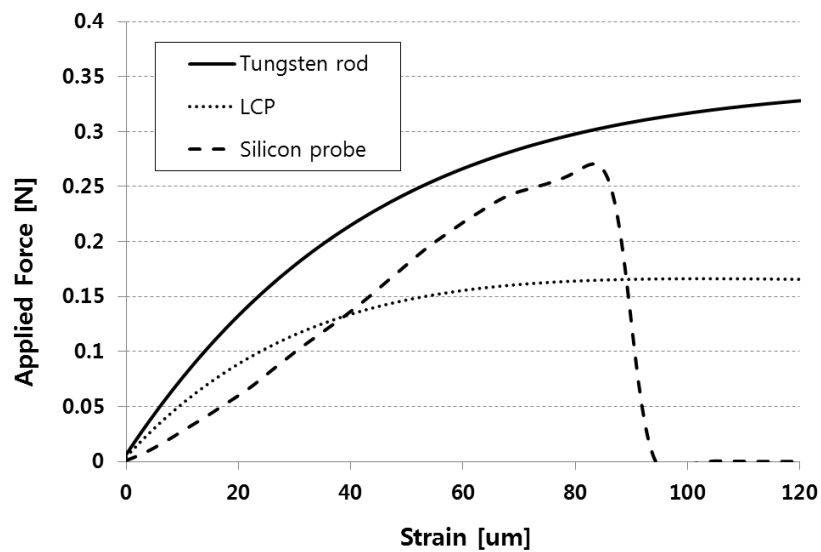


Figure 3-6. Results of material-dependent mechanical characteristics measurements (N=5, averaged data plot). LCP was stiff and elastic and showed similar curve to that of tungsten rods. The curve of LCP showed that of elastic material-based electrodes. Tungsten (diameter = 200  $\mu\text{m}$ ) and a silicon probe (cross section area = 100  $\mu\text{m}$  (W) x 100  $\mu\text{m}$  (T)) were also measured for comparison. Silicon probe showed the slowly decreased curve [1].

## 3.2 Results of preliminary experiments

Applying various stimulation on neuropathic pain model animals, two kinds of behavioral tests and LFP recording experiment were performed. According to results of preliminary experiments, the effective stimulation parameters for neuropathic pain could be determined. Changes in averaged power spectral density (PSD) were observed during painful stimulus depending on DBS.

### 3.2.1 Results of behavioral tests (von Frey and duration measurement)

Responses to pain significantly decreased in neuropathic pain model rats with DBS on VPL comparison to without DBS as shown in Figure 3-7. First, both the number of responses to von Frey stimulus and the latency of redrawing paws that means the rate of nociception decreased ( $N = 16$ ). After 21 days follow up, the von Frey score was 9.8 ~ 10 (10 is the maximum value) and the duration of showing a pain response was 3 ~ 5 sec without DBS. However, the number of response to von Frey stimulus decreased to 4.8 ~ 6.8 and duration also decreased to 1.2 ~ 3.5 sec. When we aborted DBS, the pain score and duration temporarily increased back to 9.4 ~ 10 and upto 21.8 sec ( $N = 6$ ), respectively.

As results of statistical analysis of behavioral tests shown in Figure 3-7 (a) ~ (c), the amplitude of 0.7 ~ 1.4 mA, pulse duration of 20 ~ 240  $\mu\text{sec}$ , and frequency (= 1/pulse rate) over 130 Hz were meaningfully effective for neuropathic pain (paired- $T$  test). Consequently, the effective stimulation condition was amplitude over 700  $\mu\text{A}$  ( $p = 0.044$ ), duration over 20  $\mu\text{sec}$  ( $p < 0.05$ ), and frequency over 130 Hz ( $p < 0.03$ ). The effective stimulation parameters and the finite state machine for closed-loop control could be determined as shown in Figure 3-7(d). The minimal stimulation condition with efficacy (700  $\mu\text{A}$ , 20  $\mu\text{sec}$ , 130 Hz) and the maximum effective condition (1.4 mA, 240  $\mu\text{sec}$ , 250 Hz) could be also determined as the 'state 0' and last state (state 4) for closed-loop control ( $p < 0.05$ ). The transition time for state change is the same as aforementioned over 5 min that was empirically meaningful time to reduce the pain with DBS.

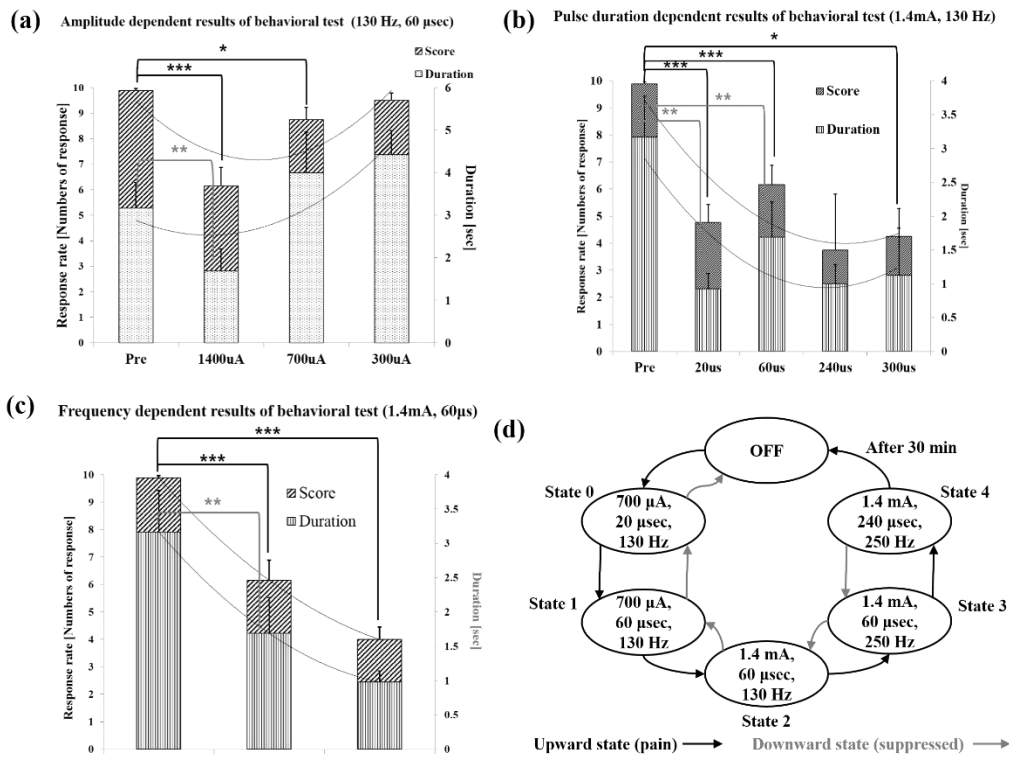


Figure 3-7. Changes in behavioral responses before and after DBS stimulation. Depending various stimulation parameters such as (a) amplitude, (b) duration, and (c) frequency, the behavioral responses were changed. From these behavioral results, 1<sup>st</sup> stimulation parameters for closed-loop control could be separated as (d). (Abbreviation: Score = results of von Frey test, Duration: results of duration test)

Table 3-2. *p*-value of statistical analysis on results of behavioral tests (Paired-*T* test)

Von Frey Test	Amplitude-dependent results (130 Hz, 60 μsec)			Duration-dependent results (1.4 mA, 130 Hz)			Frequency-dependent results (1.4 mA, 60 μsec)		
	0.3 mA	0.7 mA	1.4 mA	60 μsec	240 μsec	300 μsec	130 Hz	260 Hz	300 Hz
<i>p</i>	0.182	0.047	0	0	0.056	0.011	0	0	0.01
Star	-	*	***	***	-	*	***	***	**
Duration Test	Amplitude-dependent results (130 Hz, 60 μsec)			Duration-dependent results (1.4 mA, 130 Hz)			Frequency-dependent results (1.4 mA, 60 μsec)		
	0.3 mA	0.7 mA	1.4 mA	60 μsec	240 μsec	300 μsec	130 Hz	260 Hz	300 Hz
<i>p</i>	0.168	0.044	0.003	0.003	0.217	0.075	0.003	0.124	0.168
Star	-	*	**	**	-	-	**	-	-

### 3.2.2 Results of neural recording (Local field potential, LFP)

It was not easy to instinctively differentiate changes in raw recorded LFPs depending on painful stimulus (Figure 3-8 (a),  $N = 8$ ). We could isolate factors related to pain applying STFT method as Figure 3-8(b). We could classified differences before and after signal processing like STFT and averaging as shown in Figure 3-8. The changes in processed LFPs were different depending on their stimulation conditions such as amplitude, duration, and frequency as Figure 3-11. The delta-band LFP of 0.1 ~ 4 Hz was filtered and its changed levels of PSD was averaged. Statistical results of changes in LFPs related to pain depending on various DBS conditions were summarized in Figure 3-10 (a) ~ (c). We could observe that there were significant relationships between stimulation conditions and changes in level of PSDs of delta-band LFPs. The  $p$ -values of these analyses were listed in Table 3-3. Moreover, the changed neural response was remained for at least 20 sec after the end of the painful stimulus. Recorded and signal-processed level of PSDs increased its baseline and suppressed pain-related signal with DBS. Although electrical stimulation ended, the large impulse signals had been observed resulting from stimulation for 10 ~ 20 sec as Figure 3-11.

In addition, there was no significant differences in results of recording between bipolar and monopolar configuration as shown in Figure 3-9 ( $N = 4$ ). It was easier to differentiate neural responses related to nociceptive information from recorded and STFT-processed LFPs resulting from the bipolar configuration than from the monopolar system, if anything. Then, we used bipolar configuration for following implementation and applications of the CDBS system.

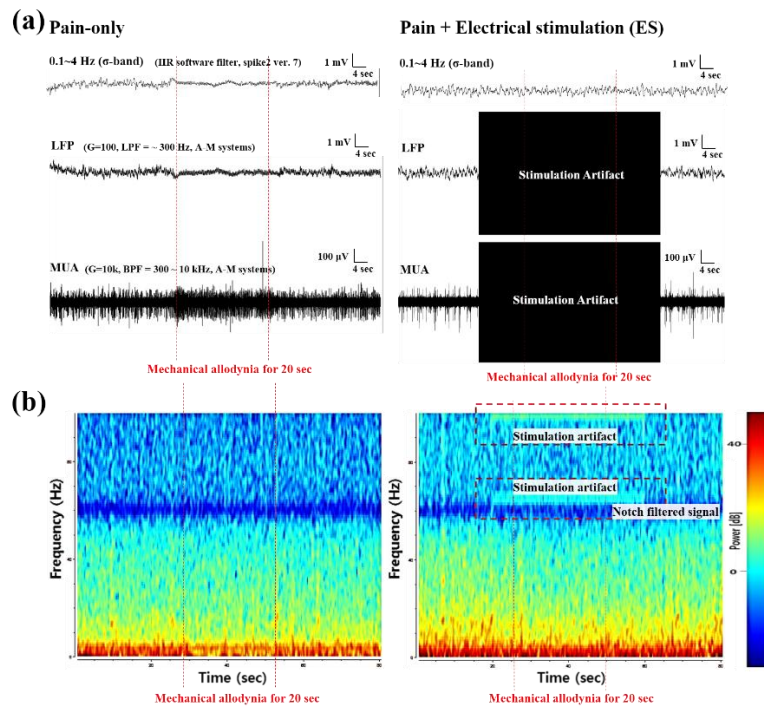


Figure 3-8. Changes in neural signals related to neuropathic pain. (a) Recorded RAW neural responses and (b) STFT-applied results.

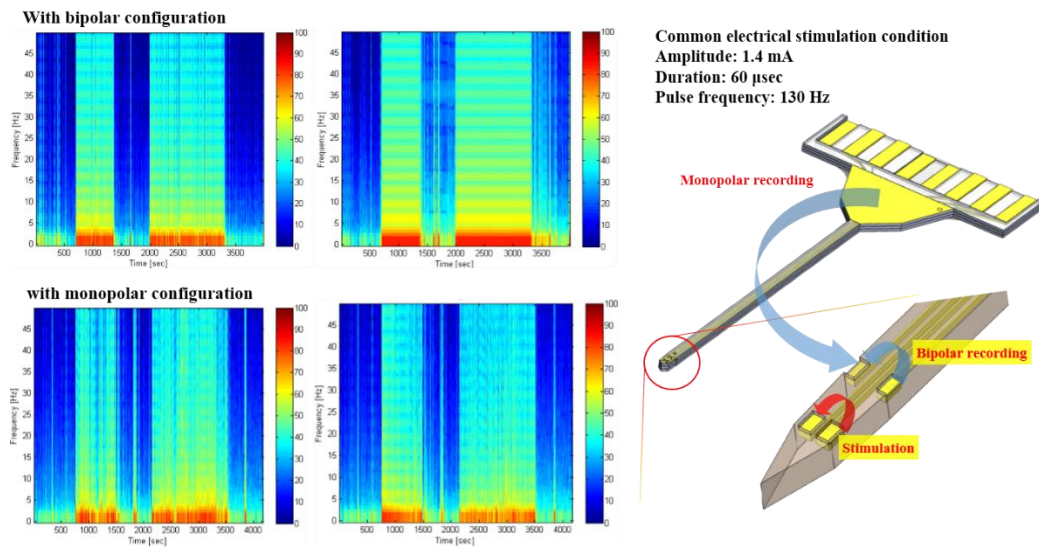


Figure 3-9. Results of neural recording with different configuration. There was no significant differences between monopolar and bipolar configuration. Then, we used bipolar configure for following CDBS experiments.

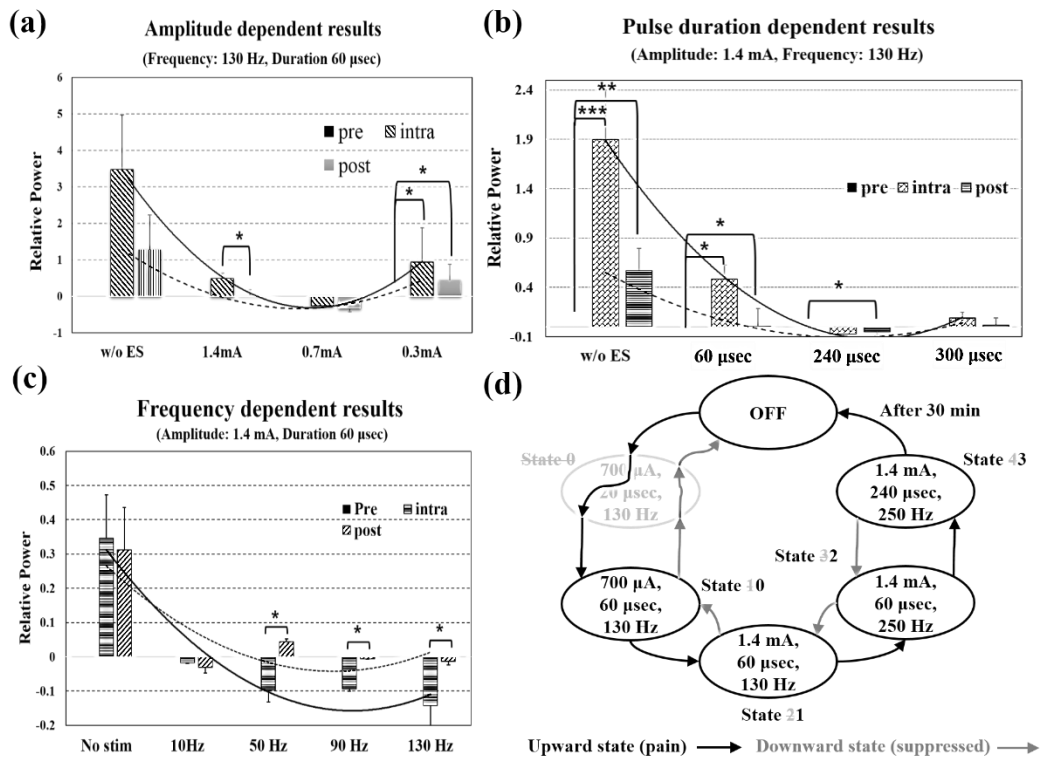


Figure 3-10. Changes in pain-related neural responses from VPL region before and after DBS stimulation. Depending various stimulation parameters such as (a) amplitude, (b) duration, and (c) frequency, the pain-related neural responses were changed. From these behavioral results, 2<sup>nd</sup> modified stimulation parameters for closed-loop control could be extracted as (d). (Abbreviation: Pre = before DBS, Intra = during DBS, Post = after DBS)

Table 3-3. *p*-value of statistical analysis on results of neural recording (paired-T test)

Parameters	Amplitude-dependent results (130 Hz, 60 µsec)						Duration-dependent results (1.4 mA, 130 Hz)						Frequency-dependent results (1.4 mA, 60 µsec)									
	0.3 mA		0.7 mA		1.4 mA		60 µsec		240 µsec		300 µsec		10 Hz		50 Hz		90 Hz		130 Hz			
<i>p</i>	I	P	I	P	I	P	I	P	I	P	I	P	I	P	I	P	I	P	I	P		
		0.003	0.015	0.031	0.108	0.191	0.519	0.004	0.046	0.022	0.018	0.17	0.014	0.91	0.282	0.248	0.39	0.005	0.014	0.037	0.068	0.022
Star	**		*		-		**		**		**		-		-		*		*		*	

\* Pre: Before DBS, I: During DBS, P: After DBS.

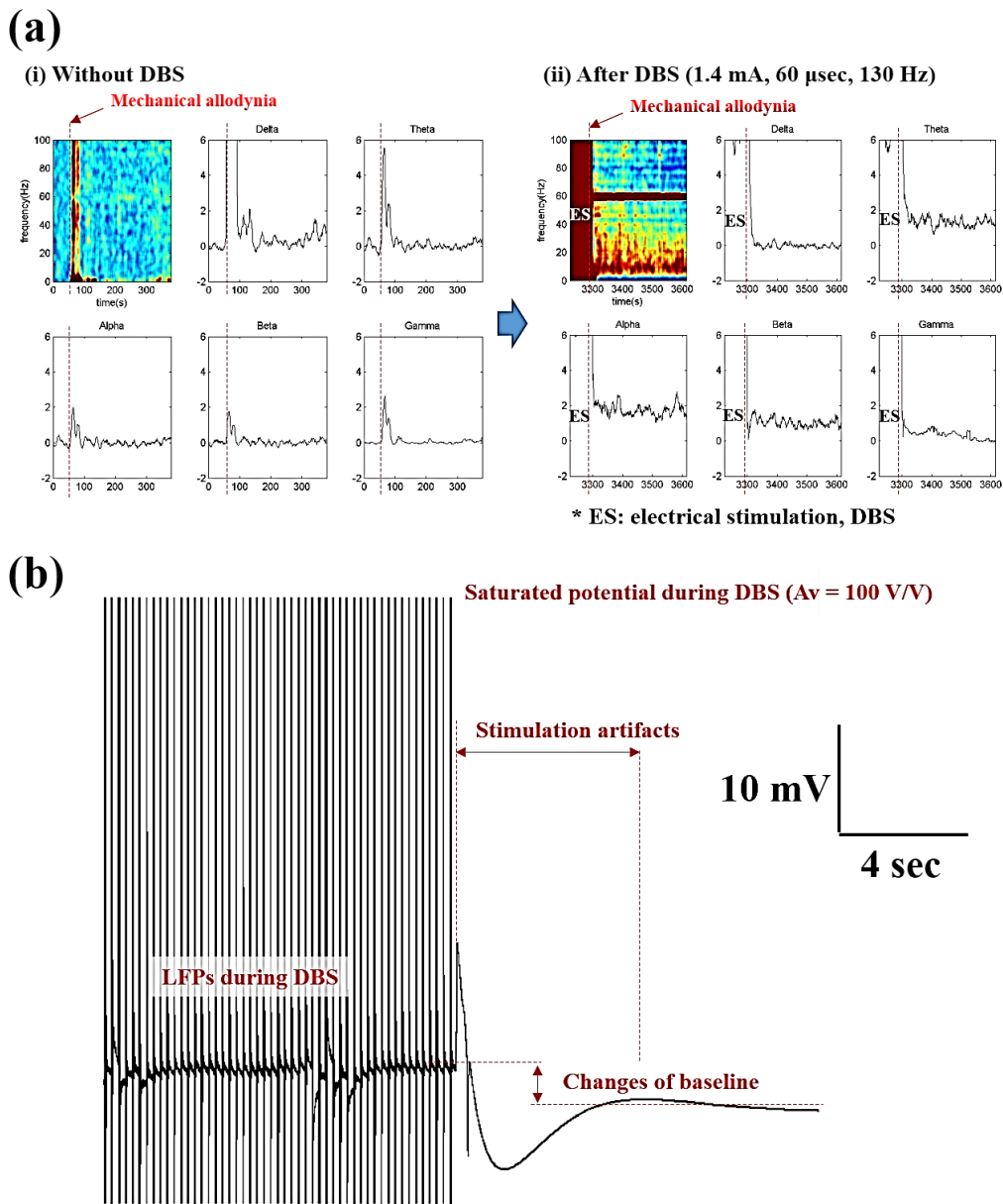


Figure 3-11 Changes in LFPs depending on painful stimulus and DBS. (a) Changes of power of LFPs before and after DBS (STFT-analysis applied results) depending on frequency-band, (b) changes of recorded raw signal. The tenable stimulation artifacts stood up to the end of DBS for 10 ~ 20 sec after DBS. The baseline changes in LFPs were observed during DBS ( $N = 8$ ).



### 3.2.3 Results of correlation analysis (Pearson analysis)

We performed correlation analysis between results changes in average PSD level and scored results of each behavioral depending various stimulation parameters of Figure 3-7 and 3-10. The correlation could be characterized with the qualification values of correlation called Pearson's correlation  $r$ -value. Consequentially, duration and frequency showed high correlation of  $r$ -value over 0.9996 comparison to low correlation of amplitude as shown in Table 3-4.

Table 3-4. Results of correlation analysis (Pearson's coefficient:  $r$ -value)

	Amplitude dependency	Duration dependency	Frequency dependency
Von Frey test	0.0519	0.9926	0.9996
Duration test	-0.0776	0.9985	0.9998
Star	-	**	***
Results	None or very weak	Strong correlation	Strong correlation

\* All values describes the correlation with the changes of neural recording for each conditions.

### 3.2.4 Results of histological study

After 6-week deep brain stimulation experiments, we performed histological study to verify the inserted position of the electrode in the rodent brain. After obtaining brain slice samples, we could confirm that the electrodes were successfully located at VPL by cresyl violet staining as shown in Figure 3-12. The electrode was vertically and straight inserted into VPL region. Since the electrodes were not bent in the brain, the electrodes were minimally invasive as much as possible in the brain.

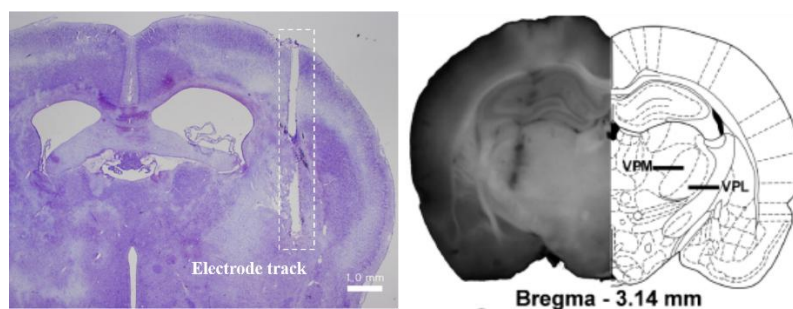


Figure 3-12. Results of histological study and the rodent brain atlas.

### **3.3 Closed-loop stimulator**

The effective stimulation parameters for neuropathic pain determined from results of preliminary experiments are important information for closed-loop control. In addition, we confirmed that the objectivity of changes in delta-band LFPs reflected nociceptive information that could be used as neural signal index for closed-loop control. From those data, the default stimulation parameter, upper bound, and lower bound of stimulation conditions were also determined. Based on the developed CDBS strategy, the prototype system was developed. We examined the performance of the developed system and applied for *in vivo* experiments.

#### **3.3.1 Developed closed-loop deep brain stimulation strategy**

We determined the finite state machine of stimulation parameters for closed-loop control of the CDBS system reflecting results of preliminary experiments of section 3.2 as shown in Figure 3-7 (d) and 3-10 (d). The finally determined FSM was shown in Figure 3-13. The final FSM was established considering high significances of results. We attached more weight to results of behavioral tests than those of neural responses. In addition, the higher level of states means that the higher amplitude, duration, and frequency.

The average response time of local field potential for stimulation was known 40 ~ 50 msec [144]. The effective stimulation time for neuropathic pain was empirically 0.5 ~ 5 min in animal behaviors (however, time of changes in neural signal was 5 sec) after electrical stimulation on motor cortex or deep brain [141, 145, 146]. The FSM was determined reflecting this empirical transition time of neuropathic pain, but we tried to implement the closed-loop system with the shorter response time including recording, ADC sampling, STFT, averaging, and stimulator control than average response time of local field potential of 40 ~ 50 msec.

The system stored the reference level of averaged PSD during the resting state, and then it derived stimulation pulses when the level of PSD was changed with the preset

rate by the fitting program. If there were no significant changes in the PSD level with DBS, the controller adjusted the state of FSM to upper state (higher stimulation condition). This tendency of changes in delta-band LFPs was generally downward by electrical stimulation as shown in Figure 3-11 (b). If the averaged PSD level decreased by DBS, the stimulation state was changed as lower level or off in the end.

Moreover, the sampled LFPs by the internal ADC module of MCU was frequently saturated due to the increasing baseline potential by electrical stimulation and the limitation of the sampling range of the ADC with a default gain ( $A_v = 100\sim 1000$  V/V) of the preamplifier during DBS period. This could cause essential problems to closed-loop control in the stand-alone mode of the closed-loop DBS (CDBS) system such as signal processing and power control of deriving stimulation pulses based on processed LFPs. For solving this problem, controlling the gain of variable gain amplifier (VGA) of Figure 2-16 (b) in section 2.3.3 to decrease the gain as 1~100 V/V and compensating the decreased gain by embedded software in the MCU module were applied.

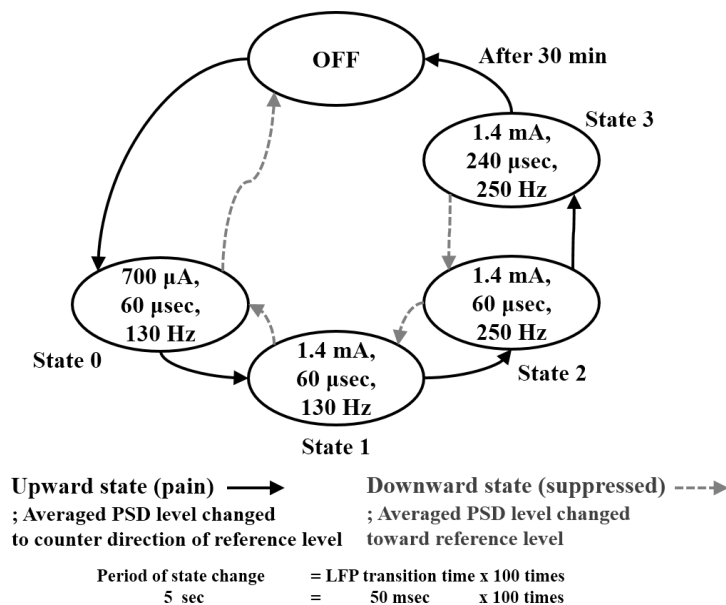


Figure 3-13. Final finite state machine (FSM) for controlling prototype CDBS system for neuropathic pain control. Depending on recorded and signal processed potential of LFPs, stimulation parameters should be adjusted according to this FSM. The period of state change was determined using the empirical state transition time of 5 sec.

### 3.3.2 Developed prototype closed-loop stimulator

We developed the prototype closed-loop DBS (CDBS) system based on the developed closed-loop strategy of section 3.2.2 as shown in Figure 3-14 (a). The size of the developed system was 70 mm (W) x 100 mm (D) x 34 mm (H). The center of the system was for a main controller (microcontroller unit, MCU) using an ARM core-based evaluation board. Top and bottom modules are organically connected with the centered controller module. The bottom module was for neural recording including LFPs (0.1 ~ 20 Hz) and spikes (300 ~ 10 kHz). The bottom included preamplifier with a VGA, two kinds of filters with source followers for each, a comparator for spikes, and power regulation circuitry for supplying power to the whole systems. The top module was for the stimulation including a custom designed stimulation chip and peripheral circuits. Each channels of the DBS electrode was connected according to its purpose; channel 1 and 2 were on the top module for DBS, and channel 3 and 4 were connected to the bottom module for recording as shown in Figure 3-14 (b).

The stimulation parameters such as amplitude, duration, and frequency were programmable and adjustable. The response time of the CDBS system from recording LFP to adjusting stimulation conditions was 12.5 msec (50 msec was required for processing and restoring the level of the resting potential at the first operation).

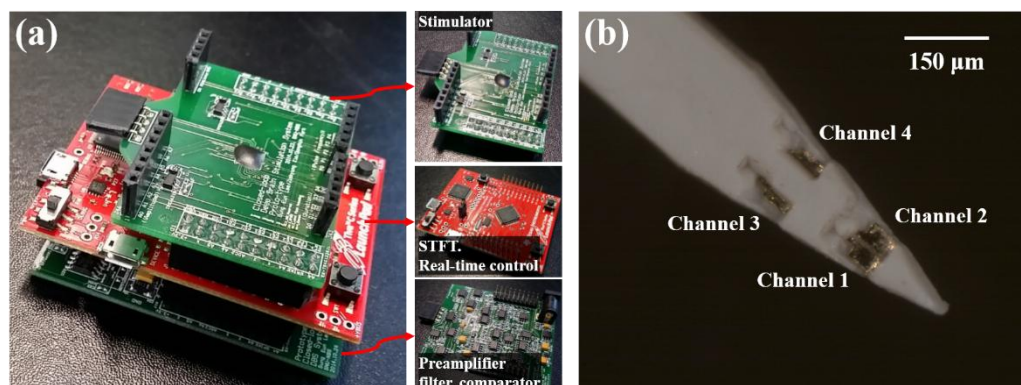


Figure 3-14. Implemented prototype CDBS system for neuropathic pain. (a) CDBS device and (b) the electrode channels for CDBS.

### 3.3.3 Results of performance measurements

As aforementioned in section 2.3.4, we performed the performance measurement before *in vivo* application. The experiment environment was shown in Figure 3-15 (a). Figure 3-15(b) showed results of performance measurement. The developed prototype CDBS system stored the averaged PSD of resting state for 30 sec as reference signal for comparison. The CDBS system controlled to derive stimulation pulses during pain period. The response time of the system for closed-loop control was 12.5 msec (worst case was 50 msec). The CDBS system successfully turned off the stimulation pulse after 3 sec from the end of painful stimulus.

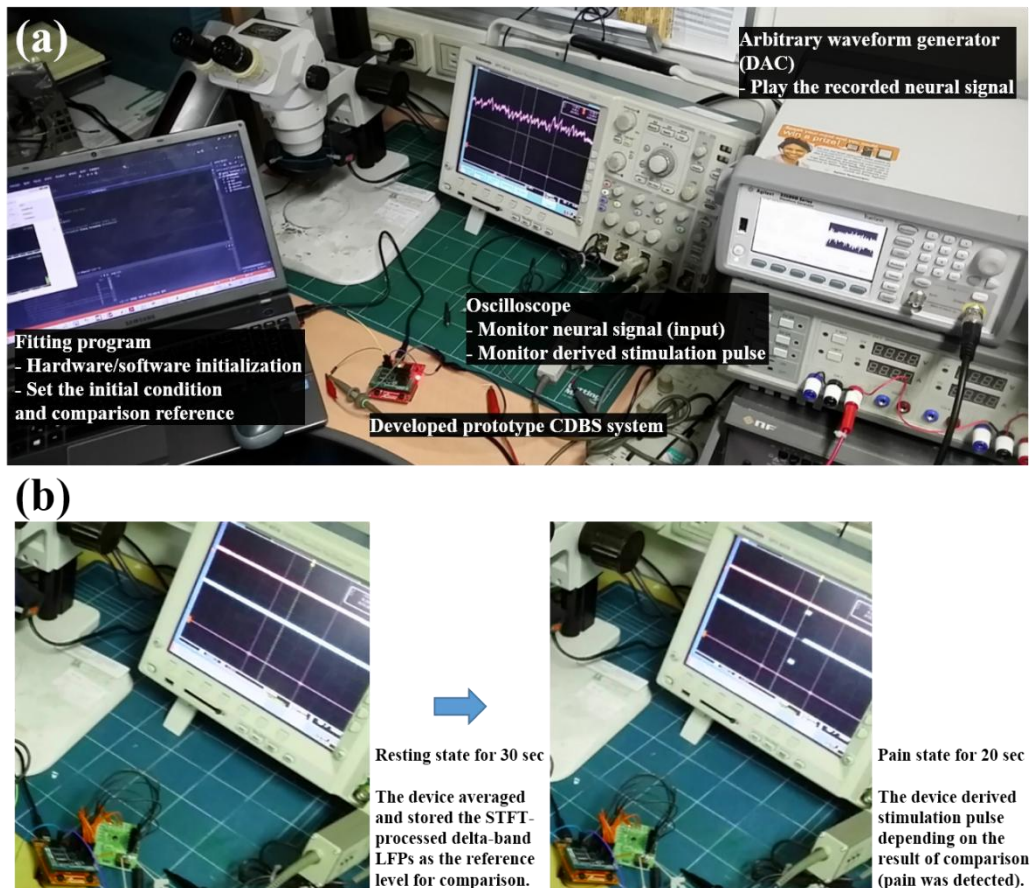


Figure 3-15. Results and test environment for performance measurements of the developed CDBS system for neuropathic pain. (a) Measurement environment and (b) results of measurement.

### 3.3.4 Results of *in vivo* experiments

We performed *in vivo* experiments applying the developed system with same environments as preliminary experiments. The experiment environment and results were described in section 2.3.5 and in Figure 3-16, respectively. The CDBS system operated according to the developed CDBS strategy for neuropathic pain as section 3.3.1. First, the averaged PSD of resting state had been continuously stored for established period by the fitting program. The system continuously updated the reference level of averaged PSD of the resting state after DBS, when there were no significant changes in LFPs for established period. Second, the CDBS system derived stimulation pulse with short response time of 12.5 ~ 50 msec. Third, the CDBS system controlled the gain of VGA to decrease during DBS as the developed control strategy. The system compensated the decreased gain by the embedded software. Fourth, the CDBS system ignored changes in neural signal for 30~40 sec after stimulation because it was require to restore base neural potential after stimulation as shown in Figure 3-11 (b). Finally, the system restored the gain of VGA to its initial condition after DBS. The reference PSD level of the resting state was also re-updated if there was no significant changes in PSD level for the established period that was previously set by the fitting program. In this way, the neuropathic pain was successfully suppressed by the developed CDBS system and the system was automatically controlled (negative feedback on nociceptive information).

Table 3-5. System response time

<b>Function</b>	<b>Required time to function</b>
<b>Analog to digital convertng (sampling)</b>	5 [ $\mu$ sec]
<b>Short time Fourier transform (STFT)</b>	10.25 [msec]
<b>Averaging</b>	1.2 [msec]
<b>Comparing the FSM</b>	< 1 [ $\mu$ sec]
<b>Control signal generation</b>	< 1 [ $\mu$ sec]
<b>Other works</b>	43 [ $\mu$ sec]
<b>Total response time</b>	12.5 [msec]

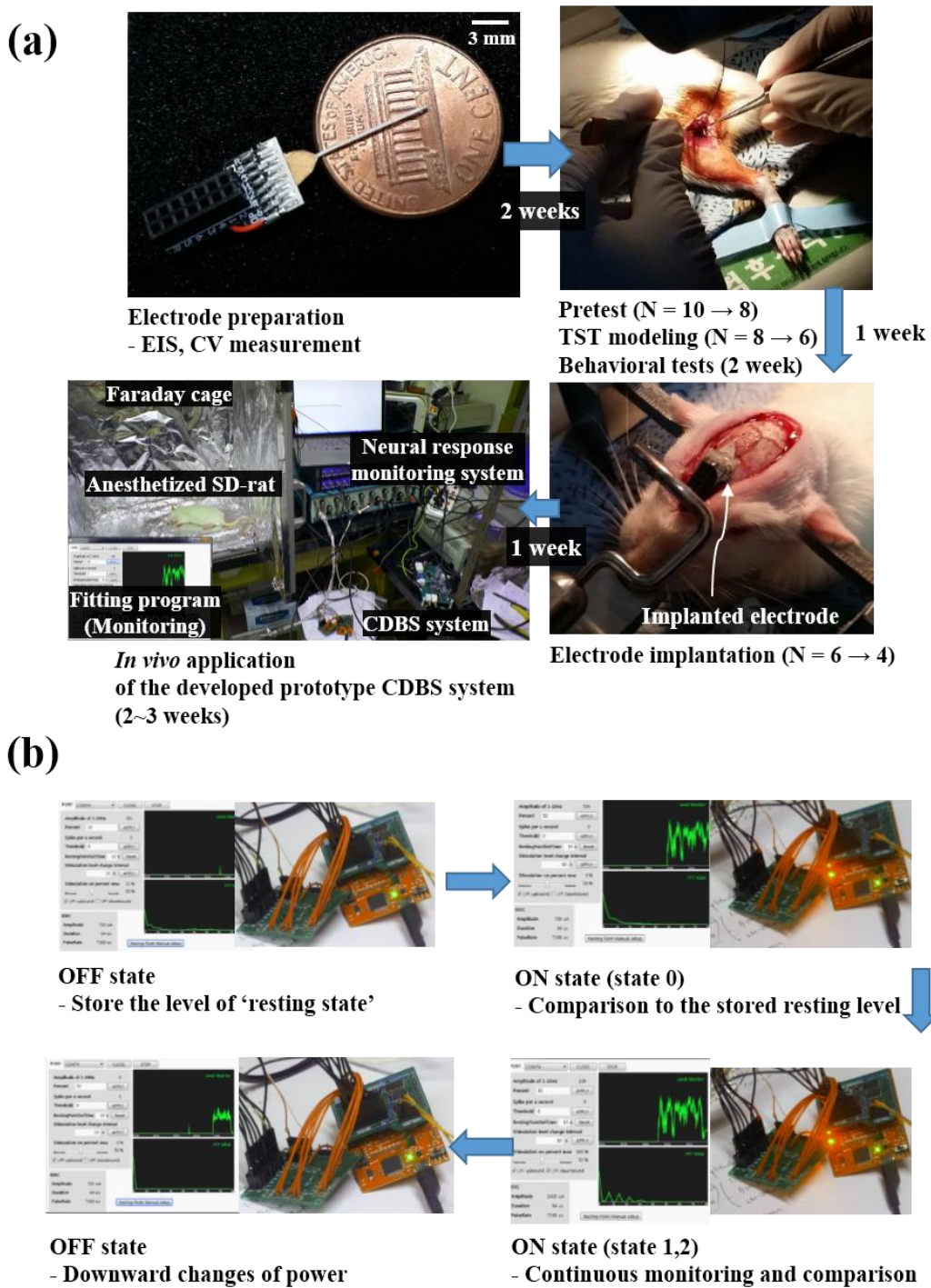


Figure 3-16. *In vivo* performance tests of prototype CDBS system for neuropathic pain. (a) Whole procedure of experiments. (b) Results of *in vivo* tests. The stimulation state was ordinarily adjusted depending on the change of recorded and processed LFPs.

## ***4. Discussion***

---

***4.1 Improved LCP process for multiple LCP layers***

***4.2 Volume of tissue active issues***

***4.3 Correlation analysis***

***4.4 Closed-loop stimulator***

***4.5 Gliosis***



## 4.1 Improved LCP process for multiple LCP layers

There were several reasons that conventional LCP process has low yield for developing LCP-based depth-type electrodes. (1) Blockage problems after lamination process due to the melt down of LCP substrate and preformed contact holes on a cover LCP layer was a major reason. (2) Some pads for contacts and connectors were not exposed due to misalignments between cover and substrate layers. (3) There were several failures during the final laser cutting process. It was because misalignment during laser micromachining process. In general, the laser machine had used circle shaped metal patterns of 1 mm in diameter at the corners of LCP substrates. However, several thermal processes could cause local thermal-expansion upon the polymer during LCP fabrication process. For example, E-gun evaporation, bake process for lithography, and O<sub>2</sub> plasma process could cause the thermal expansion of LCP. LCPs that were used in this study has thermal expansion coefficients of lower than 0.2 % HAS (Hot air shrink 180 °C, 30 min) and lower than 0.2 % BWS (Boiling water shrinkage, 180 °C, 30 min).

The laser ablation process for small sized contacts which was suggested by our group's previous work [129] could be a solution of the problem (1). Separately, for multilayered process, a precise alignment method of multiple LCP layers should be required to solve problem (2) and (3). Although all LCP layers were applied for the same LCP process for metal patterning, there might be variance of thermal-expansion in each LCP layers. It means that the probability of misalignments could increase. Applying the suggested new layer arrangement and interlayer alignment method for multiple LCP layers, the failure rate remarkably could decrease during lamination, laser drilling, and final laser cutting process to achieve high yield. Practically, the yield of electrode was improved from about 30 % to over 69 % in this study. Of course that the throughput was reduced because the frequency for alignment increased.

The improved LCP process is outstanding process to implement double side-electrode with simplification and high reliability comparison to other material-based processes [147, 148]. An enhanced method for multiple LCP layers including metal

pattern arrangement and interlayer alignment methods of this study could contribute to fabricate double side electrodes. For example, three layers (Cover + M1 + M2) and the other three layers (M2 + M1 + Cover) could compose the double-side electrode as shown in Figure 4-1.

The new alignment method has still limitations. At over the melting point of LCP which is higher temperature than the liquid crystal point, the LCP was melted and filled in the LCP align-key patterns as Figure 4-2 (a). Solving this problem, laser ablation process was additionally applied after lamination step using other align-keys to expose buried align-keys. Then, follow-up laser drilling and final laser cutting process were performed using the exposed align-keys. Nevertheless, metal align-keys could be broken away from its original position due to excessive power or frequency of laser patterns during laser ablation process upon metal align-keys as Figure 4-2(b). The broken align-keys could cause misalignment problems. To solve this problem, we optimized recipes of laser process as shown in Table 2-3. We optimized the recipe by the more number of patterns rather than the more power of laser. We relatively decreased the frequency of laser pattern to guarantee enough time for cooling down heated metal patterns.

We considered newly suggested align-keys for interlayer alignment method to apply to industrial laser machine for mass production (or improvement the throughput). In general, flexible PCBs or flat cables using polyimide or other flexible materials are fabricated using laser milling, drilling, and cutting process in industries. We frequently used industrial laser machines of LPKF Laser & Electronics (Garbsen, Germany) that require several circle patterns of 1 mm in diameter for auto-alignments. That is why we designed cross line patterns in a circle of 1 mm in diameter. If this align-key was used for auto-alignment process, the throughput could be improved.

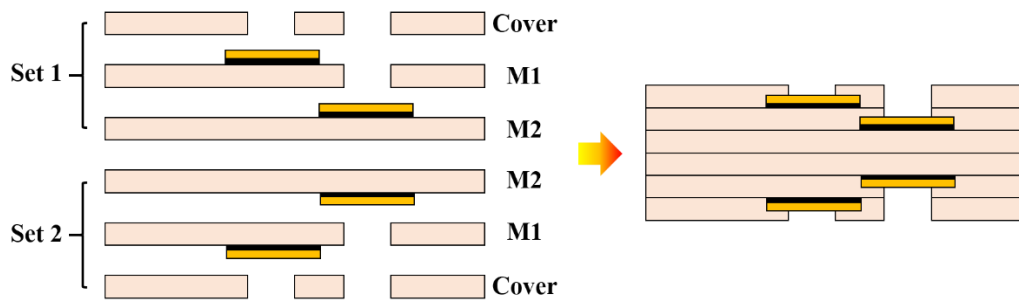


Figure 4-1. Layer arrangement for double-side LCP-based electrode based on the improved LCP process for multiple LCP layers of this study.

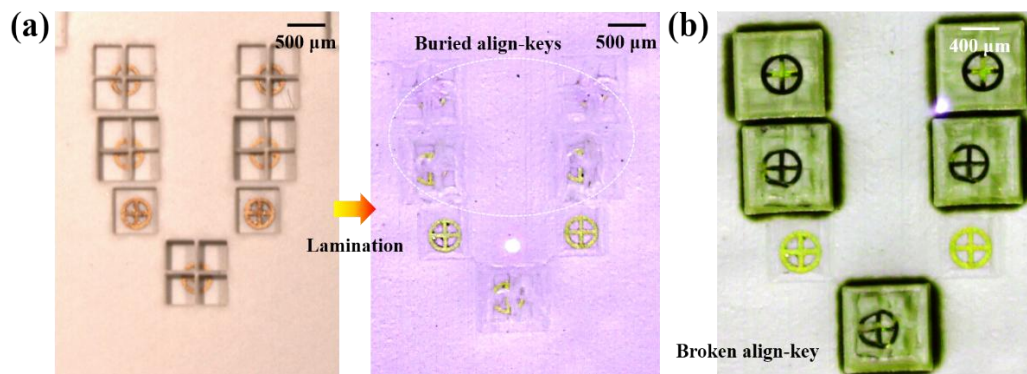


Figure 4-2. Problems during new interlayer alignment method; (a) buried LCP align-key structures after the lamination process and (b) transformation of metal align-keys during laser ablation process.

## 4.2 Volume of tissue activated (VTA) issues

In this study, we suggested the newly designed electrode structure and fabrication process implantable DBS electrode as well as surgical procedure for electrode implantation. The electrode should be strongly fixed on the skull during implantation. Moreover the developed surgical tools and procedure were compatible to conventional stereotaxic tools for precise electrode implantation. The electrode was accurately implanted into VPL region and fixed for 4~6 weeks without severe tissue damage using the developed surgical tools as shown in Figure 2-6 and Figure 2-15. We performed preliminary experiments and *in vivo* application several times of the prototype CDBS system including the multichannel DBS electrode. Various pressing forces were applied on the interface board and connector due to frequent experiments. Although there was not breakaway of the electrode from the brain, it could cause some wounds and inflammation on sutured region. It could be naturally solved if the whole system was minimized to be fully implantable.

Furthermore, we designed structure of the DBS electrode reflecting results of simulation. Comparison to a commercial electrode using simulation parameters of Table 2-2, the designed LCP electrode showed smaller VTA than the volume of VPL region in the brain by the default stimulation condition (Amplitude: 0.7 mA, frequency: 130 Hz, duration: 60  $\mu$ sec). However, the result of simulation could be different from empirical data due to several assumptions of this simulation. First, the simulation parameters for tissues of Table 2-2 were not exact value for brain. Second, the formula for calculating VTA was for cellular model [127], but not for tissue level. If there were accurate tissue modeling for rodent VPL region, the more practical VTA could be acquired. Finally, each brain regions of brain has its own electrical characteristics such as conductivity, permeability, density, and so on. These factors could change the result of simulation such as VTA and impedance of double layer [149, 150]. If these were applied for practical simulation, it could be possible to design a novel DBS electrode for localized stimulation with high spatial resolution as shown in Figure 4-4. For example, there was the similar

research for artificial retinal implant called a hexagonal electrode for bipolar stimulation for retina as shown in Figure 4-5 [151].

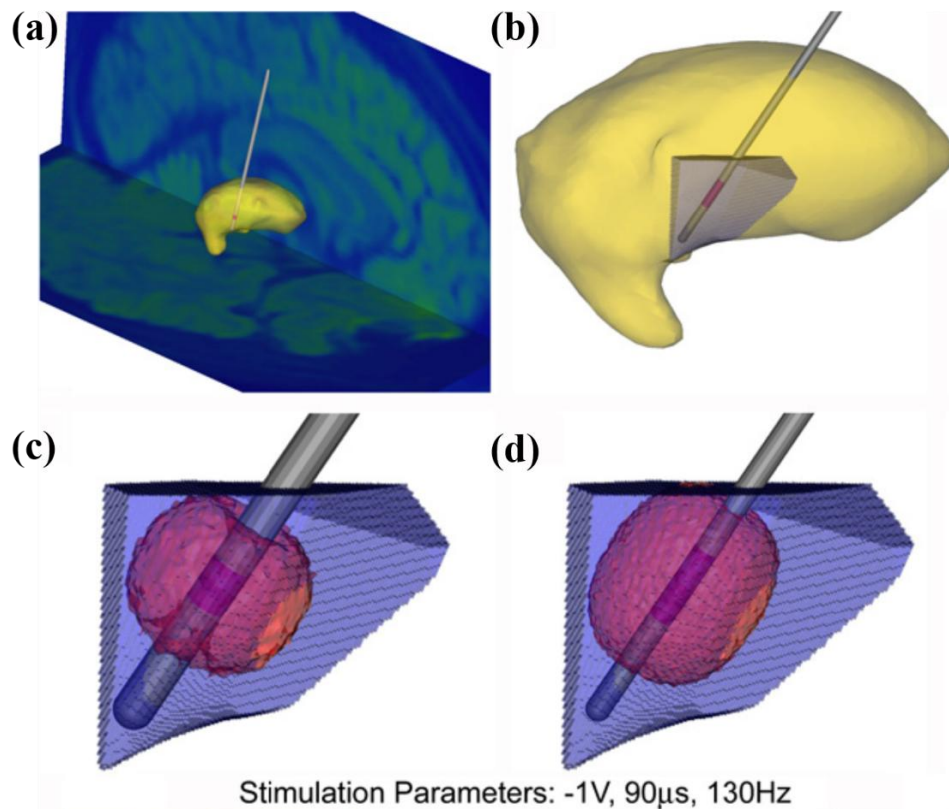


Figure 4-3. Results of TVA simulation for Thalamic VIM stimulation. (a) 3D view of thalamus with DBS electrode and T1 MRI projected onto background slices. (b) VIM with a DBS electrode. (c) The Medtronic electrode with stimulation (26% of the VIM). (d) The VIM is better stimulated using an electrode with 0.75 mm diameter and 2.54 mm height, producing a VTA (33% of the volume) [150].

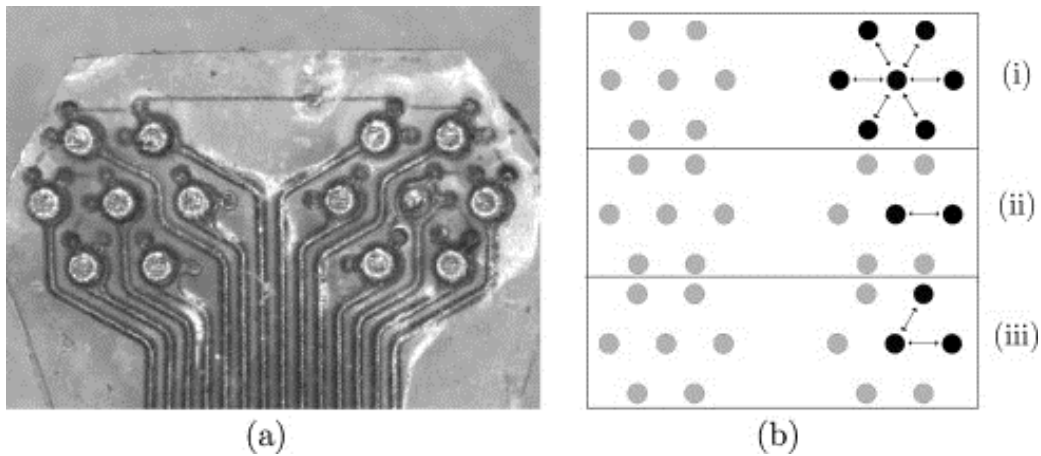


Figure 4-4. Hexagonal electrode design and its various stimulation scheme. (a) The 14-channel platinum stimulating electrode array tip. Electrodes are grouped into two hexagons with the circular contacts with a diameter of 230  $\mu\text{m}$ . (b) The electrode can be used to stimulate in three different electrode configurations, (top) six-return electrodes, (middle) a single-return electrode, and (bottom) two-return electrode stimulation. These configurations can be moved so that any electrode can act as the stimulating or return electrode [151].

### 4.3 Correlation analysis

We considered the correlation analysis between changes in local field potential and changes in behavioral responses to neuropathic pain as very meaningful. It is because there was no researches that determined the objective neural signal index from the recorded and processed neural responses reflecting the nociceptive behaviors. This study could play a major role in connection among several results of previous pain-related researches using behavioral tests [32, 34, 139] and neural response monitoring [119]. In addition, we worked for trying to develop a closed-loop system for neuropathic pain based on the principle studies. Moreover, we tried searching effective DBS parameters for neuropathic pain control such as amplitude, duration, and frequency through preliminary experiments of section 2.2 and 3.2. We developed the FSM of stimulation parameter based on the effective stimulation parameter and applied for implementing the

CDBS system for neuropathic pain control. As a result, the system operated for suppressing pain (negative feedback), and then the system successfully turned off stimulator near the end of the painful stimulus. From statistical results of preliminary experiments, amplitude had low correlation between changes of neural responses and animal behaviors. Duration and frequency had strong relationship to reduce the pain, but the amplitude did not have according to results. If we examined more conditions of amplitude, it could be available to observe 'correlation'. It is required to apply more various amplitude conditions to animal experiments using high-resolution stimulators.

In addition, the tendency of changes in neural response against painful stimulus in this study was opposite to results of Bae's [141]. The almost results of preliminary experiments ( $N = 18$ ) were different even with the results of the first trial ( $N = 6$ ). In this study, the averaged power spectral density (PSD) level of LFPs related to pain increased during mechanical stimulation in delta-band (0.1 ~ 4 Hz), theta-band (4 ~ 7 Hz), and alpha-band (7 ~ 15 Hz). Whereas both Bae [141] and the first trial of preliminary experiment that used urethane for anesthesia showed different results from the other preliminary experiments during pain period. It could be different effects relating to anesthetic drugs or excipients for anesthesia such as atropine that was used to reduce airway secretion in this study. Kramis *et al.* [152] demonstrated that there was no significant differences in lower band LFPs using pentobarbital and urethane for anesthesia, but atropine could influence on activities of lower band of LFPs. Same additional experiments without atropine anesthesia or only with urethane anesthesia are required in the future. If the tendency of neural responses was same as the Bae's results [141], the results of correlation analysis would be slightly different. Although the strength of correlation was same as the results of Table 3-4, the characteristics of correlation would be 'strong anti-correlation' Reflecting these different tendencies, we implemented the prototype CDBS system for neuropathic pain control of this study operates in these two kinds of changes in LFPs (downward and upward changes in PSD of lower frequency band LFPs).

## 4.4 Closed-loop stimulator

### 4.4.1 Correction method based on neural spikes

Although the spike-based correction method was implemented for closed-loop control as shown in Figure 2-20 and 2-22, it could not be used for practical experiments. It was too difficult to capture the neural spike during preliminary experiments. Spikes could be recorded just twice from SD-rat of No. 6 of 1<sup>st</sup> preliminary experiment as shown in Figure 3-8(a) ( $N = 2$ ). Even the recorded spikes were vanished after 2 weeks. It was not enough to apply as correction methods for closed-loop control. If the correction method was applied as we expected, the accuracy of the closed-loop control could be improved [153]. Bae [141] and results of 1<sup>st</sup> trial of preliminary experiments of this study (Figure 3-8(a)) showed general changes in spikes during pain period. Rate of spikes increased during pain stimulus. If the signal processing using (Eq. 5-1) was applied, it would be available to improve the accuracy of the CDBS system for neuropathic pain.

Signal index

$$= \left\{ \begin{array}{l} \text{Changed rate of spikes} \times \text{Rate of changed PSD in LFPs (upward change)} \\ \frac{\text{Changed rate of spikes}}{\text{Rate of changed PSD in LFPs (downward change)}} \end{array} \right. \quad (\text{Eq. 5 - 1})$$

### 4.4.2 Power consumption

In addition, for implementing the CDBS system, an ARM M4 module (lower power consumption module among ARM cores and high performance ADC of 2 Msps, power consumption = 93.39 mW) and preamp/filters used commercialized discrete components including OP Amps (AD620, LF441 and LTC6910-1 required 4.29 mW, 1 mW, and 34.1 mW for normal performance, respectively) were used. Although the performance of the MCU was sufficient to analyze and process recorded signals, internal ADC has the lower limitation of input voltage range that required DC-offset. There was problem that the signal below of '0 V' was sampled as '0' without offset voltage. Then, the DC offset



adder circuit and compensation function was used in embedded software as shown in Figure 4-6 was used to add offset level for identifying sampled LFPs and analyzing. However, because of its offset, there were other problems such the upper limitation of input range and frequent saturation. Besides, because of addition of trimmer and VGA circuits (LTC6910-1, 34.1 mW), the system became larger and required more power. If whole functions including amplifier, filter, ADC, and microcontroller for signal processing and system control were integrated into an integrated circuit (IC) such as RHD2000 (Intan technology, CA, USA) as Figure 4-6.

#### 4.4.3 Size of the system

The developed prototype CDBS system in this study was 70 mm (W) x 100 mm (D) x 34 mm (H) which was too large to be fully implanted. Then, the minimization of the system is essentially required as an implantable system. As section 4.4.2, if the IC filter and ADC modules that are specified for neural signal recording were used, the system could be smaller than before. If it is possible to integrate whole functions with the wireless power transmission method into an IC, head mountable CDBS system could be also available as shown in Figure 4-7.

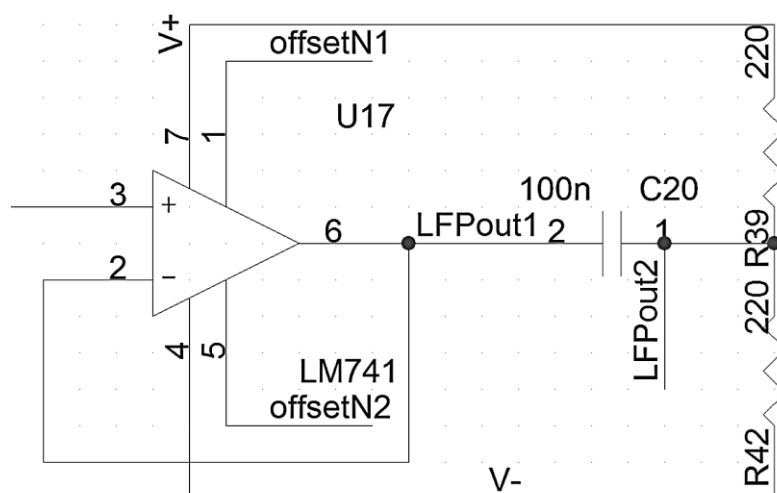


Figure 4-5. Compensation circuit for DC offset.

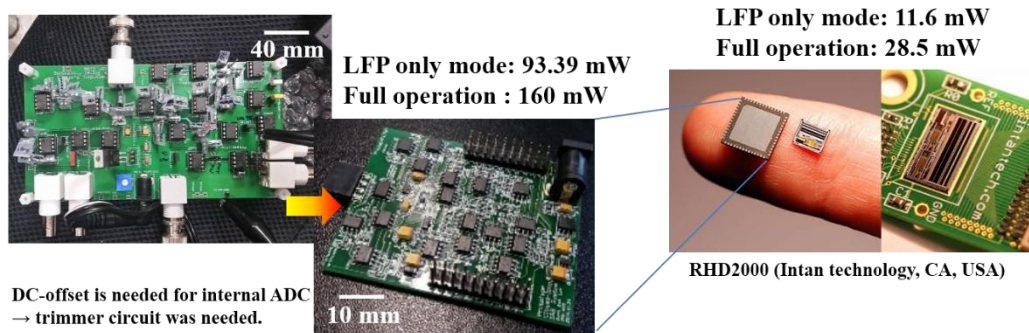


Figure 4-6. Integrated circuit-based CDBS system.

#### 4.4.4 Response time of closed-loop control

The developed CDBS system operated with the average response time ( $T_c$ ) of 12.5 msec (50 msec was firstly required for setting reference level of resting state). As aforementioned in section 3.3.1, the determined closed-loop FSM was considered to have shorter response time (recording, ADC sampling, STFT, averaging, and stimulator control, Figure 4-7(b)) than the average transition and transport time of local field potential (40 ~ 50 msec, Figure 4-7(a)) as shown in Figure 4-7. The slowest step was ‘short time Fourier transform (STFT, 10.25 msec) and moving averaging (1.2 msec)’. The maximum capacity of internal ADC of microcontroller was 20,000 samples/sec and sampling data was applied to STFT function for signal processing every 5  $\mu$ sec. This frequency was conservatively selected because the focused frequency band of LFP was only lower than 20 Hz (delta-, theta-, and alpha-band) filtered by a hardware low pass filter. For ADC sampling, the minimum sampling frequency without antialiasing is 51.2 Hz for raw signal of 20 Hz. Then, the signal processing was performed with four moving windows of sampled LFP signals every 10.25 msec as shown in Figure 4-7. By applying the thread method for signal processing and control the stimulator, we could prevent the data bottleneck phenomenon that causes the system down. If the more efficient STFT algorithm and effective signal process set were applied, the shorter response time for each time block of Figure 4-7 could be achieved.

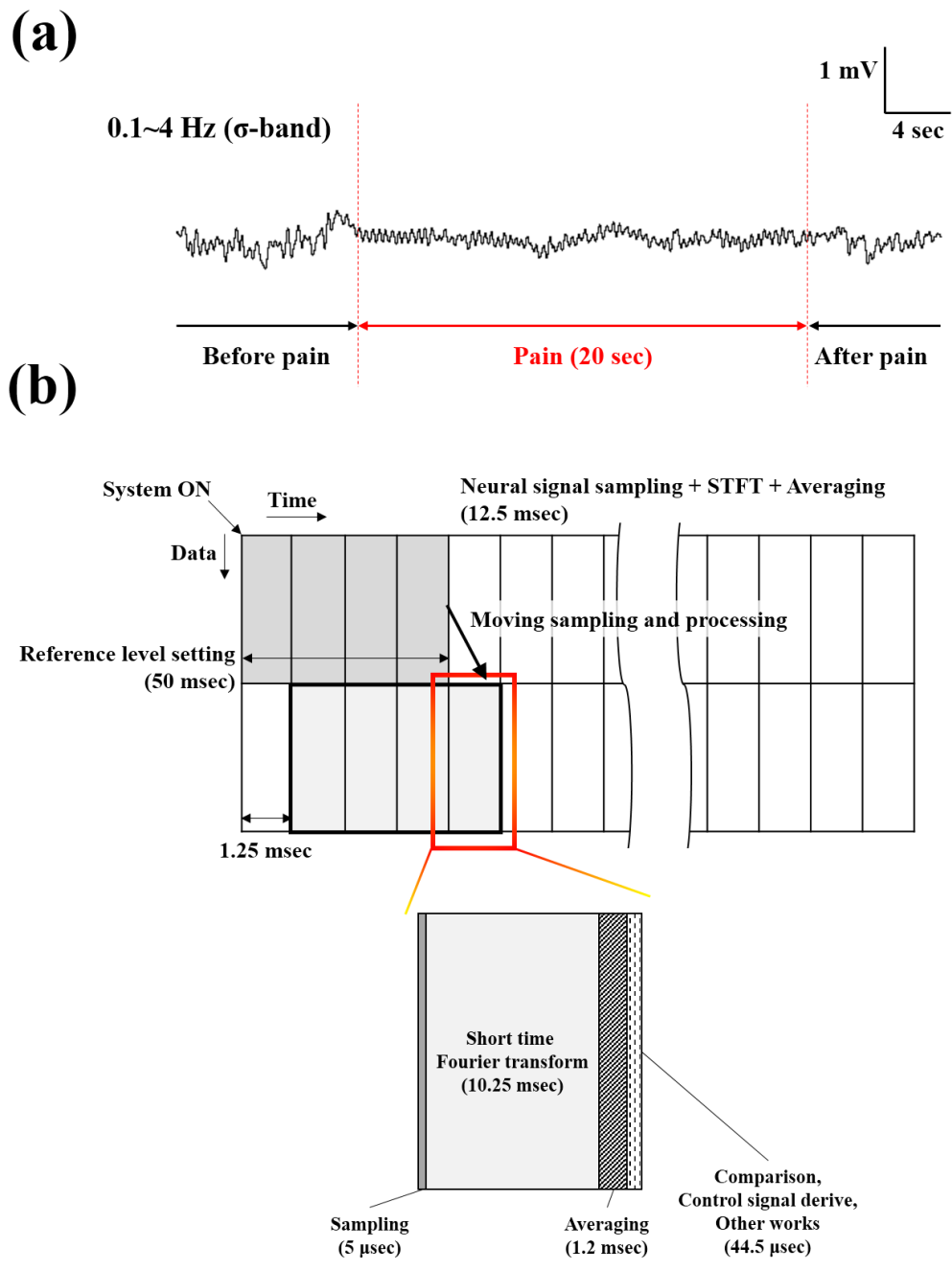


Figure 4-7. Comparison of changes in LFP and system response time. (a) LFP changes during pain stimulus (recorded during preliminary experiments) and (b) composition of system response time for closed-loop control.

## 4.5 Gliosis

Chronically implanted recording electrode arrays linked to prosthetics have the potential to make positive impacts. However, the developed LCP-based DBS electrode as an invasive electrode, it can cause gliosis. Gliosis is a nonspecific reactive change of glial cells in response to damage to the central nervous system (CNS) including brain. In most cases, gliosis involves the proliferation or hypertrophy of several different types of glial cells, including astrocytes, microglia, and oligodendrocytes. In its extreme form, the proliferation associated with gliosis leads to the formation of a glial scar. Current theories hold that glial encapsulation (gliosis) insulates the electrode from nearby neurons, thereby hindering diffusion and increasing impedance [154, 155], or extends the distance between the electrode and its nearest target neurons [154].

Our group have been researched not only tissue response during device insertion, but also the effective electrode design and insertion condition for minimal damage [131, 155]. Previous studies demonstrated that faster insertion of sharp devices resulted in lower mean effective strain. Moreover, tip geometry had little effect on the tissue damage with hundreds-micrometers-level devices [131]. As other groups' trials, there are various efforts to reduce tissue responses such as optimized electrode design, optimized implantation procedure [131], applications of biocompatible materials for the insulating layer [156], and application of microfluidics [157]. It could be possible to apply various techniques above for LCP-based devices to improve biocompatibility [158]. It is our hope that a rational approach to limiting or eliminating the foreign body response in the CNS through biologically active mediators will augment implant designs and overcome the obstacles to introducing chronic CNS implants into the clinic by the future works.

## ***5. Conclusion***

---

We developed a prototype closed-loop deep brain stimulation system for neuropathic pain. For implementing the system, we identified and validated the neural signal index and effective stimulation parameters by preliminary experiments including behavioral tests and neural signal recording. Correlation analysis between changes in local field potential and changes in animal behaviors against the painful stimulus gave scientific objectivity to the use of changes in local field potential as a neural signal index for closed-loop control. In addition, we implemented the prototype CDBS system including a multichannel CDBS electrode and a closed-loop stimulator. For this implementation, we improved LCP process and closed-loop control algorithm that automatically adjusts the stimulation parameters based on results of preliminary experiments. The developed CDBS system for neuropathic pain control was applied for *in vivo* experiments to validate its functionality and efficacy.

### **Achievements**

- 1) We developed fundamental technologies for developing a closed-loop deep brain stimulation system for neuropathic pain such as an improved LCP process and closed-loop control strategy.
- 2) We performed preliminary experiments such as behavioral tests and LFP recording for determining and examining effective stimulation conditions and extracting neural signal index.
- 3) Correlation analysis was also performed to acquire scientific objectivity the use of changes in LFP as nociceptive information for closed-loop control.
- 4) We developed and applied *in vivo* the prototype closed-loop deep brain stimulation system for neuropathic pain.

## ***References***

---

- [1] S. E. Lee, S. B. Jun, H. J. Lee, J. Kim, S. W. Lee, C. Im, *et al.*, "A flexible depth probe using liquid crystal polymer," *Biomedical Engineering, IEEE Transactions on*, vol. 59, pp. 2085-2094, 2012.
- [2] J. Jeong, S. W. Lee, K. S. Min, and S. J. Kim, "A novel multilayered planar coil based on biocompatible liquid crystal polymer for chronic implantation," *Sensors and Actuators A: Physical*, vol. 197, pp. 38-46, 2013.
- [3] J. Jeong, S. W. Lee, K. S. Min, S. Shin, S. B. Jun, and S. J. Kim, "Liquid Crystal Polymer(LCP), an Attractive Substrate for Retinal Implant," *Sensors and Materials*, vol. 24, pp. 189-203, 2012.
- [4] W. F. House, "Cochlear implants," *The Annals of otology, rhinology, and laryngology*, vol. 85, p. 1, 1976.
- [5] S. K. An, S. I. Park, S. B. Jun, C. J. Lee, K. M. Byun, J. H. Sung, *et al.*, "Design for a simplified cochlear implant system," *Biomedical Engineering, IEEE Transactions on*, vol. 54, pp. 973-982, 2007.
- [6] A. Y. Chow, V. Y. Chow, K. H. Packo, J. S. Pollack, G. A. Peyman, and R. Schuchard, "The artificial silicon retina microchip for the treatment of visionloss from retinitis pigmentosa," *Archives of ophthalmology*, vol. 122, pp. 460-469, 2004.
- [7] E. T. Kim, J.-M. Seo, S. J. Woo, J. A. Zhou, H. Chung, and S. J. Kim, "Fabrication of pillar shaped electrode arrays for artificial retinal implants," *Sensors*, vol. 8, pp. 5845-5856, 2008.
- [8] S. W. Lee, J.-M. Seo, S. Ha, E. T. Kim, H. Chung, and S. J. Kim, "Development of microelectrode arrays for artificial retinal implants using liquid crystal polymers," *Investigative ophthalmology & visual science*, vol. 50, pp. 5859-5866, 2009.
- [9] M. L. Kringelbach, N. Jenkinson, S. L. Owen, and T. Z. Aziz, "Translational principles of deep brain stimulation," *Nature Reviews Neuroscience*, vol. 8, pp. 623-635, 2007.
- [10] A. L. Benabid, "Deep brain stimulation for Parkinson's disease," *Current opinion in neurobiology*, vol. 13, pp. 696-706, 2003.
- [11] C. Hammond, R. Ammari, B. Bioulac, and L. Garcia, "Latest view on the mechanism of action of deep brain stimulation," *Movement disorders*, vol. 23,



- pp. 2111-2121, 2008.
- [12] M. R. García, B. A. Pearlmutter, P. E. Wellstead, and R. H. Middleton, "A slow axon antidromic blockade hypothesis for tremor reduction via Deep Brain Stimulation," *PloS one*, vol. 8, p. e73456, 2013.
  - [13] H. E. Merskey, "Classification of chronic pain: descriptions of chronic pain syndromes and definitions of pain terms," *Pain*, 1986.
  - [14] M. Costigan, J. Scholz, and C. J. Woolf, "Neuropathic pain: a maladaptive response of the nervous system to damage," *Annual review of neuroscience*, vol. 32, p. 1, 2009.
  - [15] A. F. DaSilva, C. Granziera, J. Snyder, and N. Hadjikhani, "Thickening in the somatosensory cortex of patients with migraine," *Neurology*, vol. 69, pp. 1990-1995, 2007.
  - [16] C. J. Woolf, "Pain: moving from symptom control toward mechanism-specific pharmacologic management," *Annals of internal medicine*, vol. 140, pp. 441-451, 2004.
  - [17] E. Shipton, "Post-surgical neuropathic pain," *ANZ journal of surgery*, vol. 78, pp. 548-555, 2008.
  - [18] M.-M. Backonja, "Defining neuropathic pain," *Anesthesia & Analgesia*, vol. 97, pp. 785-790, 2003.
  - [19] M. Zhuo, "Cortical excitation and chronic pain," *Trends in neurosciences*, vol. 31, pp. 199-207, 2008.
  - [20] B. Bingham, S. K. Ajit, D. R. Blake, and T. A. Samad, "The molecular basis of pain and its clinical implications in rheumatology," *Nature Clinical Practice Rheumatology*, vol. 5, pp. 28-37, 2009.
  - [21] R. Baron, A. Binder, and G. Wasner, "Neuropathic pain: diagnosis, pathophysiological mechanisms, and treatment," *The Lancet Neurology*, vol. 9, pp. 807-819, 2010.
  - [22] J. Spooner, H. Yu, C. Kao, K. Sillay, and P. Konrad, "Neuromodulation of the cingulum for neuropathic pain after spinal cord injury," 2007.
  - [23] M. Zhao, J. Wang, H. Jia, and J. Tang, "Roles of different subtypes of opioid receptors in mediating the ventrolateral orbital cortex opioid-induced inhibition of mirror-neuropathic pain in the rat," *Neuroscience*, vol. 144, pp. 1486-1494,

- 2007.
- [24] M. Zhuo, "Neuronal mechanism for neuropathic pain," *Mol Pain*, vol. 3, p. 14, 2007.
- [25] T. S. Jensen and R. Baron, "Translation of symptoms and signs into mechanisms in neuropathic pain," *Pain*, vol. 102, pp. 1-8, 2003.
- [26] M. C. Bushnell, M. Čeko, and L. A. Low, "Cognitive and emotional control of pain and its disruption in chronic pain," *Nature Reviews Neuroscience*, vol. 14, pp. 502-511, 2013.
- [27] P. Blomstedt, U. Sandvik, and S. Tisch, "Deep brain stimulation in the posterior subthalamic area in the treatment of essential tremor," *Movement Disorders*, vol. 25, pp. 1350-1356, 2010.
- [28] C. B. McCracken and A. A. Grace, "High-frequency deep brain stimulation of the nucleus accumbens region suppresses neuronal activity and selectively modulates afferent drive in rat orbitofrontal cortex in vivo," *The Journal of Neuroscience*, vol. 27, pp. 12601-12610, 2007.
- [29] G. Cruccu, T. Aziz, L. Garcia-Larrea, P. Hansson, T. Jensen, J. P. Lefaucheur, *et al.*, "EFNS guidelines on neurostimulation therapy for neuropathic pain," *European Journal of Neurology*, vol. 14, pp. 952-970, 2007.
- [30] E. A. Pereira, A. L. Green, K. M. Bradley, N. Soper, L. Moir, J. F. Stein, *et al.*, "Regional cerebral perfusion differences between periventricular grey, thalamic and dual target deep brain stimulation for chronic neuropathic pain," *Stereotactic and functional neurosurgery*, vol. 85, pp. 175-183, 2007.
- [31] R. G. Bittar, I. Kar-Purkayastha, S. L. Owen, R. E. Bear, A. Green, S. Wang, *et al.*, "Deep brain stimulation for pain relief: a meta-analysis," *Journal of Clinical Neuroscience*, vol. 12, pp. 515-519, 2005.
- [32] C. Hamani, J. M. Schwalb, A. R. Rezai, J. O. Dostrovsky, K. D. Davis, and A. M. Lozano, "Deep brain stimulation for chronic neuropathic pain: long-term outcome and the incidence of insertional effect," *Pain*, vol. 125, pp. 188-196, 2006.
- [33] C. L. Wu, S. Agarwal, P. K. Tella, B. Klick, M. R. Clark, J. A. Haythornthwaite, *et al.*, "Morphine versus mexiletine for treatment of postamputation pain: a randomized, placebo-controlled, crossover trial,"

- Anesthesiology*, vol. 109, p. 289, 2008.
- [34] D. Nandi and T. Z. Aziz, "Deep brain stimulation in the management of neuropathic pain and multiple sclerosis tremor," *Journal of clinical neurophysiology*, vol. 21, pp. 31-39, 2004.
- [35] T. Anderson, B. Hu, Q. Pittman, and Z. H. Kiss, "Mechanisms of deep brain stimulation: an intracellular study in rat thalamus," *The Journal of physiology*, vol. 559, pp. 301-313, 2004.
- [36] G. Paxinos and C. Watson, *The rat brain in stereotaxic coordinates: hard cover edition*: Academic press, 2006.
- [37] B. MacFarlane, A. Wright, J. O'callaghan, and H. Benson, "Chronic neuropathic pain and its control by drugs," *Pharmacology & therapeutics*, vol. 75, pp. 1-19, 1997.
- [38] A. L. Benabid, S. Chabardes, J. Mitrofanis, and P. Pollak, "Deep brain stimulation of the subthalamic nucleus for the treatment of Parkinson's disease," *The Lancet Neurology*, vol. 8, pp. 67-81, 2009.
- [39] L. Garcia-Larrea, R. Peyron, P. Mertens, M. Gregoire, F. Lavenne, D. Le Bars, *et al.*, "Electrical stimulation of motor cortex for pain control: a combined PET-scan and electrophysiological study," *Pain*, vol. 83, pp. 259-273, 1999.
- [40] S. Lisanby and H. Sackeim, "Therapeutic brain interventions and the nature of emotion," ed: *The Neuropsychology of Emotion*. Edited by Borod J. New York, Oxford University Press, 2000.
- [41] M. S. Nobler, M. A. Oquendo, L. S. Kegeles, K. M. Malone, C. Campbell, H. A. Sackeim, *et al.*, "Decreased regional brain metabolism after ECT," *American Journal of Psychiatry*, vol. 158, pp. 305-308, 2001.
- [42] M. S. George, S. H. Lisanby, and H. A. Sackeim, "Transcranial magnetic stimulation: applications in neuropsychiatry," *Archives of General Psychiatry*, vol. 56, pp. 300-311, 1999.
- [43] A. T. Barker, R. Jalinous, and I. L. Freeston, "Non-invasive magnetic stimulation of human motor cortex," *The Lancet*, vol. 325, pp. 1106-1107, 1985.
- [44] J. P. Lorberbaum and E. M. Wassermann, "Safety concerns of TMS," *Transcranial magnetic stimulation in neuropsychiatry*. *American Psychiatric*

- Press, Washington*, pp. 141-161, 2000.
- [45] M. S. George, "Stimulating the brain," *Scientific American*, vol. 289, pp. 66-73, 2003.
  - [46] D. Panescu, "Vagus nerve stimulation for the treatment of depression," *Engineering in Medicine and Biology Magazine, IEEE*, vol. 24, pp. 68-72, 2005.
  - [47] J. Zabara, "Peripheral control of hypersynchronous discharge in epilepsy," *Electroencephalography and Clinical Neurophysiology*, vol. 61, p. S162, 1985.
  - [48] D. A. Groves and V. J. Brown, "Vagal nerve stimulation: a review of its applications and potential mechanisms that mediate its clinical effects," *Neuroscience & Biobehavioral Reviews*, vol. 29, pp. 493-500, 2005.
  - [49] S. Ansari, K. Chaudhri, and K. Al Moutaery, "Vagus nerve stimulation: indications and limitations," in *Operative Neuromodulation*, ed: Springer, 2007, pp. 281-286.
  - [50] R. P. Lesser, S. Arroyo, N. Crone, and B. Gordon, "Motor and sensory mapping of the frontal and occipital lobes," *Epilepsia*, vol. 39, pp. S69-S80, 1998.
  - [51] D. Fishlock, "Doctor volts," *IEE Review*, vol. 47, pp. 23-28, 2001.
  - [52] T. A. Zesiewicz, R. Elble, E. Louis, R. A. Hauser, K. Sullivan, R. Dewey, *et al.*, "Practice parameter: therapies for essential tremor report of the quality standards subcommittee of the American Academy of Neurology," *Neurology*, vol. 64, pp. 2008-2020, 2005.
  - [53] U. D. o. Health and H. Services, "FDA approves implanted brain stimulator to control tremors," *Press Release P97-24 (August 4, 1997)*, 2006.
  - [54] T. Loher, H.-H. Capelle, A. Kaelin-Lang, S. Weber, R. Weigel, J. Burgunder, *et al.*, "Deep brain stimulation for dystonia: outcome at long-term follow-up," *Journal of neurology*, vol. 255, pp. 881-884, 2008.
  - [55] T. E. Schlaepfer and K. Lieb, "Deep brain stimulation for treatment of refractory depression," *The Lancet*, vol. 366, pp. 1420-1422, 2005.
  - [56] J. O. Dostrovsky and A. M. Lozano, "Mechanisms of deep brain stimulation," *Movement Disorders*, vol. 17, pp. S63-S68, 2002.
  - [57] D.-B. S. f. P. s. D. S. Group, "Deep-brain stimulation of the subthalamic

- nucleus or the pars interna of the globus pallidus in Parkinson's disease," *The New England journal of medicine*, vol. 345, p. 956, 2001.
- [58] C. W. Olanow, C. G. Goetz, J. H. Kordower, A. J. Stoessl, V. Sossi, M. F. Brin, *et al.*, "A double-blind controlled trial of bilateral fetal nigral transplantation in Parkinson's disease," *Annals of neurology*, vol. 54, pp. 403-414, 2003.
- [59] A. Stefani, A. M. Lozano, A. Peppe, P. Stanzione, S. Galati, D. Tropepi, *et al.*, "Bilateral deep brain stimulation of the pedunculopontine and subthalamic nuclei in severe Parkinson's disease," *Brain*, vol. 130, pp. 1596-1607, 2007.
- [60] L. Wojtecki, L. Timmermann, S. Jorgens, M. Sudmeyer, M. Maarouf, H. Treuer, *et al.*, "Frequency-dependent reciprocal modulation of verbal fluency and motor functions in subthalamic deep brain stimulation," *Archives of neurology*, vol. 63, p. 1273, 2006.
- [61] E. B. Montgomery Jr, "Deep brain stimulation for hyperkinetic disorders," *Neurosurgical focus*, vol. 17, pp. 1-8, 2004.
- [62] E. B. Montgomery Jr, "Dynamically coupled, high-frequency reentrant, non-linear oscillators embedded in scale-free basal ganglia-thalamic-cortical networks mediating function and deep brain stimulation effects," *Nonlinear Studies*, vol. 11, pp. 385-422, 2004.
- [63] E. B. Montgomery Jr and J. T. Gale, "Mechanisms of action of deep brain stimulation (DBS)," *Neuroscience & Biobehavioral Reviews*, vol. 32, pp. 388-407, 2008.
- [64] A. M. Lozano and H. Eltahawy, "How does DBS work?," *Supplements to Clinical neurophysiology*, vol. 57, pp. 733-736, 2004.
- [65] K. J. Iremonger, T. R. Anderson, B. Hu, and Z. H. Kiss, "Cellular mechanisms preventing sustained activation of cortex during subcortical high-frequency stimulation," *Journal of neurophysiology*, vol. 96, pp. 613-621, 2006.
- [66] M. E. Anderson, N. Postupna, and M. Ruffo, "Effects of high-frequency stimulation in the internal globus pallidus on the activity of thalamic neurons in the awake monkey," *Journal of neurophysiology*, vol. 89, pp. 1150-1160, 2003.
- [67] C. C. McIntyre and W. M. Grill, "Excitation of central nervous system neurons by nonuniform electric fields," *Biophysical journal*, vol. 76, pp. 878-888, 1999.

- [68] J. Coombs, D. Curtis, and J. Eccles, "The interpretation of spike potentials of motoneurons," *The Journal of physiology*, vol. 139, pp. 198-231, 1957.
- [69] R. Llinas and C. Terzuolo, "Mechanisms of supraspinal actions upon spinal cord activities. Reticular inhibitory mechanisms on alpha-extensor motoneurons," *Journal of neurophysiology*, vol. 27, pp. 579-591, 1964.
- [70] M. Steriade, M. Deschênes, and G. Oakson, "Inhibitory processes and interneuronal apparatus in motor cortex during sleep and waking. I. Background firing and responsiveness of pyramidal tract neurons and interneurons," *Journal of Neurophysiology*, vol. 37, pp. 1065-1092, 1974.
- [71] J. Gale and E. Montgomery Jr, "Stimulation-induced resonance frequencies in the basal ganglia-thalamic-cortical (BG-Th-Ctx) network. 2003 Abstract Viewer," *Itinerary Planner: Program*, 2003.
- [72] T. Hashimoto, C. M. Elder, M. S. Okun, S. K. Patrick, and J. L. Vitek, "Stimulation of the subthalamic nucleus changes the firing pattern of pallidal neurons," *The Journal of neuroscience*, vol. 23, pp. 1916-1923, 2003.
- [73] E. B. Montgomery Jr, "Effects of GPi stimulation on human thalamic neuronal activity," *Clinical Neurophysiology*, vol. 117, pp. 2691-2702, 2006.
- [74] I. Bar-Gad, S. Elias, E. Vaadia, and H. Bergman, "Complex locking rather than complete cessation of neuronal activity in the globus pallidus of a 1-methyl-4-phenyl-1, 2, 3, 6-tetrahydropyridine-treated primate in response to pallidal microstimulation," *The Journal of neuroscience*, vol. 24, pp. 7410-7419, 2004.
- [75] T. R. Anderson, B. Hu, K. Iremonger, and Z. H. Kiss, "Selective attenuation of afferent synaptic transmission as a mechanism of thalamic deep brain stimulation-induced tremor arrest," *The Journal of neuroscience*, vol. 26, pp. 841-850, 2006.
- [76] J. Dostrovsky, R. Levy, J. Wu, W. Hutchison, R. Tasker, and A. Lozano, "Microstimulation-induced inhibition of neuronal firing in human globus pallidus," *Journal of neurophysiology*, vol. 84, pp. 570-574, 2000.
- [77] H. Kita, Y. Tachibana, A. Nambu, and S. Chiken, "Balance of monosynaptic excitatory and disynaptic inhibitory responses of the globus pallidus induced after stimulation of the subthalamic nucleus in the monkey," *The Journal of neuroscience*, vol. 25, pp. 8611-8619, 2005.

- [78] J. E. Rubin and D. Terman, "High frequency stimulation of the subthalamic nucleus eliminates pathological thalamic rhythmicity in a computational model," *Journal of computational neuroscience*, vol. 16, pp. 211-235, 2004.
- [79] E. Salinas, I. Opris, A. Zainos, A. Hernandez, and R. Romo, "Motor and non-motor roles of the cortico-basal ganglia circuitry," *Brain Dynamics and the Striatal Complex*, pp. 237-255, 2000.
- [80] E. B. Montgomery Jr and S. R. Buchholz, "The striatum and motor cortex in motor initiation and execution," *Brain research*, vol. 549, pp. 222-229, 1991.
- [81] P. D. Wall and W. H. Sweet, "Temporary abolition of pain in man," *Science*, vol. 155, pp. 108-109, 1967.
- [82] D. Nandi, X. Liu, C. Joint, J. Stein, and T. Aziz, "Thalamic field potentials during deep brain stimulation of periventricular gray in chronic pain," *Pain*, vol. 97, pp. 47-51, 2002.
- [83] A. A. Calejesan, S. J. Kim, and M. Zhuo, "Descending facilitatory modulation of a behavioral nociceptive response by stimulation in the adult rat anterior cingulate cortex," *European Journal of Pain*, vol. 4, pp. 83-96, 2000.
- [84] M. J. Millan, "Descending control of pain," *Progress in neurobiology*, vol. 66, pp. 355-474, 2002.
- [85] A. K. Senapati, S. C. Lagraize, P. J. Huntington, H. D. Wilson, P. N. Fuchs, and Y. B. Peng, "Electrical stimulation of the anterior cingulate cortex reduces responses of rat dorsal horn neurons to mechanical stimuli," *Journal of neurophysiology*, vol. 94, pp. 845-851, 2005.
- [86] U. Gimsa, U. Schreiber, B. Habel, J. Flehr, U. van Rienen, and J. Gimsa, "Matching geometry and stimulation parameters of electrodes for deep brain stimulation experiments—numerical considerations," *Journal of neuroscience methods*, vol. 150, pp. 212-227, 2006.
- [87] D. Harnack, C. Winter, W. Meissner, T. Reum, A. Kupsch, and R. Morgenstern, "The effects of electrode material, charge density and stimulation duration on the safety of high-frequency stimulation of the subthalamic nucleus in rats," *Journal of neuroscience methods*, vol. 138, pp. 207-216, 2004.
- [88] D. V. Reynolds, "Surgery in the rat during electrical analgesia induced by focal brain stimulation," *Science*, vol. 164, pp. 444-445, 1969.

- [89] D. E. Richardson and H. Akil, "Long term results of periventricular gray self-stimulation," *Neurosurgery*, vol. 1, pp. 199-202, 1977.
- [90] Y. Hosobuchi, J. E. Adams, and R. Linchitz, "Pain relief by electrical stimulation of the central gray matter in humans and its reversal by naloxone," *Science*, vol. 197, pp. 183-186, 1977.
- [91] G. Mazars, L. Merienne, and C. Cioloca, "[Treatment of certain types of pain with implantable thalamic stimulators]," *Neuro-Chirurgie*, vol. 20, pp. 117-124, 1973.
- [92] G. Mazars, L. Merienne, and C. Ciolocca, "Intermittent analgesic thalamic stimulation. Preliminary note," *Revue neurologique*, vol. 128, p. 273, 1973.
- [93] Y. Hosobuchi, J. E. Adams, and B. Rutkin, "Chronic thalamic stimulation for the control of facial anesthesia dolorosa," *Archives of Neurology*, vol. 29, pp. 158-161, 1973.
- [94] J. E. Adams, Y. Hosobuchi, and H. L. Fields, "Stimulation of internal capsule for relief of chronic pain," *Journal of neurosurgery*, vol. 41, pp. 740-744, 1974.
- [95] U. Thoden, M. Doerr, G. Dieckmann, and J.-U. Krainick, "Medial thalamic permanent electrodes for pain control in man: an electrophysiological and clinical study," *Electroencephalography and clinical neurophysiology*, vol. 47, pp. 582-591, 1979.
- [96] D. Nandi, T. Aziz, H. Carter, and J. Stein, "Thalamic field potentials in chronic central pain treated by periventricular gray stimulation—a series of eight cases," *Pain*, vol. 101, pp. 97-107, 2003.
- [97] A. M. Kuncel and W. M. Grill, "Selection of stimulus parameters for deep brain stimulation," *Clinical Neurophysiology*, vol. 115, pp. 2431-2441, 2004.
- [98] M. E. Wewers and N. K. Lowe, "A critical review of visual analogue scales in the measurement of clinical phenomena," *Research in nursing & health*, vol. 13, pp. 227-236, 1990.
- [99] G. M. Pitcher, J. Ritchie, and J. L. Henry, "Paw withdrawal threshold in the von Frey hair test is influenced by the surface on which the rat stands," *Journal of neuroscience methods*, vol. 87, pp. 185-193, 1999.
- [100] A. Viswanathan and R. D. Freeman, "Neurometabolic coupling in cerebral cortex reflects synaptic more than spiking activity," *Nature neuroscience*, vol.



- 10, pp. 1308-1312, 2007.
- [101] I. Nauhaus, L. Busse, D. L. Ringach, and M. Carandini, "Robustness of traveling waves in ongoing activity of visual cortex," *The Journal of Neuroscience*, vol. 32, pp. 3088-3094, 2012.
- [102] C. Kayser, M. A. Montemurro, N. K. Logothetis, and S. Panzeri, "Spike-phase coding boosts and stabilizes information carried by spatial and temporal spike patterns," *Neuron*, vol. 61, pp. 597-608, 2009.
- [103] J. Liu and W. T. Newsome, "Local field potential in cortical area MT: stimulus tuning and behavioral correlations," *The Journal of neuroscience*, vol. 26, pp. 7779-7790, 2006.
- [104] L. Rossi, G. Foffani, S. Marceglia, F. Bracchi, S. Barbieri, and A. Priori, "An electronic device for artefact suppression in human local field potential recordings during deep brain stimulation," *Journal of neural engineering*, vol. 4, p. 96, 2007.
- [105] C. Reck, E. Florin, L. Wojtecki, H. Krause, S. Groiss, J. Voges, *et al.*, "Characterisation of tremor-associated local field potentials in the subthalamic nucleus in Parkinson's disease," *European Journal of Neuroscience*, vol. 29, pp. 599-612, 2009.
- [106] A. Berényi, M. Belluscio, D. Mao, and G. Buzsáki, "Closed-loop control of epilepsy by transcranial electrical stimulation," *Science*, vol. 337, pp. 735-737, 2012.
- [107] S. Little, A. Pogosyan, S. Neal, B. Zavala, L. Zrinzo, M. Hariz, *et al.*, "Adaptive deep brain stimulation in advanced Parkinson disease," *Annals of neurology*, vol. 74, pp. 449-457, 2013.
- [108] J. Lee, H.-G. Rhew, D. Kipke, and M. Flynn, "A 64 channelprogrammable closed-loop deep brain stimulator with 8 channel neural amplifier and logarithmic adc," in *VLSI Circuits, 2008 IEEE Symposium on*, 2008, pp. 76-77.
- [109] P. J. Grahn, G. W. Mallory, O. U. Khurram, B. M. Berry, J. T. Hachmann, A. J. Bieber, *et al.*, "A neurochemical closed-loop controller for deep brain stimulation: toward individualized smart neuromodulation therapies," *Frontiers in Neuroscience*, p. 0, 2014.
- [110] M. K. Hosain, A. Kouzani, and S. Tye, "Closed loop deep brain stimulation: an

- evolving technology," *Australasian Physical & Engineering Sciences in Medicine*, pp. 1-16, 2014.
- [111] X.-J. Feng, E. Shea-Brown, B. Greenwald, R. Kosut, and H. Rabitz, "Optimal deep brain stimulation of the subthalamic nucleus—a computational study," *Journal of computational neuroscience*, vol. 23, pp. 265-282, 2007.
- [112] C. J. Lee, S. J. Oh, J. K. Song, and S. J. Kim, "Neural signal recording using microelectrode arrays fabricated on liquid crystal polymer material," *Materials Science and Engineering: C*, vol. 24, pp. 265-268, 2004.
- [113] K. S. Min, "Accelerated Soak Test of Various Polymeric Biomaterials for Implantable Device Packing," Master Degree, Department of Electrical and Computer Engineering, Seoul National University, Seoul, 2009.
- [114] S. W. Lee, K. S. Min, J. Jeong, J. Kim, and S. J. Kim, "Monolithic encapsulation of implantable neuroprosthetic devices using liquid crystal polymers," *Biomedical Engineering, IEEE Transactions on*, vol. 58, pp. 2255-2263, 2011.
- [115] C. Hassler, T. Boretius, and T. Stieglitz, "Polymers for neural implants," *Journal of Polymer Science Part B: Polymer Physics*, vol. 49, pp. 18-33, 2011.
- [116] S. Corbett, J. Ketterl, and T. Johnson, "Polymer-based microelectrode arrays," in *MRS Proceedings*, 2006.
- [117] X. Wang, J. Engel, and C. Liu, "Liquid crystal polymer (LCP) for MEMS: processes and applications," *Journal of Micromechanics and Microengineering*, vol. 13, p. 628, 2003.
- [118] D. J. Edell and B. Farrell, "Implantable devices having a liquid crystal polymer substrate," ed: Google Patents, 2003.
- [119] S. H. Bae, J.-H. Che, J.-M. Seo, J. Jeong, E. T. Kim, S. W. Lee, *et al.*, "In vitro biocompatibility of various polymer-based microelectrode arrays for retinal prosthesis," *Investigative ophthalmology & visual science*, vol. 53, pp. 2653-2657, 2012.
- [120] L. Kuraray Co. (2010, March 21). *VECSTAR Liquid Crystalline Polymer Film Products*. Available: <http://www.kuraray.co.jp/>
- [121] U. E. GmbH, "Material Data Sheet," U. E. GmbH, Ed., UBE U-Varnish-S version 2005 ed. UBE Europe GmbH UBE Europe GmbH 2005.

- [122] P. C. S. Inc, "Material Datasheet Parylene," P. C. S. Inc, Ed., version 2009 ed. Parylene Coating Services Inc: Parylene Coating Services Inc, 2009.
- [123] N. S. Technology, "MED-1000 and MED-1011 Silicone Adhesives - Product Profile," N. S. Technology, Ed., version 2005 ed. Nusil Silicone Technology: Nusil Silicone Technology, 2005.
- [124] M. Corporation., "Material Data Sheet SU-8 2000/3000," M. Corporation., Ed., version 2009 ed. MicroChem Corporation., MA, USA: MicroChem Corporation., 2009.
- [125] T. GmbH, "Material Data Sheet Vectra MT1300," T. GmbH, Ed., version 2008 ed. Ticona GmbH, Kelsterbach, Germany: Ticona GmbH, 2008.
- [126] S. F. Cogan, "Neural stimulation and recording electrodes," *Annu. Rev. Biomed. Eng.*, vol. 10, pp. 275-309, 2008.
- [127] C. C. McIntyre, W. M. Grill, D. L. Sherman, and N. V. Thakor, "Cellular effects of deep brain stimulation: model-based analysis of activation and inhibition," *Journal of neurophysiology*, vol. 91, pp. 1457-1469, 2004.
- [128] C. Wu, M. Wais, E. Sheppy, M. del Campo, and L. Zhang, "A glue-based, screw-free method for implantation of intra-cranial electrodes in young mice," *Journal of neuroscience methods*, vol. 171, pp. 126-131, 2008.
- [129] C. K. Joonsoo Jeong, Seung Hee Ahn, Gwan Jung Kim, Jungmin Seo, Sung June Kim, "Simply Fabricated Protruding Microelectrode Array using Liquid Crystal Polymer (LCP)," presented at the BMES annual meeting 2014, San Antonio, Texas, USA, 2014.
- [130] K. Yamanaka, "Anodically electrodeposited iridium oxide films (AEIROF) from alkaline solutions for electrochromic display devices," *Japanese journal of applied physics*, vol. 28, p. 632, 1989.
- [131] C. Bjornsson, S. J. Oh, Y. Al-Kofahi, Y. Lim, K. Smith, J. Turner, *et al.*, "Effects of insertion conditions on tissue strain and vascular damage during neuroprosthetic device insertion," *Journal of neural engineering*, vol. 3, p. 196, 2006.
- [132] B. Wester, R. Lee, and M. LaPlaca, "Development and characterization of in vivo flexible electrodes compatible with large tissue displacements," *Journal of neural engineering*, vol. 6, p. 024002, 2009.

- [133] W. Jensen, K. Yoshida, and U. G. Hofmann, "In-vivo implant mechanics of flexible, silicon-based ACREO microelectrode arrays in rat cerebral cortex," *Biomedical Engineering, IEEE Transactions on*, vol. 53, pp. 934-940, 2006.
- [134] N. Haj Hosseini, R. Hoffmann, S. Kisban, T. Stieglitz, O. Paul, and P. Ruther, "Comparative study on the insertion behavior of cerebral microprobes," in *Engineering in Medicine and Biology Society, 2007. EMBS 2007. 29th Annual International Conference of the IEEE*, 2007, pp. 4711-4714.
- [135] P. S. Motta and J. W. Judy, "Multielectrode microprobes for deep-brain stimulation fabricated with a customizable 3-D electroplating process," *Biomedical Engineering, IEEE Transactions on*, vol. 52, pp. 923-933, 2005.
- [136] T. Dowdall, I. Robinson, and T. F. Meert, "Comparison of five different rat models of peripheral nerve injury," *Pharmacology Biochemistry and Behavior*, vol. 80, pp. 93-108, 2005.
- [137] B. H. Lee, R. Won, E. J. Baik, S. H. Lee, and C. H. Moon, "An animal model of neuropathic pain employing injury to the sciatic nerve branches," *Neuroreport*, vol. 11, pp. 657-661, 2000.
- [138] M. Zimmermann, "Ethical guidelines for investigations of experimental pain in conscious animals," *Pain*, vol. 16, pp. 109-110, 1983.
- [139] S. I. Park, J. H. Oh, Y. S. Hwang, S. J. Kim, and J. W. Chang, "Electrical stimulation of the anterior cingulate cortex in a rat neuropathic pain model," in *Advances in Functional and Reparative Neurosurgery*, ed: Springer, 2006, pp. 65-71.
- [140] R. M. Rangayyan and N. P. Reddy, "Biomedical signal analysis: a case-study approach," *Annals of Biomedical Engineering*, vol. 30, pp. 983-983, 2002.
- [141] E. K. Bae, "Characterization of analgesic effects of cortical electrical stimulation based on time-spectral analysis of neural activities in ventral posterolateral nucleus," Master degree, Department of Biomedical Engineering, Yonsei University, Yonsei University, 2014.
- [142] G. W. King, "Apparatus and method for treating peripheral vascular disease and organ ischemia by electrical stimulation with closed loop feedback control," ed: Google Patents, 2000.
- [143] J. M. Lucas, Y. Ji, and R. Masri, "Motor cortex stimulation reduces

- hyperalgesia in an animal model of central pain," *Pain*, vol. 152, pp. 1398-1407, 2011.
- [144] Q. Li, Y. Ke, D. C. Chan, Z.-M. Qian, K. K. Yung, H. Ko, *et al.*, "Therapeutic deep brain stimulation in Parkinsonian rats directly influences motor cortex," *Neuron*, vol. 76, pp. 1030-1041, 2012.
- [145] J. Kim, S. Eun Lee, K. Sik Min, H. H. Jung, J. E. Lee, S. J. Kim, *et al.*, "Ventral posterolateral deep brain stimulation treatment for neuropathic pain shortens pain response after cold stimuli," *Journal of neuroscience research*, vol. 91, pp. 997-1004, 2013.
- [146] J. Kim, J. Kim, K. S. Min, S. E. Lee, S. J. Kim, and J. W. Chang, "VPL-DBS on neuropathic pain rat model is effective in mechanical allodynia than cold allodynia," *Neurological Sciences*, vol. 33, pp. 1265-1270, 2012.
- [147] J. H. Meier, E. Flach, and T. Breskot, "Neural electrode arrangement," ed: Google Patents, 2001.
- [148] T. Stieglitz, "Flexible biomedical microdevices with double-sided electrode arrangements for neural applications," *Sensors and Actuators A: Physical*, vol. 90, pp. 203-211, 2001.
- [149] S. F. Lempka, S. Miocinovic, M. D. Johnson, J. L. Vitek, and C. C. McIntyre, "In vivo impedance spectroscopy of deep brain stimulation electrodes," *Journal of neural engineering*, vol. 6, p. 046001, 2009.
- [150] C. R. Butson and C. C. McIntyre, "Role of electrode design on the volume of tissue activated during deep brain stimulation," *Journal of Neural Engineering*, vol. 3, p. 1, 2006.
- [151] Y. Wong, S. Chen, J. Seo, J. Morley, N. Lovell, and G. Suaning, "Focal activation of the feline retina via a suprachoroidal electrode array," *Vision research*, vol. 49, pp. 825-833, 2009.
- [152] R. Kramis, C. Vanderwolf, and B. H. Bland, "Two types of hippocampal rhythmical slow activity in both the rabbit and the rat: relations to behavior and effects of atropine, diethyl ether, urethane, and pentobarbital," *Experimental neurology*, vol. 49, pp. 58-85, 1975.
- [153] T. M. Hall, K. Nazarpour, and A. Jackson, "Real-time estimation and biofeedback of single-neuron firing rates using local field potentials," *Nature*

*communications*, vol. 5, 2014.

- [154] X. Liu, D. B. McCreery, R. R. Carter, L. A. Bullara, T. G. Yuen, and W. F. Agnew, "Stability of the interface between neural tissue and chronically implanted intracortical microelectrodes," *Rehabilitation Engineering, IEEE Transactions on*, vol. 7, pp. 315-326, 1999.
- [155] J. Turner, W. Shain, D. Szarowski, M. Andersen, S. Martins, M. Isaacson, *et al.*, "Cerebral astrocyte response to micromachined silicon implants," *Experimental neurology*, vol. 156, pp. 33-49, 1999.
- [156] N. Wisniewski, F. Moussy, and W. Reichert, "Characterization of implantable biosensor membrane biofouling," *Fresenius' Journal of Analytical Chemistry*, vol. 366, pp. 611-621, 2000.
- [157] L. M. Garcia-Segura and J. Balthazart, "Steroids and neuroprotection: new advances," *Frontiers in neuroendocrinology*, vol. 30, pp. v-ix, 2009.
- [158] S. E. Lee, J. Jeong, J. Kim, S.-H. Ahn, J. H. Park, K. S. Min, S. B. Jun, N. L. Jeon, S. J. Kim, "128-CHANNEL FLEXIBLE MEA WITH DRUG DELIVERY CHANNELS FOR IN VIVO NERVE STIMULATION AND RECORDING," in *MicroTAS 2014*, San Antonio, TX, USA, 2014, p. 3 pages.

## 국문초록

심부 뇌 자극술은 뇌의 특정 부위를 전기적으로 자극함으로써 관련 신경질환들을 치료하는 신경외과적 기법이다. 이는 미국 식약처(FDA)의 승인을 받아 파킨슨씨 병, 경직장애, 우울증, 강박장애 등과 같은 다양한 질환 치료에 적용되고 있다. 그러나, 현 시스템은 개회로(開回路, open-loop)구조로, 환자의 증상 경중 여부와 무관한 동일 자극조건 전기신호를 인가함으로써, 조직에 무리를 주거나 시간에 따른 질환치료효과가 경감되는 등의 한계를 가지고 있다. 또한, 지속적인 전기자극과형을 발생시킴으로써 자극기 내의 배터리수명이 단축되어, 자극기 교체수술의 주기가 단축되어 환자의 불편을 야기하기도 한다.

이에, 본 연구는 신경병증성 통증의 증상 경중에 따라 자극조건을 조정하는 폐회로 (閉回路, closed-loop) 심부 뇌 자극시스템과 그 기반 기술을 개발하고자 하였다. 본 연구에서는 이를 위해 다채널 전극과 뇌 국소 전위 (Local field potential, LFP) 기반의 폐회로 심부 뇌 자극장치를 개발하였으며, 이와 관련된 기반 기술들을 개발하였다. 먼저, 다채널 전극을 집적하기 위하여 기존의 액정폴리머 공정을 개선하였다. 다음으로, 제작된 액정폴리머 기반의 다채널 심부 뇌 전극을 이용하여 다양한 자극 조건에 따른 통증모델 동물의 행동반응 실험과 신경신호의 변화들을 측정 및 분석함으로써 신경병증성 통증에의 효과적인 자극조건을 획득하였다. 그리고 두 실험방법론에 따라 얻어진 결과들간 연관성 분석 (Pearson's correlation analysis)을 수행함으로써 뇌 국소 전위의 특정 주파수에서의 변화가 신경병증성 통증의 신경신호 지표로 사용될 수 있음을 객관적으로 검증하였다. 이러한 결과들을 바탕으로 뇌 국소 전위 기반의 폐회로 제어

알고리즘을 개발하고, 이를 적용한 프로토타입 장치를 개발하였다. 개발된 폐회로 시스템의 효과와 성능을 검증하기 위하여, 시스템 동작성 시험과 함께 신경병증성 동물 모델에 적용하는 실험을 수행하였으며, 개발된 시스템이 통증 관련 뇌 국소 전위 신호의 발생과 그 정도에 따라 자동적으로 조정된 심부 뇌 자극을 인가하여 신경병증성 통증을 조절함을 확인하였다.

**주요어 : 폐회로 심부 뇌 자극, 뇌 국소 전위, 심부 뇌 자극술, 신경병증성 통증**

**학 번: 2010-30944**